Faculty of Physics and Astronomy
University of Heidelberg

Diploma thesis
in Physics

submitted by
Tina Jurkat
born in Marburg

Januar 2007

Atmospheric Gaseous Sulfuric Acid and Methanesulfonic Acid in the Marine Boundary Layer: Mass Spectrometric Measurements on a Research Ship Cruise

This diploma thesis was carried out by Tina Jurkat at the
Max-Planck-Institute for Nuclear Physics, Heidelberg
(Atmospheric physics division)
under supervision of
Prof. Dr. Frank Arnold

Atmospheric Gaseous Sulfuric Acid and Methanesulfonic Acid in the Marine Boundary Layer: Mass Spectrometric Measurements on a Research Ship Cruise

This work is focused on the presentation and analysis of measurements of gaseous sulfuric acid (H_2SO_4) and methanesulfonic acid (MSA, CH_4SO_3) performed during the 3 week ship campaign on the research vessel "Celtic Explorer", as part of the European project on Marine Aerosol Production (MAP). The Max Planck-Institute for Nuclear Physics (MPI-K) adapted the CIMS - measurement setup (Chemical Ionization Mass Spectrometry) equipped with an Ion Trap Mass Spectrometer (ITMS) to a sea-container, which was for the first time employed for measurements in remote marine air on the Atlantic Ocean. The course was set at latitudes between 50° and 58° North during the season of high plankton bloom. Plankton is due to its emission of dimethyl sulfide (DMS, $(CH_3)_2S$) of relevance for sulfate aerosol production and cloud formation. High concentrations of the DMS oxidation products MSA with values of the order of $10^7 cm^{-3}$ and low concentrations of H_2SO_4 with an average of $1.70 \cdot 10^6 cm^{-3}$ were observed. The comparison with additional data such as SO_2 concentrations, which were also measured with the CIMS-method by the MPI-K, aerosol number and size distributions, as well as aerosol composition measured during the cruise were used for the analysis of possible sinks and sources of the two gaseous species in the Marine Boundary Layer.

Atmosphärische gasförmige Schwefelsäure und Methansulfonsäure in der Marinen Grenzschicht: Messungen mit einem Massenspektrometer während einer Forschungsschifffahrt

Diese Arbeit konzentriert sich auf die Darstellung und Analyse von Messungen gasförmiger Schwefelsäure (H_2SO_4) und Methansulfonsäure (MSA, CH_4SO_3), die während einer dreiwöchigen Schiffskampagne auf dem Forschungsschiff "Celtic Explorer" im Rahmen des Europäischen Projekts zur Marinen Aerosol Produktion (MAP) durchgeführt wurden. Die Methode der chemischen Ionisations-Massenspektrometrie (IT-CIMS) wurde am Max-Planck Institut für Kernphysik in einen Messcontainer integriert und zum ersten Mal für Messungen in der Marinen Grenzschicht des Atlantischen Ozeans eingesetzt. Der Kurs bewegte sich zwischen dem 50° und 58° Breitengrad Nord, während der Zeit der höchsten Algenblüte. Hohe Konzentrationen der DMS Oxidationsprodukte MSA in der Grössenordnung von $10^7 cm^{-3}$ und niedrige H_2SO_4 Werte mit einem Durchschnitt von $1.70 \cdot 10^6 cm^{-3}$ wurden gemessen. Die Emission von DMS durch Algen ist aufgrund ihrer Relevanz für die Produktion von Sulfataerosolen und der Wolkenbildung über dem Ozean von Interesse. Vergleichsdaten wie Schwefeldioxidkonzentrationen, Aerosolgrößenverteilung und Aerosolzusammensetzung wurden zur Analyse möglicher Quellen und Senken der Gasphasensäuren in der Marinen Grenzschicht herangezogen.

Contents

1 Introduction **1**

2 Scientific Background **5**

2.1 Atmospheric Sulfurous Trace Gases 5

2.1.1 Marine Aerosol Size Distributions 6

2.1.2 Dimethyl Sulfide 6

2.1.3 Dimethyl Sulfoxide 8

2.1.4 Methanesulfonic Acid 10

2.1.5 Sulfur Dioxide 11

2.1.6 Sulphuric Acid 13

2.1.7 OH-Radicals 14

2.2 Sinks of H_2SO_4 and MSA 15

2.2.1 Nucleation 15

2.2.2 Condensation 19

3 Measurement Principle **23**

3.1 Chemical Ionization Mass Spectrometry (CIMS) 23

3.2 Ion Trap Mass Spectrometer (ITMS) 25

4 Marine Aerosol Production (MAP) **31**

5 Experimental Setup and Calibration **35**

5.1 Experimental Setup 35

5.1.1 Inlet System 36

5.1.2 Ion Source and Ion Reaction 37

5.1.3 Ion-Molecule Reactions of H_2SO_4 and MSA 39

5.1.4 Detection of Sulfur Dioxide 40

5.1.5 Instrumental Settings 42

5.1.6 Additional Data . . . 43
5.2 Sulfuric Acid Calibration . . . 44
5.2.1 Production of OH-radicals . . . 44
5.2.2 Discrimination of Mass 125 . . . 46
5.2.3 Calculation of the Calibration Factor . . . 47

6 Atmospheric Measurements 53
6.1 Further Considerations . . . 53
6.1.1 Background and Detection Limit . . . 53
6.1.2 Temperature and Pressure Factor . . . 56
6.1.3 Isotopic Corrections . . . 57
6.2 Experimental Data . . . 57
6.2.1 Sulfuric Acid, MSA and Sulfur Dioxide . . . 57
6.2.2 Additional Data: Aerosol parameters, Chlorophyll-a and Halocarbons 60

7 Data Analysis and Discussion 63
7.1 Sulfuric Acid . . . 63
7.2 Sulfur Dioxide . . . 72
7.3 Methanesulfonic Acid . . . 76

8 Conclusions and Perspectives 83

A Experimental Data 85
A.1 Influence of NO_x . . . 101
A.2 Experimental Setup . . . 107

B Additional Data 109

C Air Mass Trajectories 113

List of Figures 116

Bibliography 123

Chapter 1

Introduction

Sulfate aerosols present in the Marine Boundary Layer (MBL) influence the global climate in various ways. Sulfuric acid is the only known oxidation product of dimethyl sulfide (DMS), emitted by marine phytoplankton, that nucleates to form new particles, contributing to the marine sulfate aerosol budget. Methanesulfonic acid (MSA), also produced through DMS oxidation, is known to be involved in the growth of particles and influences their composition. Understanding how these gases evolve from DMS emissions and how they act on climate forcing is pivotal for climate change studies.

Questions about the Earth's self regulating ability have led to a vital discussion during the last decades. Ever since James Lovelock presented the GAIA hypothesis (GAIA is the name of the Greek Goddess of Earth) stating that the Earth System and its organism regulate and stabilize its environment, indirectly as well as for its own benefit, various criticism have become loud. Up to now it has not been possible to discern a clear cut consensus. The CLAW hypothesis [Charlson et al., 1987], named after their creators R. Charlson, J. Lovelock, M. Andreae and S. Warren, a GAIA supporting theory concerning biogenic emissions, postulates the global thermostat stemming from marine algae that produce DMS, stimulating cloud formation and thereby increasing Earth's albedo which results in a cooling effect on Earth. As a consequence algae production is reduced resulting in a negative feedback effect.

Many investigations have been carried out for a better understanding of the interaction between the biological and atmospherical system with a specific focus on the sulfur cycle. Not only to prove or disprove such a provoking hypothesis as the one of GAIA, but for a thorough quantification of the biogenic contribution of sulfur emissions to the Earth's climate further

research is necessary. Contributions of anthropogenic emissions can only be evaluated with the knowledge of natural sources and their emission rates.

Aerosols, being an essential element of this algae feedback effect, are of major concern, due to their importance for cloud formation. The ocean covers 70% of the Earth's surface, of while 50% are covered with stratus clouds. Stratus clouds form in the lower tropospheric regions. They have a low water content and rarely produce precipitation but they have a high reflectivity and therefore reduce incoming solar radiation. The impact of clouds over the ocean and their importance for the climate becomes clear with the comparison of the uncovered ocean albedo (vertical radiation) of 4% and the stratus cloud covered ocean of 60 to 70 % [Roedel, 2000]. This is one crucial aspect of oceanic aerosols and their influence on the radiative budget of the Earth.

There are three main classes of aerosols in the Marine Boundary Layer: Sea salt aerosol, non-sea-salt aerosols (nss) and free tropospheric aerosols (also known as background aerosols, which are injected through vertical entrainment). They are either directly emitted into the atmosphere through primary production or they are formed through nucleation processes of trace gases (secondary aerosols). Their contribution depends on various factors such as wind speed, ocean temperature, precipitation and the oxidation of DMS.

Among other secondary aerosols, sulfate aerosols in particular acting as cloud condensation nuclei (CCN) influence regional precipitation patters and optical properties of clouds. By increasing Earth's albedo they provoke a cooling effect. This is known to be the direct effect of radiative forcing of aerosols. The indirect effect considers their influence on cloud properties such as size and number distributions of droplets and composition of CCN. High aerosol number concentrations lead to an increase in the number of cloud droplets, with a higher total cross section for backscattering of incoming sunlight. This again leads to a cooling effect due to an increased albedo. The indirect effect can be estimated to range between -0.5 to -5.0 W/m depending on whether clean air masses or polluted air masses over industrial regions are present [Brasseur et al., 1999]. Size distribution also affects the lifetime of a cloud. Thus, whether direct or indirect, both effects contribute to planetary cooling which partially counteracts the anthropogenic greenhouse effect. Apart from their effect on the climate several studies report of additional, more immediate impacts that aerosols can have on human well-being. Inhalation of aerosols is observed to emerge asthma, lung cancer and premature death. [Zylka-Menhorn, 2005].

The quantitative as well as qualitative contribution of dimethyl sulfide emission to new particle formation is still poorly understood, however any effect depends critically on the production of gas-phase sulfuric acid. As a final oxidation product of DMS, sulfuric acid is observed to be strongly involved in nucleation processes, particle formation and growth. [Reiner and Arnold, 1993][Reiner and Arnold, 1994][Boy et al., 2004][Kulmala, 2003] [Kulmala et al., 2005]. Nucleation processes include homogeneous, heterogeneous as well as ion induced nucleation [Arnold, 1982][Korhonen et al., 1999][Yue and Chan, 1979]. Sulfuric acid (H_2SO_4) is known to be the only oxidation product of DMS which leads to new particle formation. Other reaction pathways lead to the formation of methansulfonic acid (CH_4SO_3) and sulfur dioxide (SO_2). SO_2 as a direct precursor of H_2SO_4 is in the atmosphere mainly oxidized by OH radicals. MSA on the other hand does not favor particle formation but contributes to their growth due to a very low saturation vapor pressure. The two end products have therefore different influences on particle number and size distributions, contributing to Earth's albedo in different ways.

A complex oxidation scheme of two temperature dependent pathways with several intermediate products, such as dimethyl sulfoxid (DMSO), complicates the determination of the yields and identity of the final products stemming from biogenic sulfur. Their importance can vary with the different prevailing atmospheric conditions.

The present work deals with the recent measurements of H_2SO_4, MSA, DMSO and SO_2 made during a ship cruise on the Northern Atlantic ocean at latitudes between 50° and 58° North as part of the European project on Marine Aerosol Production (MAP). The project is focused on the investigation of primary and secondary marine aerosol production and their influence on the global climate, concentrating on the secondary aerosol formation mechanism involving iodine oxides and the primary production of marine organic matter aerosols produced by plankton. For a better quantification of their relative influence, sulfur trace gases need to be quantified. These measurements were performed during a three-week ship cruise on the research vessel "Celtic Explorer" in June/July 2006 during the season of high plankton bloom in the Atlantic north and west of Ireland.

A sea-container mounted with two CIMS (Chemical Ionization Mass Spectrometry) instruments of our MPI-K group was deployed on the front deck of the ship. A general introduction to the measurement principles as well as detailed description of the experimental setup on the ship will be given in chapter 5 and 6. The calibration methods used will be

discussed in chapter 5. A data set acquired during 15 days of the cruise will be discussed with specific focus on one day in June when nucleation was observed and the last five days in July when 24 h measurements were performed. Additional data from Differential Mobility Particle Sizer (DMPS) systems provided by the University of Helsinki and Aerosol Mass Spectrometers (AMS) from the University of Manchester acquired during the cruise will be used to support trends of formation and loss of sulfurous acidic gases in the MBL. High MSA-concentrations up to 6 $\cdot 10^7 \mathrm{cm}^{-3}$ and relatively low H_2SO_4-concentrations with an average around 1.7 $\cdot 10^6 \mathrm{cm}^{-3}$ to 2.9 $\cdot 10^6$ cm^{-3} were measured. A possible explanation of the low H_2SO_4-concentrations is the short lifetime of H_2SO_4 due to high aerosol surface of pre-existing particles and low SO_2-concentrations. High relative humidity and memory effects are possible explanations for a high detection limit (around 1 $\cdot 10^6 \mathrm{cm}^{-3}$). SO_2, measured by the second CIMS-instrument ranged between the detection limit of 30 ppt (parts per trillion) and several ppb (parts per billion). The higher SO_2-mole fractions were due to ship emissions.

Chapter 2

Scientific Background

This chapter will give an overview on DMS oxidation pathways leading to the formation of H_2SO_4 and MSA. The focus will be on the sulfur containing trace gases as precursors of aerosols and their impact on cloud formation over the ocean.

2.1 Atmospheric Sulfurous Trace Gases

Atmospheric climate is strongly influenced by both anthropogenic and natural emissions of sulfur gases. There are still many uncertainties regarding the relative amount emitted by the two sources and their effect on the climate. For an estimate of climate forcing by anthropogenic sulfur sources, an understanding of the biogenic sulfur cycle and its contribution to aerosol formation is necessary.

Natural sulfur sources can be divided into terrestrial and marine. Land emissions include a variety of species such as H_2S, CS, OCS and CS_2 and have an estimated emission flux of 0.25 Tmol/a (for the total land surface). The marine emissions are almost exclusively in the form of DMS. It accounts for the largest source of natural sulfur to the global atmosphere and the largest overall source of sulfur in the Southern Hemisphere [Bates et al., 1987]. DMS undergoes a complex series of gas-phase reactions in the atmosphere leading to the formation of sulfur species that favor the generation of new particles or the alteration of pre-existing particles.

Due to high reactivity the concentration of the different sulfur compounds varies regionally and seasonally in the atmosphere. Sulfur is present in five different oxidation stages. The reduced sulfur compounds (oxidation stage -1,-2) is rapidly oxidized by hydroxyl radicals. These species occur mainly in the gas phase and because of high reactivity their residence time in the lower atmosphere is no longer than a few days. Higher oxidation stages are mainly

found in particles and cloud droplets but also in the form of SO_2 in the gaseous phase. Aerosol scavenging therefore becomes a major sink of oxidized sulfur species. Apart from chemical mechanisms and scavenging by aerosols, vertical mixing and surface deposition on the ocean are additional sinks of sulfur containing molecules in the Marine Boundary Layer. The discussion of formation and loss and the influence on aerosol growth and nucleation for the major products of the DMS oxidation chain will be a major objective of this chapter and this thesis in general.

2.1.1 Marine Aerosol Size Distributions

Marine aerosol size distributions are governed by sulfur compounds significantly. Shown in F 2.1 is the particle size distribution plotted vs the particle radius taken from
[O'Dowd et al., 1997]. The first maximum on the right can be explained by sea salt aerosols produced through bubble bursting at the seawater surface. Air is trapped by waves in the water at high wind speeds forming bubbles with a diameter of 100 μm which in turn produce smaller droplets (about 10% of the bubble size) when bursting at the surface. Typical concentrations in the MBL are around 5 to 30 cm^{-3} comprising 95% of the total aerosol mass [O'Dowd et al., 1997]. These droplets evaporate partially to one third of their original size thereby forming aerosols with a radius of 0.2 μm, known as the accumulation mode, which is partly dominated by secondary aerosols and generated through coagulation of smaller, newly-formed particles. Particle sizes in the super micron region are dominated by coarse/sea-salt particles as well. Another mode can be seen at 0.005 μm which is known as the "new particle sub range". It is formed mainly by nss-sulfate particles and particles containing organic matter. The maxima at 0.02-0.03 μm is known as the nucleation mode and consists of newly formed particles generated by homogeneous nucleation. Total number concentrations are usually dominated by the nucleation mode and the accumulation mode.

2.1.2 Dimethyl Sulfide

Dimethyl sulfide ($(CH_3)_2S$) is know to be the primary source of biogenic sulfur next to other volatile sulfur gases such as CS_2, H_2S and OCS [Bates, 1992]. With 15 Tg/a it accounts for 60% of the natural sulfur gases released to the atmosphere. DMS is produced in the surface water by most species of marine phytoplankton by enzymatic cleavage of dimethylsulphoniopropionate, DMPS. A typical DMS producer is the plankton species emiliania huxleyi. DMS surface seawater concentrations vary substantially on a regional and seasonal basis, with lowest values at high latitudes in winter and highest values in summer at the same

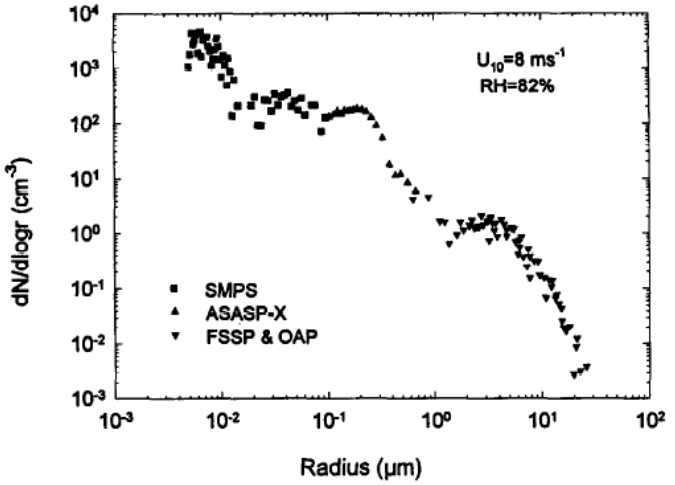

Figure 2.1: Typical marine aerosol number distributions measured in North East Atlantic maritime air masses at the Outer Hebrides, taken from [O'Dowd et al., 1997]

latitudes [Bates et al., 1987]. Transport into marine air, meaning the flux of gases across the air-sea interface depends on concentration differences, the wind speed and the molecular diffusivity of the gas. Typical concentrations in higher latitudes are between 20 and 160 pptv [Jefferson et al., 1998]. DMS yield is however only weakly correlated with the usual measures of phytoplankton productions such as chlorophyll. As stated in Simó et al., DMS concentration depends mainly on the depth of the actual mixing layer [Simó and Pedrós-Alló, 1999]. Increase in solar radiation does further shoal the mixing layer and cause stimulation of DMS production. Consequently on a seasonal scale DMS productions during summer would be highest and considering the radiative effect of DMS, which will be discussed later in more detail, would lead to a climatic feedback effect. It appears that the warmest, most saline, and most intensely illuminated regions have the highest DMS emissions to the atmosphere [Charlson et al., 1987].
DMS has a relatively long lifetime (compared to oxidized sulfur compounds) in the Marine Boundary Layer reaching as long as 7-9 days, which can be explained by low OH levels and will be discussed later [Davis et al., 1998]. A further potential loss of DMS is dissolution in aqueous particles followed by oxidation of OH and O_3. This however has a minor effect on the DMS lifetime [Barnes et al., 2006].

In remote marine air DMS is mainly oxidized in the gaseous phase by OH radicals via two main reaction pathways: Addition of an O atom and abstraction of an H atom. The

reaction with OH contributes to both pathways and leads to the formation of H_2SO_4 and MSA. Additional oxidation candidates such the NO_3 radical can also be responsible for DMS oxidation, especially during night when no OH is present. This candidate takes only part in the abstraction pathway and should be of minor importance in the remote MBL due to low concentrations.
Initialization by halogens also play an important role for to the additional branch. Model studies have shown that inclusion of halogen chemistry leads to higher destruction of DMS and lowers therein the conversion efficiency of DMS to SO_2 [von Glasow and Crutzen, 2004]. F 2.2 shows the two reaction pathways and the intermediate products. Assuming a diurnal average concentration of OH radicals of $1{\cdot}10^6 \mathrm{cm}^{-3}$ the lifetime of DMS can be estimated to be 58 h. This estimate leads to the hypothesis that DMS undergoes vertical transport in the atmosphere as observed by [Lucas and Prinn, 2002] and [Mitchell, 2001]. Vertical concentration profiles reflect the variations of most of the products of DMS oxidation, since the time for vertical mixing of DMS in the Marine Boundary Layer and the layer above, also known as Buffer Layer, is shorter than the chemical lifetime of DMS.

2.1.3 Dimethyl Sulfoxide

Dimethyl sulfoxide (DMSO, $(CH_3)_2SO$) is one of the major intermediate reaction products of DMS with OH leading to gaseous methansulfinic acid (MSIA, CH_4SO_2) and $DMSO_2$, respectively. In the second case further oxidation is not expected to produce MSA and is therefore lost to further reactions. The addition reaction pathway of DMS with OH to DMSO is favored at low temperatures therefore suggesting a latitude and altitude depended variation [Bardouki et al., 2003]. DMSO can also be produced via multiphase reactions of DMS with O_3 [Lee and Zhu, 1994] and NO_x radicals which are mainly important during night. Its lifetime in the Marine Boundary Layer is relatively short due to uptake on pre-existing particles. The reaction of DMSO with OH radicals as well as O_3 leads to MSIA, a precursor of MSA at low temperatures under cloud free conditions. There are still many uncertainties about the formation of DMSO from DMS since their removal pathways and lifetimes are different. For a comprehensive overview on DMS atmospheric chemistry and kinetics see [Barnes et al., 2006].

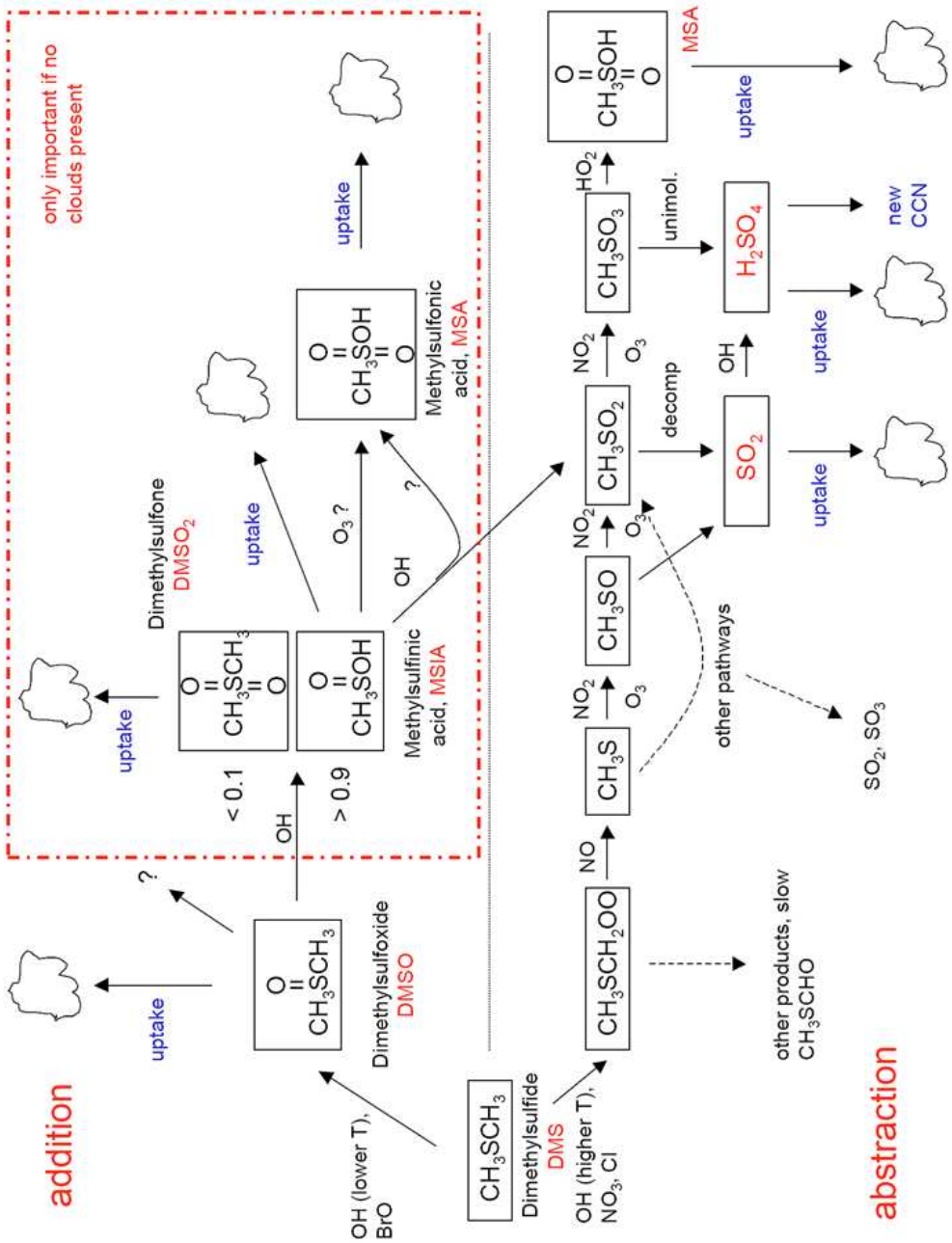

Figure 2.2: The two reaction pathways leading to the formation of MSA and H_2SO_4 taken from [von Glasow and Crutzen, 2004].

2.1.4 Methanesulfonic Acid

Currently, atmospheric methanesulfonic acid (MSA) is thought to be exclusively produced by DMS oxidation [Seinfeld and Pandis, 1998] and therefore a strong indicator of biogenic contributions to the global sulfur budged. It has a higher vapor pressure than H_2SO_4 but condenses easily on preexisting particles, contributing to their growth and composition. In contrast to H_2SO_4 MSA is not involved in nucleation processes [Kreidenweis and Seinfeld, 1988]. It appears to be more sensitive than H_2SO_4 to changes in relative humidity and aerosol surface [Berresheim et al., 2002][Mauldin III et al., 1999].

Recent measurements of MSA-concentrations range from $8.0{\cdot}10^6$ cm^{-3} at the northeastern coast of Crete [Bardouki et al., 2003], $8.0{\cdot}10^5 cm^{-3}$ western coast of Ireland (median values) [Berresheim et al., 2002], down to $1.1{\cdot}10^5 cm^{-3}$ in the coastal Antarctic boundary layer showing a strong latitude dependent production rate [Davis et al., 1998].

The formation of MSA as already shown in the above diagram F 2.2 is initiated via two reaction pathways:

$$CH_3SCH_3 + OH \longrightarrow CH_3SCH_2 + H_2O \qquad \text{(abstraction)} \tag{2.1}$$

$$CH_3SCH_3 + OH \longrightarrow CH_3S(OH)CH_3 \qquad \text{(addition).} \tag{2.2}$$

Both rate coefficients are temperature and pressure dependent. The abstraction reaction pathway (2.1) has a weak, positive temperature dependence, while the addition reaction pathway (2.2) shows a negative dependence on temperature. The rate constant for the first reaction (2.1) has a value of $4.8{\cdot}10^{-12}$ $cm^3 molecules^{-1} s^{-1}$at a temperature of 298K [Atkinson et al., 1997]. The rate constants for reaction (2.2) has been determined to be $1.7{\cdot}10^{-12}$ $cm^3 molecules^{-1} s^{-1}$ [Atkinson et al., 1997]. At 298 K, 80% of the total reaction proceeds by abstraction, while at 273 K both reactions occur at equal rates.

Further possible reactions that lead to the formation of MSA are numerous, of high complexity and not well understood yet. Since measurements of the intermediate products such as DMSO and MSIA are difficult to operate there are still many uncertainties about MSA production. The addition channel as mentioned above favors the production of DMSO (under NO_x free conditions via the reaction of O_2).

$$((CH_3)_2S - OH) + O_2 \longrightarrow HO_2 + CH_3S(O)CH_3 \tag{2.3}$$

$$((CH_3)_2S - OH) + O_2 \longrightarrow OH + CH_3S(O)_2CH_3 \tag{2.4}$$

the latter reaction leading to the formation of $DMSO_2$ [Barnes et al., 2006].

In Brasseur et.al (1999) the following reaction is suggested for the abstraction channel:

$$CH_3SCH_2 + O_2 + M \longrightarrow CH_3SCH_2O_2 + M \quad (2.5)$$

$$CH_3SCH_2O_2 + NO \longrightarrow CH_3SCH_2O + NO_2 \quad (2.6)$$

$$CH_3SCH_2O + M \longrightarrow CH_3S + CH_2O + M \quad (2.7)$$

The CH_3S is then oxidized by ozone or NO_2 to form CH_3SO and by further oxidation to CH_3SO_3. The abstraction of an H atom leads to the formation of MSA. These processes however can only be explained if NO_x is present as it is the case of coastal regions.

Lucas and Prinn (2002) suggested the reaction of MSIA with O_3, which is dominant at low temperatures and in a cloud free atmosphere. However the second branch (abstraction pathway) in the above diagram involves both the CH_3SO_2 reactions leading to MSA competing with the CH_3SO_2 dissociations. Great uncertainties arise from the poorly quantified steps of the unimolecular decomposition of the two DMS products CH_3SO_3 and CH_3SO_2, the magnitudes of which affects the yield of MSA and SO_2. The need of OH radicals for both reaction pathways suggests a diurnal pattern depending on the light intensity. However different loss mechanism of intermediate products, different lifetimes with respect to photochemical removal allowing vertical transport as well as heterogeneous reactions complicate the determination of the origin of the different sulfur species.

Thorough studies of the two reaction pathways reveal their importance for climate change. The addition pathway mainly produces sulfur species, such as MSA which can easily condense on pre-existing particles increasing their size but not their number. Higher MSA concentrations are associated with larger particles [Huebert et al., 1993]. In turn MSA increases the loss of H_2SO_4 and tends to reduce new particle formation by H_2SO_4 nucleation. The abstraction pathway on the other hand leads to the formation of H_2SO_4 and new particle formation, increasing the number of marine aerosol particles. This results in a higher backscattering cross section and thereby a higher albedo.

2.1.5 Sulfur Dioxide

SO_2 is expected to be another product yet the most important one from DMS oxidation. Its importance originates from being a direct precursor of H_2SO_4. Average concentrations range from 20-90 pptv in the MBL up to 1500 pptv at polluted continental air
[Seinfeld and Pandis, 1998]. Anthropogenic emissions of SO_2 account for about 70% of the total global flux, next to volcanic emissions (10%), biomass burning (2%) and DMS oxidation.

Recent studies of DMS to SO_2 conversion in the Marine Boundary Layer have shown that SO_2 is formed via the two reaction pathways [Davis et al., 1999] and the abstraction pathway is favored at high temperatures. A major fate of the above mentioned CH_3S intermediate in the MSA production is oxidation by O_3 to SO_2 as laboratory works have shown [Barnes et al., 2006], but the respresentativity of these chamber studies may be questioned. Nearly all chamber experiments are set up with NO concentrations that cannot be found in remote marine areas, not to mention their limiting effect due to their size. Photoreactor experiments on OH + DMS have reported SO_2 yields of 70-80% [Barnes et al., 2006] and have been measured earlier during field studies in the equatorial Pacific by [Davis et al., 1999]. However long range transport, loss and production rates of intermediate species, and the variability in the efficiency of these reactions with changing conditions leave many questions on the quantitative mechanism details by which SO_2 is formed in the atmosphere.

Emissions from bunker fuel burned by oceanic transport ships represents a significant contribution of SO_2 to the sulfur budget over the ocean, mainly in the Northern Hemisphere [Endresen and Sørgård, 2003]. Emission rates by ships, which are still poorly investigated, complicate the quantification of sulfur contribution by biogenic matter [Huebert, 1999]. Ship emissions further effect remote marine chemistry by contributing to the oxidation power of the atmosphere through emission of NO_x. Acidification is another problem: activation of sea salt bromide is favored at high gas phase acidity. Both products are involved in the DMS oxidation.

Long range SO_2 transport from coastal areas into remote marine areas can only partly account for marine SO_2 concentrations due to fast removal by wash-out effects or dry deposition. Vertical transport of anthropogenic emissions occurs through highly convective systems into the upper troposphere and eventually into the lower stratosphere where long distance transport takes place thus leading to a higher background concentration of sulfur containing aerosols at remote areas [Roedel, 2000][Speidel, 2005]. Further contributions to higher stratospheric SO_2 are volcanic eruptions and aircraft emissions.

SO_2 removal takes place via oxidation by O_3 and H_2O_2 in the liquid phase. Dry deposition on the ocean surface is one of the main removal mechanism of SO_2 in the Marine Boundary Layer [Lucas and Prinn, 2002][Jefferson et al., 1998]. SO_2 solubility is dependent on the solution pH, which decreases until solubility reaches the Henry's Law Constant for physical solubility [Brasseur et al., 1999]. Limited solubility of SO_2 is however the reason why SO_2 uptake by cloud particles compared to gas phase oxidation is only important under cloudy conditions, thus explaining a relatively long SO_2 lifetime of 1-9 days in the boundary layer

depending on the meteorological conditions. In the gas phase SO_2 is oxidized by OH radicals forming sulfuric acid and is thereby removed through nucleation or condensation. This removal mechanism is compared to continental sites less effective in the Marine Boundary Layer due to reduced levels of OH radicals. Further loss mechanisms in the Marine Boundary Layer involve vertical entrainment due to a long life time compared to oxidation processes, loss onto sea-salt aerosols and non sea-salt aerosols.

2.1.6 Sulphuric Acid

Sulfuric acid is despite its low concentration in the atmosphere playing an important role in nucleation processes with further effects on the climate. Due to its low vapor pressure ($< 10^{-3}$hPa at 20°C) activation of new particle formation by homogeneous, heterogeneous or ion induced nucleation occurs in the lower troposphere as well as in higher atmospheric regions.

Formation processes involve the oxidation of SO_2 by OH radicals described by the Stockwell-Calvert-Mechanism [Stockwell and Calvert, 1983], [Reiner and Arnold, 1993], [Reiner and Arnold, 1994]:

$$SO_2 + OH + M \longrightarrow HSO_3 + M, \tag{2.8}$$

$$HSO_3 + O_2 \longrightarrow SO_3 + HO_2. \tag{2.9}$$

$$\tag{2.10}$$

SO_3 reacts with water, either in the gas phase or following uptake into droplets via

$$SO_3 + H_2O + M \longrightarrow H_2SO_4 + M. \tag{2.11}$$

Values for the rate coefficient k are pressure and temperature dependent

$$k_1 = 9 \cdot 10^{-13}\text{cm}^3\text{s}^{-1} \tag{2.12}$$

(at a temperature of 295 K and a pressure of 1013 mbar) [DeMore, 1997]. The lifetime of SO_2 with respect to OH oxidation of atmospheric concentrations of $1{\cdot}10^6\text{cm}^{-3}$ therefore comprises about 13 days. The reaction of HSO_3 is very fast (k = $4.3{\cdot}10^{-13}\text{cm}^3$/s) therefore HSO_3 has a very short lifetime of the order of 1 second.

H_2SO_4 can be formed from SO_3 and water via two possible pathways [Reiner and Arnold, 1993][Reiner and A

$$SO_3 + 2H_2O \longrightarrow H_2SO_4 + H_2O \tag{2.13}$$

$$SO_3(H_2O) + H_2O \longrightarrow H_2SO_4 + H_2O. \tag{2.14}$$

An alternative to equation (2.8) might be a reaction of SO_2 and OH via the formation of the peroxy radical HSO_5, which is described in [Wayne, 2000]. But this mechanism can be neglected due to a very small rate constant.

The above DMS oxidation scheme F 2.2 shows one possible way to the formation of H_2SO_4 without the use of the intermediate SO_2 : CH_3SO_3 decomposes into

$$CH_3SO_3 \longrightarrow CH_3 + SO_3, \tag{2.15}$$

which forms H_2SO_4 immediately since large amount of water vapor are always present in the atmosphere and reaction 2.13 is fast. This reaction might explain the high nss-SO_4 contents of aerosols, which can not be explained through gas phase oxidation of SO_2 and condensation of gaseous H_2SO_4 onto aerosols.

2.1.7 OH-Radicals

The Stockwell-Calvert-Mechanism involves OH-radicals. These OH-radicals are very reactive with a lifetime of 1 s in the lower troposphere. They are the main oxidation species leading to the formation of MSA and H_2SO_4. Due to recycling processes OH can reach a concentration around $10^6 \mathrm{cm}^{-3}$.

In the troposphere OH is mainly produced by the photolysis of ozone:

$$O_3 + h\nu \longrightarrow O(^1D) + O_2, \ (\lambda \ \leq \ 320 \text{ nm}) \tag{2.16}$$

$$O(^1D) + H_2O \longrightarrow 2 \cdot OH, \ k = 2.2 \cdot 10^{-10} \mathrm{cm}^3\mathrm{s}^{-1} \tag{2.17}$$

$$O(^1D) + M \longrightarrow O(^3P) + M. \tag{2.18}$$

Ozone is dissociated into oxygen and an excited O-atom in singlet D state (metastable state). The excited oxygen atoms loose their energy through collisions with other molecules such as N_2 and O_2, making the recombination to oxygen or with oxygen to ozone possible. About 10 % collide with water molecules leading to OH formation as in reaction (2.17). The total OH production rate may be expressed as a yield of primary production from the reaction

of $O(^1D)$ with water vapor and an amplification factor due to recycling mechanism of HO_2. Recycling mechanism, involving ozone and NO radicals, can be of the form:

$$HO_2 + NO \longrightarrow OH + NO_2 \tag{2.19}$$

$$HO_2 + O_3 \longrightarrow OH + 2O_2 \tag{2.20}$$

The HO_2 radical is in equilibrium with OH.

Other sources of OH are the photolysis of nitrous acid HONO and the photolysis of hydrogen peroxide H_2O_2, which is less reactive and has a lifetime of about 1 day in clean air masses. OH formation is strongly dependent on UV-radiation and can therefore only be produced during daytime with a diurnal pattern following the light intensity. OH production rates vary also with latitude and changing solar flux.

2.2 Sinks of H_2SO_4 and MSA

Condensable vapors with low saturation vapor pressure such as H_2SO_4 and MSA are mainly removed through condensation onto pre-existing particles as well as through formation of new particles in the case of H_2SO_4. Once these vapors are in the particulate phase they are either removed through coagulation with other aerosols or droplets within hours, wet deposition, comprising washout effects through cloud-scavenging and below-cloud scavenging or sedimentation in the case of bigger aerosols ($r > 7$ μm). In the case of wet deposition multiple steps of dissolution and evaporation of liquid particles, growth through coagulation of droplets and evaporation of droplets on their way to the ground are possible. An average lifetime of particles with a diameter of 0.05 μm up to several μm is around 4 to 6 days [Roedel, 2000]. Smaller and bigger particles are removed faster. The following section will theoretically discuss the two main loss mechanisms of sulfurous trace gases: Nucleation to form new aerosol particles and condensation onto pre-existing particles.

2.2.1 Nucleation

New particle formation has been observed to occur mainly through three mechanisms:

- Homogeneous nucleation
- Heterogenous nucleation
- Ion induced nucleation

Homogeneous nucleation describes nucleation of vapor on embryos of vapor molecules only, if no foreign substances are present. Heterogeneous nucleation in comparison describes the nucleation process on a foreign substance or surface. Homogeneous nucleation can be divided into homomolecular (involving one single species) and heteromolecular (involving more than one species) nucleation processes.

Nucleation in the lower troposphere occurs mainly in the form of heteromolecular homogeneous nucleation involving more than one molecular species with a low saturation vapor pressure. Bimolecular nucleation of H_2SO_4 and H_2O and ternary nucleation of H_2SO_4, H_2O and NH_3 are the most frequent mechanisms in the boundary layer.
Ion induced nucleation happens mainly in the upper troposphere and lower stratosphere where ion density appears to have a maximum due to galactic cosmic rays. Stable clusters are formed through the interaction with polar ligands. Through recombination of clusters with opposite charges they neutralize and form bigger stable clusters with radia above the critical radius [Arnold, 1982][Speidel, 2005].

Homogeneous homomolecular nucleation can be described as follows: A phase change occurs only spontaneously if the free enthalpy change is negative. Over a flat surface of water the free enthalpy change is given through

$$\triangle G = TR\ln(p/p_0) \tag{2.21}$$

where T denotes the temperature, R the gas constant and p the partial pressure of water and p_0 the saturation vapor pressure. Only for supersaturation, $p > p_0$, $\triangle$G is negative and a phase change occurs. However to form a spherical water droplet with radius r and thereby creating a new surface area, work against the surface tension σ has to be done. This adds a positive term to the enthalpy change:

$$\triangle G = -nkT\ln(p/p_0) + 4\pi r^2\sigma = -\frac{4}{3}\pi r^3\frac{N_A}{V}kT\ln(p/p_0) + 4\pi r^2\sigma \tag{2.22}$$

$$= -\lambda r^3 + \gamma r^2 = -\alpha n + \beta n^{2/3}, \tag{2.23}$$

where α, β, γ and λ are implicitly defined, N_A is the Avogadro constant, V is the molar volume of bulk liquid water, k the Boltzmann constant and n the number of molecules.

A critical radius r^* and nucleation barrier ΔG^* can be derived by setting

$$\left(\frac{\partial \Delta G}{\partial r}\right) = 0. \tag{2.24}$$

Due to this barrier, demonstrated in F 2.3, which requires a high supersaturation that is rarely observed in the atmosphere, the formation of stable clusters through homogeneous

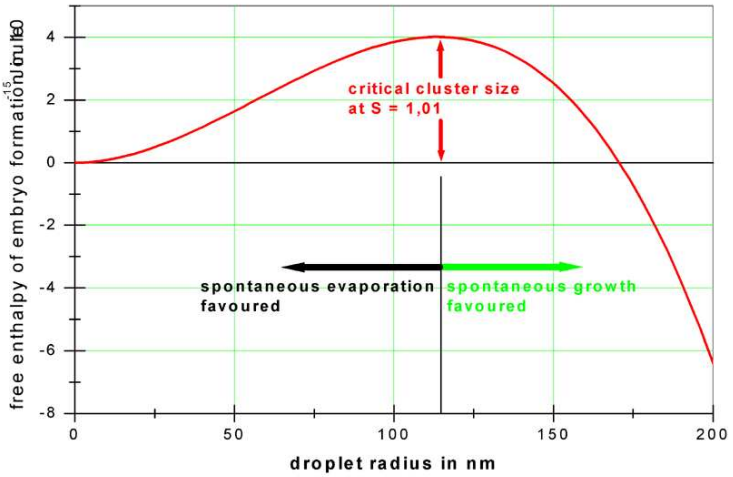

Figure 2.3: Δ G vs the particle radius, at T = 283 K and a supersaturation of S=p/p_0=1.01
.

homomolecular nucleation of water molecules in the atmosphere is very unlikely to happen. The nucleation rate depends on the probability that a newly formed cluster has reached a critical radius for stability and in addition that other molecules collide and stay attached to the new cluster. It was originally derived by Volmer and Weber [Volmer, 1939] and with the Zeldovich correction reads:

$$J = \frac{p^2}{k^2 T^2} \frac{1}{\rho_{\text{liquid}}} \left(\frac{2m\sigma}{\pi}\right)^{1/2} \exp\left(\frac{-\Delta G^*}{kT}\right) \tag{2.25}$$

with ρ_{liquid} being the density of the liquid of the droplet, p the pressure of the vapor and m the molecular mass [Roedel, 2000].
The nucleation barrier can be overcome by seeding a supersaturated volume of air with either a solid wettable particle, which can then be described by the Köhler-equation, or by adding a second hygroscopic, polar gaseous species such as H_2SO_4. If the mixture of the two gases is in the latter case supersaturated with respect to the solutions of these substances nucleation can occur. The number of molecules n of each species A and B therefore determines the free enthalpy change for the formation of a binary liquid cluster:

$$\Delta G = n_A \Delta\mu_A + n_B \Delta\mu_B + 4\pi r^2 \sigma \tag{2.26}$$

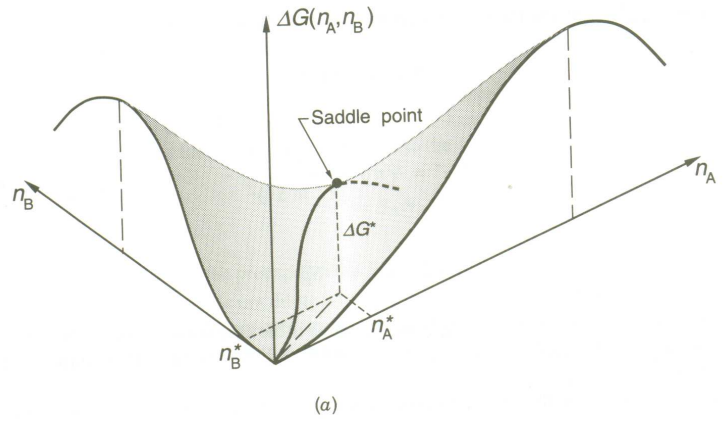

Figure 2.4: Free enthalpy of cluster formation for binary nucleation. The saddle point is given through the minimum of Δ G with respect to both molecule numbers n_A and n_B. Graphic taken from [Seinfeld and Pandis, 1998].

the chemical potentials $\Delta\mu_A$ and $\Delta\mu_B$ are given through:

$$\Delta\mu_i = -kT\ln\left(\frac{p_i}{p_{i0}}\right) \tag{2.27}$$

with the respective partial pressures p_i and saturation pressure of the solution p_{i0} of species i.

The saddle point ΔG^* is the energy barrier which has to be overcome by binary clusters in order to reach stability and can be derived solving the two equations

$$\left(\frac{\partial\Delta G}{\partial n_A}\right) = \left(\frac{\partial\Delta G}{\partial n_B}\right) = 0. \tag{2.28}$$

It depends crucially on the number of molecules of both species involved and the ratio of their partial pressure and their saturation vapor pressure over the solution and is shown in F 2.4

Ternary nucleation, such as the already mentioned most common combination involving H_2SO_4, water and NH_3 explained in [Korhonen et al., 1999], can be similarly implemented into the above equations but yields a much more complex system due to multiple dissociation and association steps in the liquid phase, forming salts and ions of these species. NH_3 has the ability to lower the vapor pressure of H_2SO_4 above the solution, which is expected to enhance particle formation in air masses containing H_2SO_4.

Thermodynamic binary nucleation involving sulfuric acid and water predicts a dependency of

the H_2SO_4 concentration with a power of 10 and more. Ternary nucleation predicts a weaker but still strong dependency with a power of 5 to 10. However atmospheric observations have shown that the boundary layer particle formation depends linearly or quadratically on H_2SO_4 concentrations. This was explained in [Kulmala et al., 2004] with an activation of molecular clusters with one H_2SO_4 molecule, where the nucleation rate depends linearly on the concentration of H_2SO_4. Thermodynamically stable clusters containing one H_2SO_4 molecule can form and grow through condensation and coagulation of organic vapors. The nucleation rate can be explained by the competition between condensational growth and cluster scavenging for particles between 1 and 3nm, which is the lower limit of current particle measurement techniques. The nucleation rate depends on further parameters such as temperature, relative humidity and the presence of organic compounds. This concept of cluster activation is still poorly understood since measurements of molecular clusters under atmospheric conditions are rare and the involvement of organic compounds in the growth rate of nm particles is still unclear. The kinetic approach predicts a quadratic dependency of H_2SO_4. Through collision of H_2SO_4 and water molecules stable clusters with two H_2SO_4 molecules are formed, which can grow through further condensation and coagulation. Although validation through measurements of the particle formation below 3 nm are currently not available, the activation and kinetic approach reflect nucleation processes more accurately than the thermodynamically binary approach.
To conclude, one can say that the formation of new particles involving sulfuric acid always depends on meteorological conditions such as temperature, relative humidity and UV radiation, as well as the presence of organic vapors and/or NH_3 and low concentration of pre-existing particles.

2.2.2 Condensation

One sink for atmospheric gaseous H_2SO_4 is nucleation, but as the necessary conditions for nucleation are rare in the atmosphere, aerosol scavenging is the main removal mechanism. These processes exhibit a mass transfer to a surface and a gas-to-aerosol transfer which is only for the most soluble sulfur species efficient. To describe the mass transfer to the aerosol surface the Knudsen number (Kn) is employed. Kn is defined as the ratio of the mean free path λ to the particle radius. The steady state flow J_c of vapor molecules to a sphere for Kn < 1 is given by

$$J_c = 4\pi R_p D_g (c_\infty - c_s), \tag{2.29}$$

where R_p denotes the radius of the particle, D_g the diffusion constant and c_∞ and c_s the concentration of the gas at a distance larger than the diameter of the particle and at the surface of the particle, respectively. For Kn > 1 the molar flow J_k is given by

$$J_k = 4\pi R_p^2 v\alpha(c_\infty - c_s) \tag{2.30}$$

where v denotes the average thermal velocity and α the mass accommodation coefficient. The mass accommodation coefficient α represents the probability that a gas phase molecule enters into the liquid on striking the liquid surface. A net flux can be expressed as

$$J = c_g v\gamma/4 \tag{2.31}$$

where c_g is the gas phase density, and γ is the uptake coefficient, which takes into account the diverse processes which limit the uptake of the gaseous species by the liquid. These processes are gas phase diffusion, liquid phase solubility and mass accommodation coefficient (α).
α has been measured for DMSO and MSA and range between 0.1 and 0.2. For H_2SO_4 α is assumed to be 0.6 [De Bruyn et al., 1994][Lucas and Prinn, 2002]. The total uptake coefficient is given by

$$\frac{1}{\gamma_{\text{meas}}} = \frac{1}{\alpha} + \frac{1}{\gamma_{\text{diffusion}}} + \frac{1}{\gamma_{\text{solubility}}} \tag{2.32}$$

For such highly soluble gases as MSA and DMSO (Henry's law constant $= 10^9$) the uptake by cloud droplets is diffusion limited $\gamma \sim R_p D_g^{-1} A^{-1}$ (R_p being the cloud aerosol radius, D_g being the gas-phase molecular diffusion coefficient and A being aerosol surface). Under noncloud conditions when aerosols diameter are smaller the uptake tends to be limited by the free molecular collision. α is temperature dependent and increases with decreasing temperature suggesting that in cloud free conditions and high temperature less uptake of MSA by particles occurs and the MSA lifetime is longer.

For imperfect mass accommodation $\alpha < 1$ and Kn ≈ 1, when the mean free path equals the particle radius, a correction of the kinetic regime flow to the continuum regime flow, given by the Fuchs-Sutugin equation, is employed [Fuchs and Sutugin, 1971]:

$$\frac{J}{J_c} = \beta_M(r) = \frac{0.75\alpha(1 + \text{Kn})}{\text{Kn}^2 + \text{Kn} + 0.283\text{Kn}\alpha + 0.75\alpha} \tag{2.33}$$

The net loss by condensation is given by the condensation sink.

Condensation Sink

The aerosol condensation sink (CS) describes how rapidly molecules will condense on aerosols [Kulmala et al., 2005] and is determined from size spectra measurements. The CS - value can be calculated from

$$\mathrm{CS} = 4\pi D \int_0^\infty r\beta_M(r)n(r)dr = 4\pi D \sum_i \beta_M r_i N_i \tag{2.34}$$

with D being the diffusion coefficient (in this case the diffusion coefficient of sulphuric acid), β_M the transitional correction factor, N_i and r_i are the number concentration and the radius of the particles in the ith size class measured with a DMPS system which will be introduced at dry relative humidity. Therefore it is referred to as dry condensation sink.

Higher values of CS indicate a higher degree of pollution and therefore a more effective removal of the two species. The CS can be interpreted as the inverse lifetime of gas phase species with a low vapor pressure. Low values of MSA that range below the detection limit could be associated with high CS values due to pollution. On the other hand higher values of MSA are associated with larger particles since MSA favors particle growth, especially on particles in the supermicron range [Huebert et al., 1993].

Multiphase reactions

Very little is known about the multiphase dynamics of MSA. These processes seem to be of major importance when explaining MSA concentrations in both the gaseous and the aqueous phase. Field studies of simultaneous measurements of gaseous and particulate MSA and models have shown, that gaseous MSA can only account for 10% or less of the particulate MSA, thus in-cloud oxidation contributes the biggest part to the total MSA concentration [von Glasow and Crutzen, 2004] [Huebert et al., 1993][Bardouki et al., 2003].

While DMS is not very soluble (Henry's Law constant: 0.48 M atm^{-1} at 298 K), its oxidation products DMSO, DMSO_2, MSIA and MSA (Henry's Law Constants with a lower limit of 10^6 M atm^{-1}) are very soluble. MSA is believed to have an even higher (about 3 orders of magnitude) solubility than the other products [Lee et al., 2003]. Multiphase reactions can compete with the analogous gasphase reactions when the species are highly soluble or the reaction rates are higher in the aqueous medium.

Barnes et al. (2006) estimates the oxidation of DMS by O_3 in the aqueous phase to have the same importance as the reaction in the gaseous phase. This in-cloud oxidation occurs

throughout the day while OH and NO_3 gas phase oxidation are restricted to daytime or pollution events, respectively.

The oxidation rates of DMSO and MSIA through OH radicals in the aqueous phase are of similar magnitude or even higher than the gas-phase reactions. The lifetime of DMSO in the aqueous phase is shorter compared to its lifetime with respect to OH oxidation in the gaseous phase. DMSO oxidation products are less volatile therefore DMSO can contribute to evaporation cycling.

Transition of the final products from the liquid to the gas-phase are scarcely reported, reflecting that still very little is known about these processes. [Mauldin III et al., 1999] reported a significant effect of particle neutralization by NH_3 upon MSA vapor pressure at low relative humidities. MSA vapor pressure was increased with the amount of particle neutralization (measured by NH_4^+ ions in the particulate aerosol phase) decreasing. Similar effects are known in the case of H_2SO_4 but the relative humidity ($< 10\%$) has to be very low in order to re-evaporate H_2SO_4 from the particles. MSA being more volatile than H_2SO_4 shows increased gas phase partitioning at RH $< 20\%$, which are practically not observed in the MBL but contributes significantly to gaseous MSA concentrations in dryer locations at bigger altitudes.

Chapter 3

Measurement Principle

Chemical Ionization Mass Spectrometry (CIMS) is a highly selective technique with fast time response for measuring atmospheric trace gases with concentration values down to $10^5 - 10^7$ cm^{-3}. The detection principle is based on a highly efficient bimolecular ion-molecule reaction where educt ions produced by an ion source react with the analyte molecules to form product ions of known masses and charge which can be detected by a quadrupole mass spectrometer. The principles of this method was first applied by [Arnold, 1978][Arnold and Fabian, 1980] [Arnold and Viggiano, 1980][Knop and Arnold, 1985] and further developed by [Eisele and Tanner, 1993][Reiner et al., 1998]. In this chapter a short introduction on the instrument used during MAP shall be given next to the principles of the measurement technique with ACIMS.

3.1 Chemical Ionization Mass Spectrometry (CIMS)

The detection of atmospheric trace gases is achieved via an ion-molecule reaction with artificially produced ions: In a flow reactor neutral molecules of the trace gas (A) specifically react with educt ions ($E^{\pm}$) of known mass and charge which were produced by a radioactive alpha source and a glow-discharge source, respectively. The educt ions are produced in the flow channel connected to the ion source. A source gas of high purity is injected, ionized and pumped into the flow reactor where the reaction to detectable product ions ($P^{\pm}$) takes place. A small part of the flow through the flow reactor is guided into the prechamber of the ion trap mass spectrometer (ITMS) via the front electrode and directed towards the first octapole lense. The instrument will be explained in more detail in the next section. The main gas stream leaves the system through an outflow tube, where additional data such as temperature, flow velocities and humidity are measured.

A reaction with negative ions inside the flow reactor occurs preferably when the neutral molecules have a greater gas-phase acidity. If the educt ions in turn also have a high gas-phase acidity they are stable with respect to proton transfer.

Permanent or induced dipole moments result in a high cross-sections of ion-molecule reaction leading to a very efficient conversion, achieving a reaction rate that is close to the collision rate. The efficiency of the conversion of educt to product ions can be improved through a longer ion-molecule residence time (t_{IMR}).

The trace gas concentration can be derived from the ratio of product to educt ion via the following consideration: Assuming only one type of product ions is produced, the ion molecule reaction is generally described by:

$$\mathrm{E}^{\pm} + \mathrm{A} \longrightarrow \mathrm{P}^{\pm} + \mathrm{B} \tag{3.1}$$

where A are the neutral gas molecules to be measured, E are the educt ions, P are the product ions and B a neutral reaction product.

The reaction rate is proportional to the concentration of the neutral reactant A and of the educt ions, $[E^{\pm}]$:

$$R(t) = -\frac{d}{dt}[\mathrm{E}^{\pm}] = \frac{d}{dt}[\mathrm{P}^{\pm}] = -k[\mathrm{E}^{\pm}][\mathrm{A}] \tag{3.2}$$

in which k is the temperature and pressure dependent rate coefficient.

If A exceeds the amount of educt ions, meaning $[A] >> [E^{\pm}]$, A can be presumed to be constant in time [A](t) =[A]. Thus integration of equation (3.2) yields the time evolution of the educt ions:

$$[\mathrm{E}^{\pm}] = [\mathrm{E}^{\pm}]_0 \cdot e^{-k[\mathrm{A}]\mathrm{t}} \tag{3.3}$$

with [E](0) =$[\mathrm{E}]_0$.

Assuming that all masses and charges are conserved ($[\mathrm{E}^{\pm}]_0$=$[\mathrm{E}^{\pm}]$+ $[\mathrm{P}^{\pm}]$),$[\mathrm{P}^{\pm}]$ is:

$$[\mathrm{P}^{\pm}] = [\mathrm{E}^{\pm}]_0 \cdot (1 - e^{-k[\mathrm{A}]t}) \tag{3.4}$$

Equation (3.4) divided by equation (3.3) leads to an expression for the concentration of the neutral analyte A, the so-called **ACIMS-Formula**:

$$[\mathrm{A}] = \frac{1}{k \cdot t_{IMR}} \ln\left(1 + \frac{[\mathrm{P}^{\pm}]}{[\mathrm{E}^{\pm}]}\right) \tag{3.5}$$

in which t_{IMR} is the reaction time.

At a given ion-molecule-residence-time and rate constant, the absolute concentration of the gaseous species, which undergoes the above ion-molecule reaction, is given through the ratio of product to educt ions $R = [P^{\pm}]/[E^{\pm}]$. High sensitivity for the detection of trace gases through the CIMS-method can thus be achieved for small values of R. The sensitivity of the detection method which uses only the ratio of the two components measured by the same instrument is therefore independent of the sensitivity of the instrument. Losses to the walls do not effect the derived concentration if ions are affected equally. However discrimination of the product or the educt mass, which can happen through tuning in a certain mass range that comprises only one of the two masses, needs to be corrected. This will be discussed in chapter 6.

The assumption that educt ions usually react with only one type of molecules is usually not given, therefore equation 3.1 has to be reformulated:

$$E^{\pm} + A_i \longrightarrow P_i^{\pm} + B_i \tag{3.6}$$

The above derived ACIMS-Formula thus leads to the Parallel-ACIMS-Formula that takes simultaneous reactions with other trace gases into account:

Parallel-ACIMS-Formula

$$[A_i] = \frac{1}{k \cdot t_{IMR}} \cdot \frac{[P_i^{\pm}]}{\sum_{j=1}^{n}[P_j^{\pm}]} \cdot \ln\left(1 + \frac{\sum_{j=1}^{n}[P_j^{\pm}]}{[E^{\pm}]}\right) \tag{3.7}$$

A detailed derivation is given in [Wollny, 1998].

The detection of H_2SO_4, MSA and SO_2 with the CIMS-method will be introduced and discussed in chapter 5.

3.2 Ion Trap Mass Spectrometer (ITMS)

Ion traps or "Paul Traps" named after their creator are generally used for storage and analysis of charged particles and their physical properties. They work with alternating electric fields, thereby trapping kations and anions equally well.

Ion traps have great advantages in

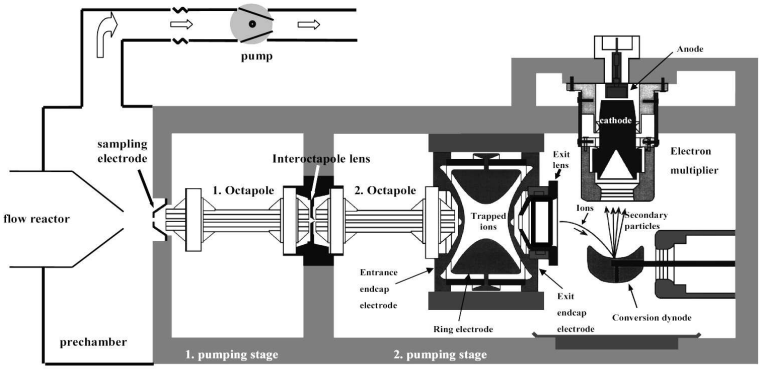

Figure 3.1: Scheme of the IT-CIMS apparatus (PITMAS). It comprises the ion optics and the detection unit. The interior is divided into two pumping stages. Figure taken from [Hanke et al., 2002].

- analysis of various processes with different reaction times
- mass analysis, when being operated in the fragmentation mode
- multi-interactions of molecules and ions of positive and negative charge
- their broad dynamic range, with high sensitivity even for low ion concentrations

The ion trap mass spectrometer (ITMS) used during MAP was a commercially purchased instrument (Finnigan LCQ, Finnigan Company, USA), configured for the detection of trace gases with the chemical ionization mass spectrometry method. The inlet system was exchange by a stainless steel adapter to fit a 40mm tubing. The mounted inlet system, originally used for detection of high molecular weight biopolymers, was replaced by a sampling electrode with a diameter of 0.015 cm used as a critical orifice for atmospheric measurements.

The ITMS is built of two chambers: The pre-chamber, where the first pumping stage is maintained, consists of the front electrode, which acts pre-selective on the type of ions (basically their charge) that will be analyzed and is supported by the tension of the first octupole-lens. The octupole centers and "guides" the ions through the inter-octupole-lens towards the second pumping stage: The main-chamber.

The main chamber of the ion trap mass spectrometer consists of a second octupole lens, the ion trap and the detection unit: the conversion dynode and the electron multiplier. The

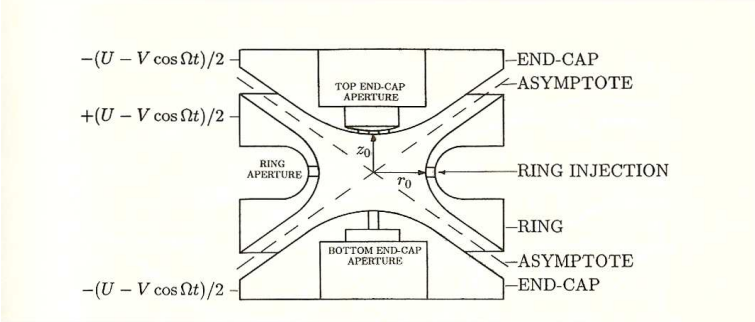

Figure 3.2: Schematic of a Paul Ion Trap. It consists of a hyperboloid ring electrode and two hyperboloid end-cap electrodes, [Gosh, 1995].

quadrupole ion-trap is built of two hyperboloid end-cab electrodes and on ring electrode in the center. The ions are confined by application of an appropriate radio frequency at the ring electrode. The end cabs are grounded. The potential that confines the ions has the shape of a rotating saddle.

The motion of ions in a quadrupole field can be described mathematically by the solutions to the second-order linear differential equation described originally by Mathieu (eq. 3.8). One can apply the solutions of stability and instability to describe the trajectories of ions confined in quadrupole devices.

Mathieu-equation:

$$\frac{d^2u}{d\xi^2} + (a_u - 2q_u\cos 2\xi)u = 0 \tag{3.8}$$

with u being the coordinate axes x, y or z, ξ is a dimensionless parameter equal to $\omega t/2$, a_u and q_u are additional dimensionless parameters known as trapping parameters. As will be explained later, ω is the radial frequency of the RF potential applied to the ring electrodes.

Rewriting equation 3.8

$$\frac{d^2u}{dt^2} = \frac{\omega^2}{4}\frac{d^2u}{d\xi^2} \tag{3.9}$$

leads to

$$m\frac{d^2u}{dt^2} = \frac{-m\omega^2}{4}(a_u - 2q_u\cos\omega t)u \tag{3.10}$$

The equations of motions in the potential given above are determined by the force acting on a charge particle with mass m and charge Q:

$$\vec{F_u} = m\vec{a} = m\frac{d^2\vec{u}}{dt^2} = -Q\nabla\phi \tag{3.11}$$

The applied electric potential is

$$\phi = \frac{\phi_0}{2}\left[\frac{\lambda x^2 + \sigma y^2 - \gamma z^2}{r_0^2}\right] \tag{3.12}$$

λ, σ and γ are weighting constants for the x,y and z coordinates.

In any electric field the Laplace condition needs to be fulfilled:

$$\Delta\phi = 0 \tag{3.13}$$

This is the case when

$$\lambda + \sigma + \gamma = 0 \tag{3.14}$$

For our ion trap $\lambda = \sigma = 1$ and $\gamma = -2$

Replacing these values in (3.12) we get (in cylindrical coordinates)

$$\phi = \frac{\phi_0}{2}\left(\frac{r^2 - 2z^2}{r_0^2}\right) \tag{3.15}$$

For an ideal quadrupole field we get $r_0^2 = 2z_0^2$, where z_0 is the shortest distance between the end cabs.

The field needs to have a time dependent periodic component to keep the particle in the center of the potential: The applied electric potential to the ring electrode ϕ_0 is a combination of a RF potential $V\cos(\Omega t)$ and a DC potential U of the form

$$\Phi_0 = U + V\cos(\Omega t) \tag{3.16}$$

After differentiating (3.15) with respect to z and replacing $\frac{\partial\phi}{\partial z}$, one obtains

$$m\frac{d^2z}{d^2t} = \frac{2z}{r_0^2}(U + V\cos(\Omega t))z \tag{3.17}$$

which can be compared to the equation (3.8) leading to the following trapping parameters in z-direction (similar considerations can be applied for the x and y component):

$$a_z = \frac{8eU}{mr_0^2\Omega^2}; \qquad q_z = \frac{-4eV}{mr_0^2\Omega^2} \tag{3.18}$$

The parameters contain the mass/charge ratio for a given ion, specific parameters of the trap, r_0, the amplitude and frequency of the RF potential, V and ω. Applying appropriate voltages U and V and the RF frequency one obtains stability constraints for an ion of known

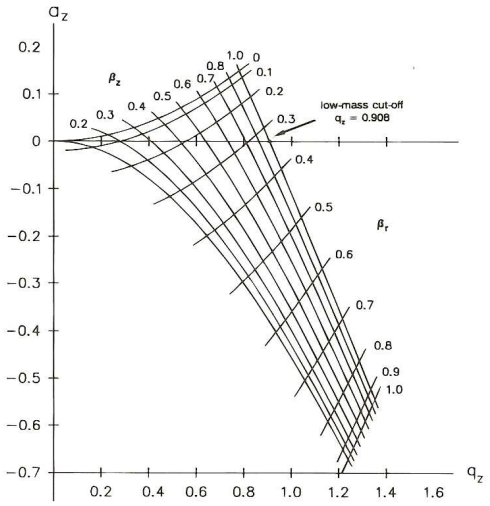

Figure 3.3: Stability diagram for the ITMS. Ions with a m/z ratio greater than the low-mass cut-off follow stable trajectories. Diagram taken from [March and Todd, 1995].

mass and charge as shown in the stability diagram 3.3.

After trapping, the ion read out process comprises the following steps: the ions are according to their mass destabilized on their trajectories in axial z-direction and then gradually ejected from the trap onto the conversion dynode. The secondary electrons emitted are counted via an electron multiplier.

To increase the sensitivity of the instrument used by our group to a certain mass-to-charge ratio, the voltages of the front electode, the octupole and inter-octupole lense, as well as the octupole radio frequency can be tuned. Semi-manual tuning allows to set an initial voltage range which then will be scanned through to find the optimal setting for detection of the desired ion mass. These voltages are recorded in a tune-file. The tuning-process can only be successful if count rates for the analyzed mass are stable and significantly higher than the background. Tuning, however, can lead to a discrimination of other masses that differ greatly from the tuned mass, particularly low masses. Comparison of the count rates with different tune files may help to analyze the amount of discrimination.

To regulate the number of ions inside the trap a device called "Automatic Gain Control" is employed. This is done by operating a pre-scan: The trap opens for a short time to generate a mass scan that reflects the actual ion concentration. Ion concentration can vary throughout the operation, depending for example on the water vapor content of the analyte

gas. It should be avoided to have too many ions inside the trap which leads to shielding effects between the charge molecules so that trapping becomes more difficult.
Ions are injected in a pulsed manner. A triggered closing mechanism that regulates the time of injection of the ions into the the main chamber is achieved by impressing a voltage onto the inter-octupole-lense. AGC and injection time should be set complementary, meaning that the time of one scan should be representative for a maximal amount of ions, so that the ion concentration is kept constant throughout the measurement.

For cooling or decelerating the ions, Helium is injected into the trap as damping gas. A secondary but very important aspect of the Helium gas is the removal of water ligands that attach to the ions. A detailed analysis has been carried out by [Aufmhoff, 2004].
The composition of heavy ions can be analyzed by applying the fragmentation mode, MS^n. Ions are excited through an oscillating voltage at the end cab electrodes, with frequencies corresponding to their internal vibration mode. They can then be dismantled by collisions with He-atoms. This mechanism is useful for the investigation of chemical species with high molecular masses that could not be assigned to a certain composition.

Chapter 4

Marine Aerosol Production (MAP)

The European project on Marine Aerosol Production (MAP) focuses on the primary and secondary aerosol production mechanisms and aerosol composition from natural sources in the Marine Boundary Layer. The project's aim is to quantify the seasonal and spatial variations of the newly identified precursor of aerosols with a special focus on iodine oxides for the secondary aerosols and the primary production of marine organic matter aerosols. The source of these primary and secondary aerosols have been observed to be plankton located in the Northeast Atlantic Ocean at the west coast of Ireland. Seasonal variations due to enhanced biological activity in summer are expected. The expansion of the area of high plankton concentration is visible in F 4.1. Due to high reflectivity of plankton they are visible as milky-shaded belt along the coast.

Sulfurous vapors have been observed to be the most important initiator for new particle formation in the Planetary Boundary Layer [Reiner and Arnold, 1993][Reiner and Arnold, 1994] [Boy et al., 2004][Kulmala, 2003][Kulmala et al., 2005]. However in coastal measurements ([Berresheim et al., 2002]) sulfuric acid concentrations were not able to explain nucleation events since their appearance was correlated with the tidal cycles but not with the H_2SO_4 diurnal cycles. Biogenic iodine emissions were attributed to be the main trigger for new particle formation in coastal regions [O'Dowd et al., 2002]. A thorough quantification of all condensable vapors contributing to particle formation over the ocean and in coastal regions was a major aim of the MAP campaign.

Another focus is on the investigation of primary aerosol containing organic matter produced by plankton and transferred to the atmosphere via the bubble bursting process at the ocean surface. Primary aerosol fluxes were measured by various systems to determine size distributions of bubble-mediated aerosols. Combined with laboratory experiments these results will

Figure 4.1: Satellite photo taken on the 6th of June 2006. The milky-shaded belt along the coast indicates the area of high plankton density.

be implemented into large scale model describing the impact of marine aerosol on marine boundary layer chemistry, direct and indirect radiative forcing and impacts on the climate. Measurements were performed during two field campaigns, one in June/July 2006 and January 2006, at the research station in Mace Head, Ireland and one ship-borne Intensive Observation Period (IOP) over the North Atlantic during the period of peak plankton activity in June 2006. The MPI-K participated in the latter one.

The cruise started in Cobh, South Ireland, at the 11th of June with one port call in Killybegs, Northwest Ireland, and landed in Galway on the 5th of July 2006. The course of the ship is shown in F 4.2, the color code represents the time. The ship "Celtic Explorer" (CE) is the national platform for offshore marine research and was provided by the Marine Institute, Ireland. It has a length of 65.5 m, its draught was 5.7 m and a beam of 15 m. The MAP cruise was the first time that the CE was used for atmospheric research. Next to a wet-lab inside the vessel where bubble-bursting experiments were performed and water samples were taken to be analyzed by Gas Chromatography/Mass Spectrometer (GC/MS), three containers were mounted on the front deck for atmospheric measurements. Next to the IT-CIMS technique, measurement techniques comprised Differential Mobility Particle Sizer (DMPS),

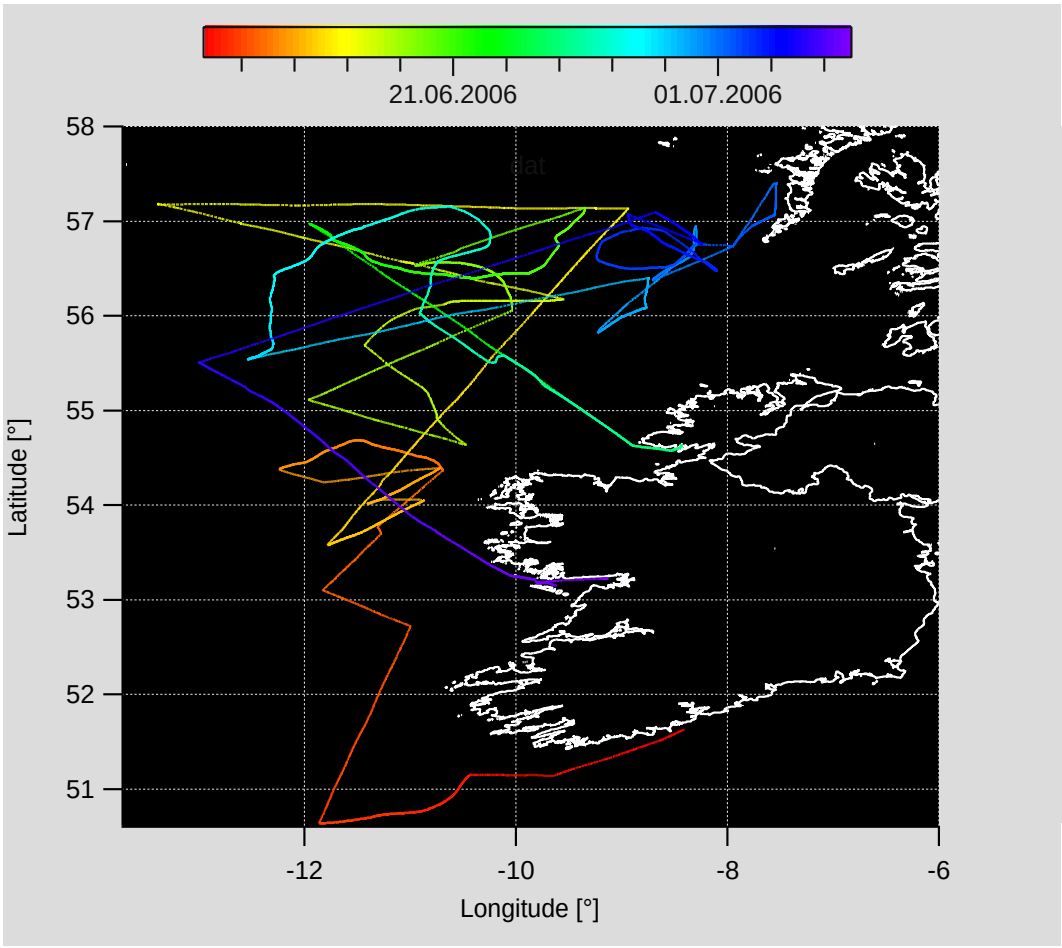

Figure 4.2: The course west of Ireland and Scotland going mainly from south to north with one port call on the 22nd of June at Killybegs, Ireland. The time is color-coded.

Condensation Particle Counter (CPC) , Hygroscopic Tandem Differential Mobility Analyzer (HTDMA), Aerosol Mass Spectrometer (AMS), impactor and filter samples. The flux of primary aerosol was observed by CPC counters with additional meteorological measurements of wind speed and surface stress and a white cap camera, which observed white cap coverage from wave braking and was installed on a "flux tower" on the front deck.

For further information regarding the MAP project see
`http://macehaed.nuigalway.ie/map/index.html`

Chapter 5

Experimental Setup and Calibration

The experimental setup used during the MAP campaign will be explained in detail in this section. Specific arrangements had to be made to adapt the CIMS measurement setup for the field campaign on the research vessel "Celtic Explorer" (CE) to endure the weather conditions as those predominant on the Atlantic Ocean. The construction and mounting of a converted 20 feet sea-container and the integration of the IT-CIMS will be presented. Calibration was done after the campaign in the laboratory and will be discussed in this section.

5.1 Experimental Setup

Measurements of atmospheric trace gases in the North Atlantic Marine Boundary Layer demand special sensitivity and robustness of the instruments. To fulfill the requirements of a successful installation of an ion trap mass spectrometer on a research vessel certain pre-arrangements had to be made. A transformed sea-container of 6 m length, 2.4 m width and 2.3 m height was equipped with two IT-CIMS (MPI-K) devices and an Enhanced Trace Level SO_2 Analyzer Thermo based on detection by pulsed fluorescence supplied by DLR (Deutsches Luft und Raumfahrtzentrum, German Aerospace Center). Supporting components for the maintenance of the IT-CIMS-measurements such as a pure air generator, several pumps, a filter system for the exhaust airstream, heating devices and a permeation oven were also integrated. The container had two circular openings on the roof for the inlet system with a hatch from where both inlets could be reached. The hatch was kept closed during atmospheric measurements to avoid influences by air from inside the container. Stainless steel pipes with a diameter of 20 cm (H_2SO_4 inlet-system) and 35 cm (SO_2 inlet-system) were set up around the

flow reactor for protection from rain and sea-salt-spray. The container was mounted on the starboard side on the front deck of the research vessel Celtic Explorer (picture is shown in the appendix). The position was ideal for minimizing the disturbance of ship emissions since the chimney for the engine exhaust was located at the after deck of the ship. Clean air conditions were maintained by heading against the wind. However a smaller exhaust (presumably the air conditioning of the kitchen) was located next to the container on the front deck. Both exhausts did affect atmospheric measurements whenever the ship was at rest and the wind conditions changed. The container was equipped with an air conditioning system to avoid overheating of the instruments. The MPI container was positioned next to one container from the Universities of Helsinki and Manchester, both mounted with instruments for aerosol characterization.

5.1.1 Inlet System

Special requirements for the inlet system had to be considered: In order to avoid losses of sulfuric acid to the walls of the container the entrance of the gas flow had to be at a decent distant to the container roof. However wall effects also take place inside the flow reactor therefore a compromise between those two effects had to be made. The distance entrance sampling tube - container roof comprised in total a length of 52 cm. The ITMS was mounted underneath the roof to keep the inlet system as short as possible. The sampling tube consisted of a 40 mm stainless steel tube with 127 cm length (inlet to front electrode) and an icon cone with an aperture of 4 mm. The icon cone was removable to be replaced by a filter system for background measurements which will be discussed later. The tube was heated at approx. 37°C by heating belts and additionally protected from seaspray or other pollution by a surrounding steel tube of 20 cm in diameter. A strong ventilation system (10^4 slm) ensured that the air that was drawn in came from above the ship. The massive air flow assured that a representative air pilar that was not in contact with the walls was cut out by the sampling tube. Analyzed air masses came from an estimated hight of about 10-15 m above the ocean surface. The sample stream pumped through the sampling line and the critical orifice of 0.15 cm aperture was 19.7 slm at 1013 hPa and 294 K.

The exhaust of the pump was connected to an air cleaning system provided by a cylindric stainless steel cartridge filled with active cole. Removal of toxic gases such as NO_2 and SO_2 used during the operation was assured. In the case of saturation or malfunctioning of the system two alert devices where linked to the cartridges. The filter gas was then pumped

Figure 5.1: The inlet system on top of the sea-container. The smaller one in the back is the inlet for H_2SO_4 measurements while the bigger on in the front is the one for SO_2 measurements. On the top right side the setup for background measurement with the filter paper is shown. On the bottom right side the inlet icon cone in the center of the protection pipes is shown.

through a 30 m exhaust tube to the after deck of the ship.

5.1.2 Ion Source and Ion Reaction

At the lower part of the flow reactor at a distance of 33 cm to the front electrode the ion source is located. A ^{210}Polonium α -source (185 MBq in June 2006, half-life 138 days), was used to produce the respective educt ions. The source was built and characterized by Hanke [Hanke, 1999]. Advantages of the α-source as compared to the glow-discharge source are a more efficient production of educt ions as well as a smaller amount of artificial HSO_4^- which is formed via the following reaction

$$HO_2^-CO_2 + SO_2 \longrightarrow HO_2SO_2^- + CO_2 \tag{5.1}$$

and reacts with HNO_3 to form the product mass at m/z = 160.

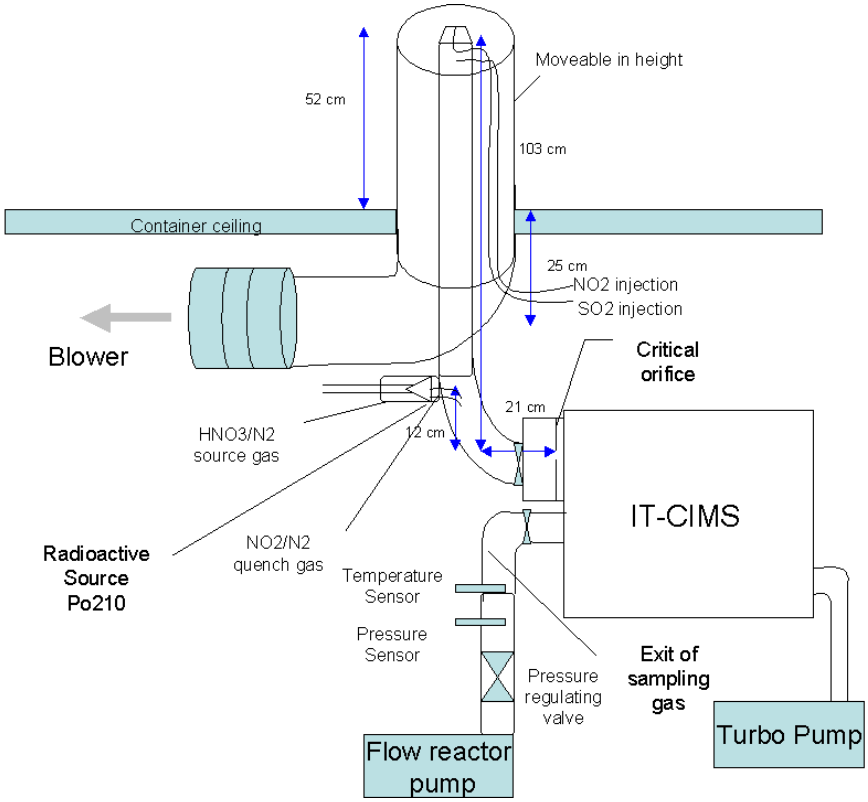

Figure 5.2: Experimental setup used during MAP for H_2SO_4 and MSA measurements. The air is drawn into a flow reactor and the H_2SO_4 and MSA molecules are ionized after approx. 91 cm by a radioactive ion source and then guided into the ITMS.

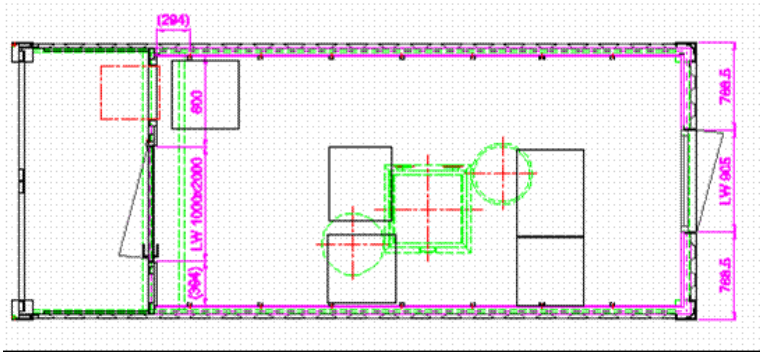

Figure 5.3: Schematic alignment of the instruments inside the container: to the left of the hatch (green square) is the IT-CIMS for SO_2 measurements, to the right the instrument to measure H_2SO_4. The green circles represent the openings for the two sampling lines. Two racks for supporting equipment are set next to the walls (black lined squares). The container has one window to the right and the exit to the left. The air conditioning system and the filter cartridges are placed in the front compartment.

The ion-source is integrated into a cylindrical stainless steel tube attached to a centered aluminium rod. The position of the ^{210}Po source with respect to the center of the flow can be varied to obtain the optimal ionization rate. This is achieved when a sufficient concentration of ions is produced but not enough to favor fast recombination of ions. The respective distance was experimentally derived to be $\sim$ 1 cm.
Into the cylinder a gas mixture composed of HNO_3 (produced through a permeation tube with a permeation rate of $\sim$ 1000 ng/min) diluted in a permeation oven by 3 slm N_2 of purity 5.0 at 50°C was injected. Due to the high electron affinity of NO_3 mainly $NO_3^-(HNO_3)_n$, n=1 with mass = 125 amu, is produced which is of an order of magnitude (or more) higher than the other ions detected.
To reduce further formation of HSO_4^- molecules through reaction 5.1 by the α-source NO_2 (2500 ppm in N_2) as quenching gas was injected below the source container. The effect of artificial production of HSO_4^- by the ion source can easily be observed if no NO_2 is injected and SO_2 is injected for titration. The NO_2 flow was determined to be at 1.65 slm, which was the appropriate amount of quench gas to supply the adequate effect and the least dilution of the analyte. An additional 0.5 slm was added at the upper part of the inlet system in 7 cm distance to the orifice. It was originally used for peroxide quenching inside the flow reactor which might lead to artificial enhancement in H_2SO_4.

5.1.3 Ion-Molecule Reactions of H_2SO_4 and MSA

H_2SO_4 undergoes the following reaction inside the flow reactor:

$$\begin{aligned} NO_3^-(HNO_3)_n(H_2O)_h + H_2SO_4 \quad &\longrightarrow \quad HSO_4^-(HNO_3)_l H_2O_m \\ &+(n-l+1)HNO_3 + (h-m)H_2O, \end{aligned} \tag{5.2}$$

and MSA undergoes:

$$\begin{aligned} (NO_3)^-(HNO_3)_n(H_2O)_h + CH_4SO_3 \quad &\longrightarrow \quad CH_3SO_3^-(HNO_3)_l(H_2O)_m \\ &+(n-l+1)HNO_3 + (h-m)(H_2O). \end{aligned} \tag{5.3}$$

where count rates for clusters with n=1 exceed the count rates for other clusters (n=0,2) by an order of magnitude. The rate coefficient for the first reaction was measured by [Viggiano et al., 1997]:

$$k_{NO_3^-(H_2SO_4)} = 1.86 \cdot 10^{-9} cm^3/s. \tag{5.4}$$

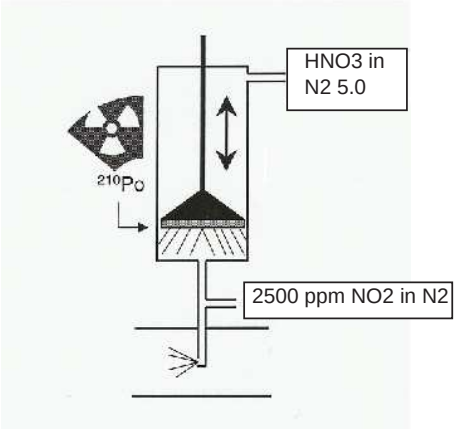

Figure 5.4: Schematic of the ^{210}Po ion source, 3 slm HNO_3 in N_2 are injected as source gas and 1.65 slm NO_2 in N_2 were added as quench gas.

The error is approximately 10-15%.

The product ion can then be detected by the mass spectrometer at mass m/z = 160 amu for H_2SO_4 and mass m/z = 158 amu for MSA . Assuming a flow of 19.7 slm, a distance of 33 cm between ion source and front electrode, the residence time of the ions inside the flow reactor is between 0.7 and 1.3 s assuming a partly laminar flow. During this time the reaction of H_2SO_4 and MSA to the known product-ions takes place.

5.1.4 Detection of Sulfur Dioxide

SO_2 was measured with the second CIMS-instrument installed in the container. The principle of the measurement technique with the CIMS method was developed by our MPI-K group and will be briefly introduced in this section.

The detection of SO_2 is achieved via the formation of SO_5^- in the following ion-molecule-reaction [Möhler et al., 1992]:

$$(CO_3)^-(H_2O)_m + SO_2 \longrightarrow SO_3^-(H_2O)_n + (m-n)H_2O + CO_2 \quad (5.5)$$

$$SO_3^-(H_2O)_n + O_2 \longrightarrow SO_5^-(H_2O)_m + (n-m)H_2O \quad (5.6)$$

To form the product ions, a glow discharge source at a pressure of 60 hPa is flushed by a continuous flow of $\sim$ 0.3 slm of oxygen [Reiner and Arnold, 1994]. This leads to the production of O_2^- primary ions through electron association. As soon as they leave the

discharge region, the oxygen ions react with CO_2. Electron affinity is not the highest for this gas (compared to NO_2 for example) but the reaction is faster due to a surplus of CO_2. The educt ions are formed via the following reaction:

$$CO_2 + O_2^- \longrightarrow CO_2^- + O_2 \tag{5.7}$$

$$CO_2^- + O_2 \longrightarrow CO_3^- + O \tag{5.8}$$

The rate coefficient for the reaction 5.5 depends on the hydration of the educt ions, which can be determined via the water vapor content measured in the reactor flow. An effective rate coefficient can be expressed through the sum of the weighted rate coefficients k_n at different water vapor concentrations:

$$k_{eff} = \sum_{n=0}^{3} k_n \frac{[CO_3^-(H_2O)_n]}{[CO_3^-]_{tot}} \tag{5.9}$$

The relative amount of $CO_3^-(H_2O)_n$ can also be determined using thermodynamical data. For a closer analysis see [Aufmhoff, 2004],[Speidel, 2005],[Nau, 2004]. The SO_2 concentration in the analyte gas can be determined via the ACIMS formula with the product to educt ratio of mass 112 (SO_5^-) and mass 60 (CO_3^-). During the MAP campaign an online calibration was used.

Online Calibration

Online calibration was first installed and used by [Nau, 2004], [Speidel, 2005] of the MPI-K group and is achieved through the injection of a defined flow of isotopically labeled $^{34}S^{16}O_2$ with a mixing ratio of 757 pptv ± 5% (inside the sampling line). The inlet is placed at the entrance of the sampling line therefore wall losses, mixing and instrument sensitivity are the same for the atmospheric SO_2 as for the calibration gas. From the corresponding count rates mass 112 and mass 114 the ambient SO_2 concentration can be calculated taking into account the isotopic purity of the standard as well as the natural isotopic ratio of the ambient air. The concentration is given by [Bandy et al., 1993]:

$$C_a = C_s \frac{K_{ss}R - K_{as}}{K_{aa} - K_{as}R} \tag{5.10}$$

where C_a denotes the ambient concentration, C_s is the concentration of the calibration gas after the injection into the flow reactor and R is the ratio of mass 112 to mass 114. K_{ij} refers to the percentage contributions of the i^{th} species in the j^{th} species with values of K_{aa}=0.939, K_{ss}=0.871, K_{as}=0.075 and K_{sa}=0.051. For a more detailed description of the method see [Nau, 2004][Speidel, 2005][Speidel et al., 2007].

5.1.5 Instrumental Settings

All mass spectrometer parameters during operation were recorded with the software TUNE PLUS from Finnigan, Fa. Thermo Finnigan. A so-called HEADER, which shows all relevant values, is stored for each spectrum. The mass spectra are recorded with the Finnigan software X-Calibure.

The prechamber pressure in front of the front electrode of the mass spectrometer was maintained constant at 110 hPa by the use of a butterfly valve. At this pressure an average educt ion rate of $1 \cdot 10^4$ inside the trap was detectable. Pressure inside the spectrometer was kept constant at $2 \cdot 10^{-5}$ torr with the combination of a flow reactor pump and the turbo molecular pump. This is about twice the pressure of an unstressed spectrometer maintained by the turbo molecular pump alone. Temperature was measured in the outflow of the spectrometer and had an average value of 36°C.
Spectra were averaged over 30 microscans. One microscan was performed during an accumulation time of $\sim$ 8000 ms. The AGC was set a $1.8 \cdot 10^9$. Consequently the time resolution was approximately 4 min. These settings were determined empirically and resemble an optimized mode between the two effects: High accumulation time results in a greater sensitivity for measuring sub-ppt trace gases. However ion-ion reactions, such as shielding effects, take place if too many ions are stored inside the trap which in turn results in a reduced sensitivity. Time resolution and noise reduction (through averaging of 30 microscans) have to be weighted against each other. A high time resolution is favorable if air masses are passed at a high speed as it is the case with airborne measurements. However on a ship with a vessel speed of maximum 6 m/s, air masses change only at a sudden change of wind direction which was also recorded. Therefore a max. time resolution of 240 s is acceptable.

setting	typical value
total flow	19.7 slm
NO_2 source quenching gas	1.65 slm
NO_2 inlet quenching	0.5 slm
N_2/HNO_3 source gas	3 slm
N_2+$S^{34}O_2$ inlet dilution	0.55 slm
pressure ion trap	$2.0 \cdot 10^{-5}$ torr
pressure prechamber	110 hPa
temperature exhaust	309 K
ion molecule reaction time	$\sim$ 1 s
pressure at ionization region	$\sim$ 1013 hPa
AGC	$1.8 \cdot 10^9$
microscans	30
max. injection time	8000 ms
mass range	50-300 amu
Multipole 1 Offset	$\sim$ 5.63 V
Lens Voltage	$\sim$ 39.88 V
Multipole 2 Offset	$\sim$ 11.78 V
Multipole RF Amplitude	$\sim$ 730.00 Vp-p
Coarse Trap DC Offset	$\sim$ 10.54
multiplier actual	$\sim$ -1176.63 V

5.1.6 Additional Data

The additional data was stored with the help of 2 personal computers. Pressure, temperature and flow controllers were recorded into a LabVIEW file by LabVIEW and measured inside the flow reactor in the outflow of the spectrometer in order to reduce disturbance to the flow or additional losses on the instrumentation. Meteorological data such as outside temperature, pressure, wind speed, relative humidity and dew point was recorded by a commercial weather station (WM 918 by Huger Electronics) mounted on top of the container.

Additional data such as water salinity, water temperature, GPS-data, speed and course of the ship as well as wind directions were recorded by standard instruments of the Celtic Explorer.

5.2 Sulfuric Acid Calibration

Calibration was done by a specifically built calibration source for atmospheric measurements of HO_2, OH and H_2SO_4 and is based on the principle of a defined photolysis of H_2O molecules, generating OH radicals which then react with SO_2 to H_2SO_4 and can be detected by the spectrometer. A detailed description and characterization of the calibration source can be found in [Reimann, 2000]. All formulas are taken from [Reimann, 2000]. The principle has been tested and applied at several field campaigns of our group [Uecker, 2002][Aufmhoff, 2004] [Fiedler, 2004]. A brief introduction of the principle will be given and additional modifications will be discussed.

5.2.1 Production of OH-radicals

OH radicals are produced via the photolytic dissociation of water molecules at atmospheric pressure and ambient temperature. By measuring the photocurrent produced by a UV-light source and the water content the production rate can be determined. Losses and inhomogeneities of the photolytic area have to be considered.
Purified air with a known water content is passed through a suprasil tube and photolyzed by the filtered and enhanced emission-frequency of 184,9 nm of a Mercury-Vapor-Lamp, which is the needed dissociation frequency for the following reaction:

$$H_2O + h\nu \longrightarrow H + OH \qquad \lambda < 185\text{nm} \tag{5.11}$$

The photocurrent is measured with a photodiode (GaAsP Schottky-diode) opposite to the UV lamp and the filters. A radiation profile inside the suprasil tube was taken and demonstrates that at the center in the direction of the flow the intensity is maximal. However towards the walls of the tube an attenuation is noticeable [Reimann, 2000]. This has to be considered when the flow is entered into the flow reactor. Furthermore a 1.5 m suprasil tube was used to assure a laminar flow profile within the tube. This profile suggests different velocities and irradiation times depending on the distance with respect to the center of the tube. To keep the error of calculated to produced OH concentration low extraction of the flow should be done at the center of the suprasil tube. According to [Reimann, 2000] if 60 % of the total flow produced inside the tube are extracted, the relative error is below 10 %. Due to a high flow rate through the critical orifice at atmospheric pressure and the dilution of 5.7 slm a slightly higher flow of 13 slm (between 65 and 74%) was taken for calibration.

The production rate (P_{OH}) of OH radicals depends on

- Φ_{OH} the quantum yield, which equals 1 in this case
- Ψ the photon flux,
- $[H_2O]$ the water vapor concentration, and
- σ_{H_20} the photo dissociation cross section of water at 185 nm:

$$\frac{d[OH]}{dt} = P_{OH} = [H_2O]\Phi_{OH}\Psi\sigma_{H_20} \tag{5.12}$$

With the assumption that for each water molecule one OH radical is produced

$$d[OH] = -d[H_2O] \Leftrightarrow [H_2O] = [H_2O]_0 - [OH] \tag{5.13}$$

which can be substituted into 5.12 and integrated over the irradiation time τ, one can determine the [OH] concentration

$$[OH] = 2[H_2O]_0 \cdot (1 - e^{\Phi_{OH} \int_0^\tau \Psi\sigma_{H_20}}) \tag{5.14}$$

with the approximation for small arguments $e^x \approx 1 + x$

$$[OH] = [H_2O]_0 \, \sigma_{H_2O} \, \Phi_{OH} \, \Psi \, \tau \tag{5.15}$$

The calibration source is able to produce OH concentrations between 10^6 cm^{-3} and 10^9 cm^{-3} which covers the range of atmospheric measurements up to very polluted air masses.

The principal setup of the calibration source is shown in F 5.5.

OH - Measurements

SO_2 was injected through a stainless steel tube of 3 mm against the flow direction at the inlet of the flow reactor. The reaction with SO_2 is very fast (OH-lifetime $\sim 10^{-2}s$) so all OH radicals are immediately converted to H_2SO_4. At a fixed OH production rate the concentration was varied until no changes in the mass spectra were seen. SO_2 mole fractions were around $15 \cdot 10^{-6}$.

The inlet of the flow reactor was originally designed for OH-measurements which can also be done by titration with isotopic label SO_2. The heavy isotope $S^{34}O_2$ is injected immediately at the entrance where it reacts with atmospheric OH radicals to form the heavier isotope of

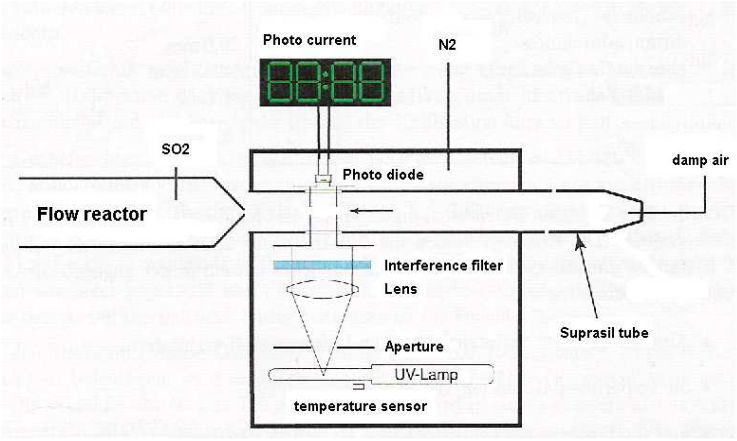

Figure 5.5: Schematic of the experimental setup during calibration: Calibration source (right) and flow reactor (left) with SO_2-injection. The source consists of a UV-lamp, photo diode and suprasil tube where humid air is irradiated.

H_2SO_4. To avoid reactions with other radicals such as HO_2, NO_2 is injected as quench gas after a reaction path of 7cm. The injection was achieved with two opposite steel needles with 1 mm in diameter to guarantee a sufficient mixture of the gases. Mole fractions for the heavy SO_2 isotope were around 2 ppm but the reaction path was sufficient to titrate the lower sub-ppt OH concentration in the atmosphere. The total conversion of OH radicals takes about 100 ms [Uecker, 2002] which means that after 4 cm all OH radicals are converted. A longer reaction path does not significantly raise the error of OH measurements.
Atmospheric measurements were performed on several days during the cruise however OH concentrations were mostly below the detection limit which ranged between 1.5 $\cdot 10^{-6}$cm^{-3} and 2.9 $\cdot 10^{-6}$ cm^{-3}.

5.2.2 Discrimination of Mass 125

During calibration an already suspected discrimination of the educt count rate was confirmed. Comparing the educt rate during background measurements, when no reaction with H_2SO_4 takes place and therefore no significant decrease in the count rates, with the educt rate when high amounts of H_2SO_4 are injected shows that educt ions do not decrease as much as the product ions increase. A discrimination of mass 125 due to tuning of the mass spectrometer may be the reason. A correction factor based on this comparison was derived and employed to the calibration factor and the atmospheric concentrations via a correction of the ACIMS formula according to:

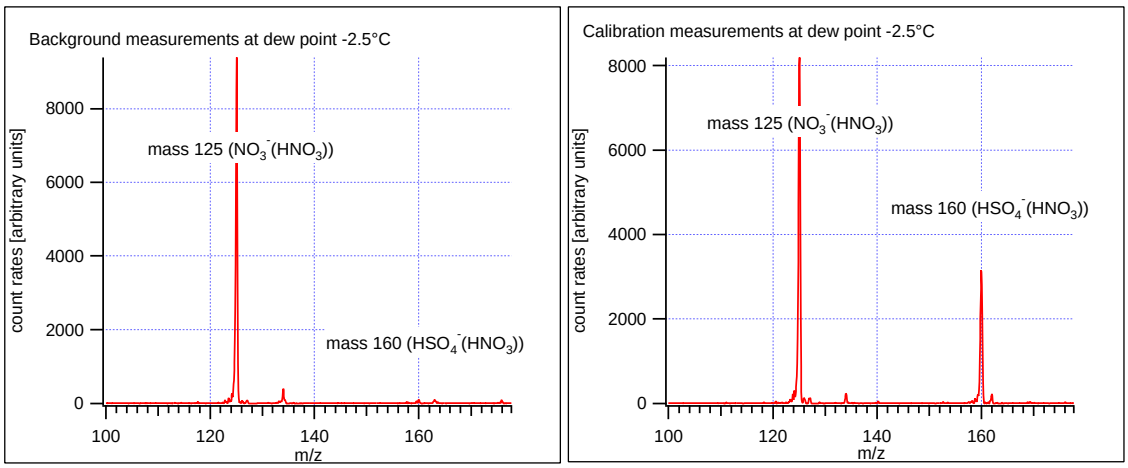

Figure 5.6: Mass spectra taken during calibration, the educt(m/z 125) and product(m/z 160) masses during background measurements (left) when the calibration source was turned off and calibration (right) with injection of SO_2 and turned on UV light source.

$$[H_2SO_4] = CF_{discr} \cdot \ln(1 + (mass160)/(2 \cdot mass125) - BG) \tag{5.16}$$

where BG denotes the background correction.

In F 5.6 two spectra taken at equal water contents in the suprasil tube during calibration are shown. The first one shows the peak height of mass 125 of 9.5 $\cdot 10^3$ which is the reference count rate. The second one shows a spectrum taken with injection of H_2SO_4 and a peak height of 3.5 $\cdot 10^3$ while the educt count rate decreases only to about 90 % of the reference count rate.

5.2.3 Calculation of the Calibration Factor

The OH-concentration is calculated according to equation 5.15.

To measure the water vapor concentration a newly calibrated dew point hygrometer (Edge Tech Model 200, Dewtrak Humidity Transmitter) combined with the data acquisition of temperature and pressure by a commercial SB Weather Station was used. Additionally the pressure at the dew point mirror was measured. Dew points between -1 and -10 °C were set, with an accuracy of 0.6°C . The hygrometer uses the chilled mirror dew point temperature condensation principle: It operates via a new electro-optical scheme to detect and maintain the condensed water vapor on the mirror surface by temperature stabilization. At lower dew

points the system became unstable due to unstable OH production inside the suprasil tube, consequently the signal of mass 160 became very noisy. For higher dew points count rates of mass 160 reached those of the educt mass in which case ACIMS is imprecise. These values were not taken into account. The water vapor concentration was determined through:

water vapor concentration

$$[\mathrm{H_2O}]_0 = \frac{p_{H_2O}}{p_0} \cdot \frac{T_0}{T_{suprasil}} \cdot \frac{N_A}{V_0} \cdot \frac{p_{suprasil}}{p_{dewpoint}} \tag{5.17}$$

so with

$$\begin{aligned}
p_{H_2O} &= 447.05 - 226.7 \text{ Pa } \pm 4.3\% && \text{Water Vapor Partial Pressure} \\
T_0 &= 273.15 \text{ K} && \text{Standard temperature} \\
N_A &= 6.022045 \cdot 10^{23} \text{ mol}^{-1} && \text{Avogadro constant} \\
p_0 &= 1.01325 \cdot 10^5 \text{ Pa} && \text{Standard pressure} \\
T_{suprasil} &= 296 \text{ K} \pm 0.2\% && \text{Suprasil tube temperature} \\
V_0 &= 2.241383 \cdot 10^{-2} \text{ m}^3\text{mol}^{-1} && \text{Standard volume} \\
p_{suprasil} &= 0.970 \cdot 10^5\text{Pa} \pm 0.2\% && \text{pressure inside the suprasil tube} \\
p_{dewpoint} &= 1.080 \cdot 10^5\text{Pa} \pm 1\% && \text{pressure at the dew point mirror}
\end{aligned} \tag{5.18}$$

the concentration ranged between

$$[\mathrm{H_2O}]_0 \approx 6.2 - 12.0 \cdot 10^{22}\ m^{-3} \pm 4.3\% \tag{5.19}$$

with

the *absorption cross-section of water* at 185 nm	σ_{H_2O}	$= 7.14 \cdot 10^{-24}\ m^2$
the *quantum yield*	Φ_{OH}	$= 1.0 \pm 1\%$

The photon flux can be determined via the ratio of the light intensity and the photon energy (at a given wavelength λ). The light intensity can be measured by the photo current I of the photo diode with defined sensitivity s and area A. Corrections have to be taken into account such as the absorption of radiation by O_2 and water vapor, reflexivity and

transmission of the walls and the broadening of the beam in direction towards the detector. The total photo current at the middle of the suprasil tube is [Reimann, 2000]

photon flux

$$\Psi = \frac{I\lambda}{sAhc} \cdot k_d \cdot k_t \cdot (e^{k_\sigma} + \rho \cdot e^{-k_\sigma}) \tag{5.20}$$

with

$$k_\sigma = (\sigma_{O_2}[\mathrm{O_2}] + \sigma_{H_2O}[\mathrm{H_2O}]_0) \cdot R \tag{5.21}$$

with the following measured values and constants.

I	=	$2.06 \cdot 10^{-8}$ A $\pm 1\%$	Photocurrent
λ	=	$1.849 \cdot 10^{-7}$ m	Wavelength
s	=	0.097 A/W $\pm 2.7\%$	Spectral sensitivity
A	=	$1.3 \cdot 10^{-5}$ m^2	Sensitive surface area of the photodiode
h	=	$6.626 \cdot 10^{-34}$ Js	Planck-constant
c	=	$2.998 \cdot 10^{8}$ m/s	Light velocity
k_d	=	$1.380 \pm 1.4\%$	Correction factor for beam divergency
k_t	=	$1.293 \pm 0.8\%$	Correction factor for transmissivity
ρ	=	$0.085 \pm 1.4\%$	Reflection ability
σ_{O_2}	=	$1.4 \cdot 10^{-24}$ m$^2 \pm 22\%$	Absorption coefficient of O_2 at $\lambda = 185$ nm
σ_{H_2O}	=	$7.14 \cdot 10^{-24}$ m$^2 \pm 2.8\%$	Absorption coefficient of H_2O at $\lambda = 185$ nm
$[\mathrm{O_2}]$	=	$5.0 \cdot 10^{24}$m^{-3}	Oxygen concentration in suprasil tube[3]
$[\mathrm{H_2O}]_0$	=	$6.2 - 12.0 \cdot 10^{22}$m^{-3}	Water vapor concentration from above
R_s	=	0.01 m	Radius of the suprasil tube

we get

$$\Psi \approx 3.15 \cdot 10^{16}\ s^{-1}m^{-2} \pm 19\% \tag{5.22}$$

as a value for the photon flux.

The irradiation time depends on the average flow through the suprasil tube as well as the fraction extracted for calibration. Optical alignments of the setup (light source - aperture -

tube) are taken into account by a geometric correction factor k_l. The *irradiation time* is

$$\tau = \frac{k_l\, b\, p_{sr}}{\chi_r\, p_0} \cdot \frac{T_0}{T_{sr}} \cdot \pi R^2 \cdot \left(1 - \sqrt{1 - \frac{\chi_r}{\chi_R}}\right) \tag{5.23}$$

with the values

k_l	=	$1.078 \pm 5\%$	Correction factor for the length of the irradiation zone
b	=	0.015 m	Aperture width
p_{sr}	=	$9.70 \cdot 10^4$ Pa $\pm 0.2\%$	Pressure in the suprasil tube
χ_r	=	12.86 slm $\pm 10\%$	Flux soaked up by the flow reactor
χ_R	=	19.7 slm $\pm 5\%$	Total flux in the suprasil tube

we obtain

$$\tau \approx 0.98 \cdot 10^{-2} s \pm 8.7\% \tag{5.24}$$

Now with the equations (5.17) to (5.23) equation (5.15) can be solved yielding a sulfuric acid concentration of

$$[H_2SO_4] = [OH] = 1.6 \cdot 10^{14}\ \mathrm{m}^{-3}\ \pm 21\% \tag{5.25}$$

and we obtain for the calibration factor according to CF= $[H_2SO_4]/ln(1 + 0.5 \cdot \mathrm{R})$ with R measured and multiplied with the factor 0.5 applied due to discrimination of the educt mass a value of

$$\textbf{Calibration Factor} \qquad \mathbf{CF} = 1.34 \cdot 10^{15}\ \mathrm{m}^{-3}\ \pm 31\% \tag{5.26}$$

The calibration procedure was carried on two days with varying temperature, pressure and different fluxes (17.1 - 20.3 slm). Thus several calibration factors were obtained. A statistical error of 10 % and a systematical error of 21% was derived. Calibration in the laboratory had the advantage that factors like photocurrent and temperature could be stabilized better than inside the container where outside temperature varied a lot and therefore influenced the photodiode. These problems have to be considered when developing an online calibration.
MSA is expected to undergo similar conditions and reactions as H_2SO_4
[Berresheim et al., 2002] therefore the same calibration factor is applied. This can be compared with the $\frac{1}{kt}$ factor in the ACIMS formula derived from the ion-molecule reaction time of ∼1 s and the rate coefficient taken from 5.4 for reaction 5.2 which is

$$\frac{1}{\mathbf{kt}} = 0.81 \cdot 10^{15}\ \mathrm{m}^{-3} \tag{5.27}$$

taken into account the dilution inside the flow reactor. Comparing the two calibration factors it is remarkable that they vary by a factor of 1.7. This discrepancy can be explained by loss of H_2SO_4 to the walls and other losses which are not considered by the ACIMS formula.

Chapter 6

Atmospheric Measurements

This chapter will discuss further corrections and considerations which have to be done for the evaluation of the data. Background, isotopic, temperature and pressure corrections will be discussed as well as difficulties in the instrumental operation during the campaign. Measurement techniques of the aerosol measurements and water samples performed by the Universities of Helsinki, Manchester and East Anglia during the campaign will briefly be introduced.

6.1 Further Considerations

6.1.1 Background and Detection Limit

Background corrections that originate from electronic noise, artificial HSO_4^- produced by the ion source, trace gases with a similar mass and atmospheric H_2SO_4 which accumulates on the walls have to be taken into account. Background measurements were performed every day, mostly during bad weather conditions such as rain and storm or at night, when photochemistry was inactive. Due to high precipitation over the ocean, background measurements often lasted several hours. The background signal was taken from the ratio of measured $HSO_4^-(HNO_3)$ (mass 160) and $NO_3^-(HNO_3)$ (mass 125), similar to the derivation of the concentration. According to [Uecker, 2002] other clusters (n=0,2) of the educt ions can be neglected. Two different measurement setups were chosen

- a filter-system, consisting of several layers of paper shown in the chapter "Experimental Setup"

- filtered air from a zero gas system "Nullgasanlage NGA19" (company Umwelttechnik MCZ GmbH)

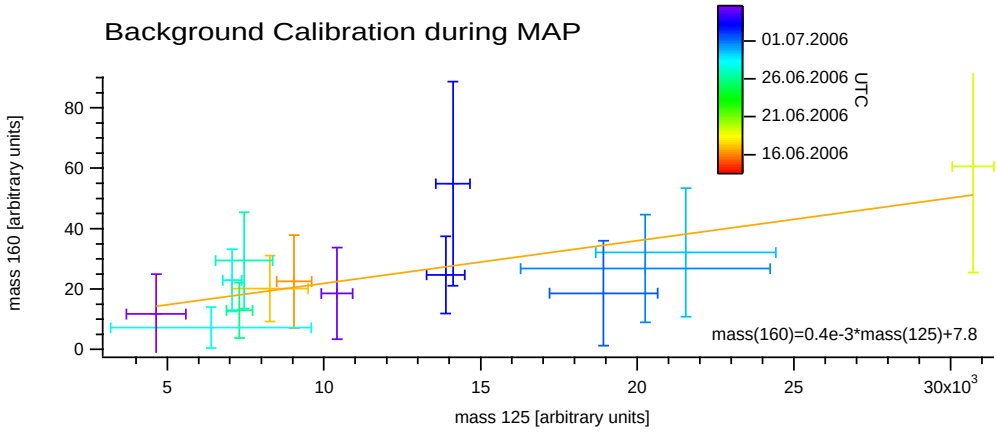

Figure 6.1: Background Measurements during MAP, mass 160 is plotted against the educt mass 125 with their respective 1σ standard deviation

The filtersystem of the zero gas system consists of an arrangement of filter cartridges which contain mainly activated charcoal, CO scrubber, NO scrubber and a molecular sieve. The molecular sieve binds molecules of about 10 Å and removes H_2O, SO_2 ammonia, carbon dioxide, hydrogen and H_2S. The NO-Oxidizer is built of a Cr-(VI)-oxid and calciumdichromate for oxidation of NO to NO_2. The charcoal removes NO_2 and ozone.

The ratio of product and educt count rates was averaged and a fixed value was subtracted from the data of the respective measurements during the day. Very high noise probably due to contaminations in the flow reactor during the first leg of the cruise raised the detection limit to $1.5 \cdot 10^6$ for H_2SO_4 and $3.3 \cdot 10^6$ cm^{-3} for MSA. F 6.1 and 6.2 show the respective background signal and 1 σ standard deviation of the count rates of mass 160. Both increase with increasing count rates at mass 125. Memory effects were observed if background measurements were performed after the atmospheric measurement in the evening. To reduce these effects filtered air was pumped through the flow reactor whenever atmospheric measurements were impossible due to weather conditions. [Hanke, 1999] reported similar effects which may stem in this case from a water-sea-salt film that forms on the walls. H_2SO_4 is highly soluble in water and therefore may be dissolved in this film and evaporates when the humidity drops. Similar effects are described in [Mauldin III et al., 1999]. Further effects have to be considered such as hydration of the educt ions that reduce the sensitivity of the instrument.

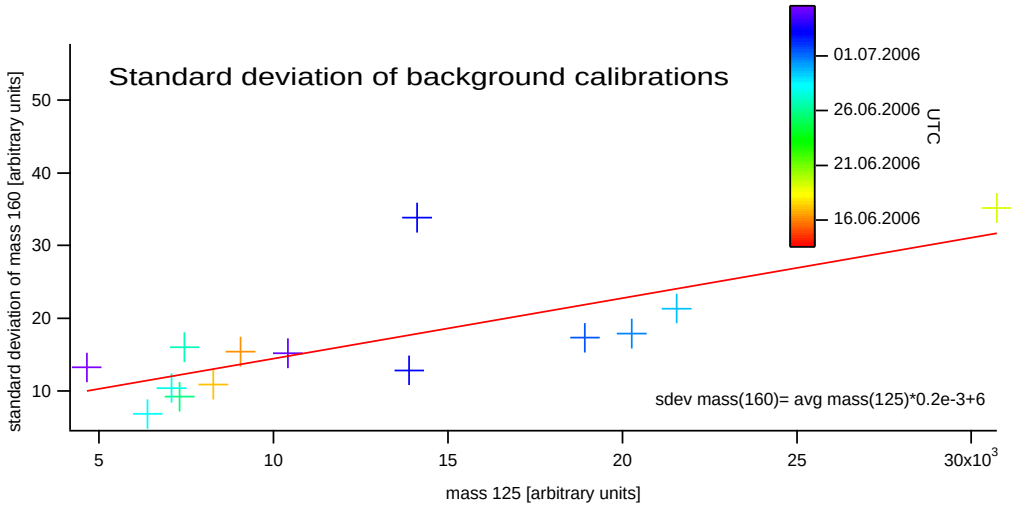

Figure 6.2: Standard Deviation of mass 160 is plotted against the educt mass 125, a trend of increased noise with higher educt rates is observed, explaining the high detection limit

Cluster Formation

Although the production of educt ions is very efficient one has to consider the effect of high relative humidity and possible sea-salt spray during atmospheric measurements in the Marine Boundary Layer. While the rate coefficient is independent of possible water clusters at a high relative humidity cluster formation has a limiting effect on the production of educt ions as discussed in [Uecker, 2002]. Water molecules attach to the $(NO_3)^-(HNO_3)_n$-ions and $(HSO_4^-)^-(HNO_3)_n$-ions to form bigger clusters that can not be detected by the spectrometer. At a temperature of 37°C the saturation vapor pressure and consequently the relative humidity inside the flow reactor is reduced to RH $\sim$ 25% as compared to the ambient air and thus cluster formation is reduced but has still a great influence on the dynamic range and the sensitivity of the instrument.

Empiric data acquired by [Uecker, 2002] have shown that the intensity of the educt count rate is remarkably reduced with rising relative humidity inside the flow reactor (F 6.3). At relative humidities about 20 % and higher the reduction of the educt count rate has already a critical impact on the dynamic range of the spectrometer. The average relative humidity inside the flow reactor ranged between 15 and 25% assuming a temperature of 37°C. The above discussed effect was mainly observed during background measurements with filtered air provided by the pure air generator when counting rates increased by a factor of four due to a lower relative humidity as can be seen in F 6.4.

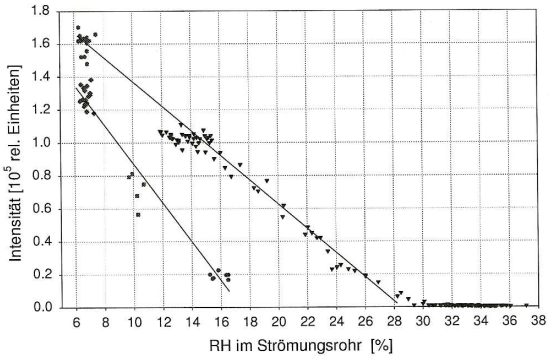

Figure 6.3: The intensity of mass 125 is plotted vs the relative humidity. At a relative humidity of 22% the count rates have already decreased by a factor of 4, thus resulting in a reduced sensitivity. Figure taken from [Uecker, 2002].

Another factor which reduced the sensitivity of the instrument was the frequent contamination of the front electrode. Sources of contamination were sea-salt spray or water droplets containing sea-salt and soot presumably emitted by the ship's exhaust. The contamination caused a drop of the pressure in the analyzer region of the IT-CIMS due to a reduced diameter of the orifice. As a result less educt ions entered the chamber. Cleaning had to be done almost every second day and measurement periods were interrupted every time for about two hours due to pumping.

6.1.2 Temperature and Pressure Factor

The flow reactor was, as mentioned above, heated at a temperature of 37°C. According to [Uecker, 2002] the possibility of aerosol evaporation inside the flow reactor at temperatures below 49°C is negligible. Due to a high flow of 19.7 slm the residence time of the analyte gas which had an average temperature of 15°C was about 3.5 s. Background measurements were performed at very high temperatures and resulted in higher background signals. If the heating belts were turned off the background signal decreased however the probability that deposition on the walls occurs is increased. The temperature difference to atmospheric conditions is about 20 K. The calibration factor was normalized to standard conditions (273 K, 1013 hPa). Therefore a correction to the specific outside temperature and pressure has to be carried out.

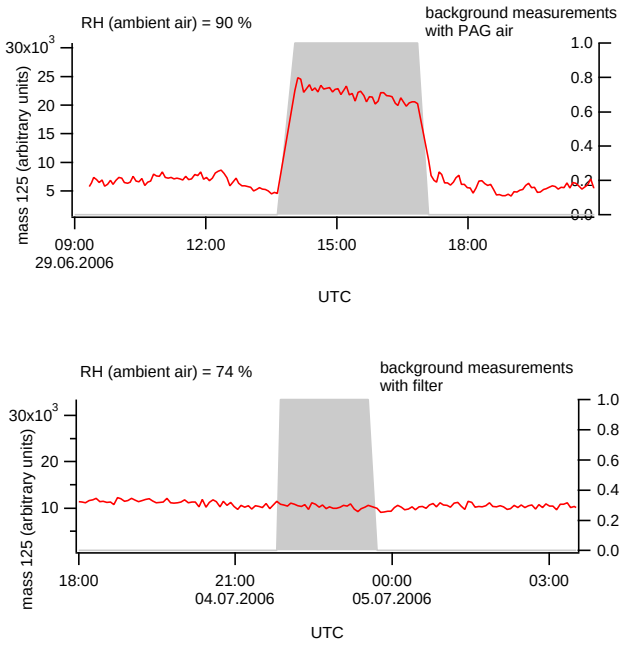

Figure 6.4: 1. Panel: Mass 125 during background measurements with a Pure Air Generator; 2. Panel: Mass 125 during background measurements with a filter

6.1.3 Isotopic Corrections

Ambient isotopic ratios were considered during simultaneous measurements of MSA and H_2SO_4. The most abundant sulfur isotopes are S^{32} (95%), S^{34} (4.2%) and S^{33} (0.75%). The heavy isotope of the product mass 158 ($CH_3S^{32}O_3^-(HNO_3)$) is at mass 160 ($CH_3S^{34}O_3^-(HNO_3)$). Therefore a correction of the relative abundance of the two species had to be subtracted from the concentration of H_2SO_4 obtained by ACIMS.

6.2 Experimental Data

6.2.1 Sulfuric Acid, MSA and Sulfur Dioxide

Measurements of H_2SO_4, MSA and SO_2 were successfully performed during 15 days of the ship cruise. Bad weather conditions during the first leg made measurements only partly successful. The second leg however allowed 24 h measurements within a very productive area of the plankton bloom. The first leg lasted from 11th of June till 22nd of June, the second leg started on the 25th of June and ended on the 5th of July. All instruments were working properly during the campaign. Lacks in the timeline were due to rainy or stormy weather or

operation of the instrument. H_2SO_4 ranged on average between $1.7{\cdot}10^6 cm^{-3}$ and $2.6{\cdot}10^6 cm^{-3}$ with the highest values of $1.7 \cdot 10^7 cm^{-3}$ which were only observed on the 13th of June. The detection limit was in general very high: The 2σ standard deviation ranged around 1.5 $\cdot 10^6 cm^{-3}$ with higher values when memory effects were observed or filter measurements were performed. In general H_2SO_4 concentrations were low compared to continental measurements carried out at Hyytiälä, Finland or Heidelberg, Germany by our MPI-K group. The highest values during continental measurements at midday, where concentrations on most days ranged around $1.0 \cdot 10^7 cm^{-3}$ to $1.5 \cdot 10^7 cm^{-3}$ were only rarely observed during the cruise. A diurnal variation can be seen during sunny days of July and the one day in June.

MSA concentrations were much higher compared to sulfuric acid with an average value of $2{\cdot}10^7 cm^{-3}$ and most of the time above the detection limit of $3.4 \cdot 10^6 cm^{-3}$. These values exceed MSA measurements also performed by our MPI-K group in boreal forests in Hyytiälä, Finland presented in [Scholz, 2004] by one order of magnitude and more, reflecting the abundance of MSA in the Marine Boundary Layer. They are however comparable to MSA measurements performed in coastal areas [Berresheim et al., 2002],[Davis et al., 1998]. Diurnal variation was only rarely observed and will be discussed in the next chapter.

The course of the ship was mostly set against the wind however when the ship was at rest, for example for measurements of temperature with water depth, contamination was high which explains most of the high valued short term events of sulfuric acid and SO_2. As an indicator for ship contaminations SO_2 values above a mole fraction of $200 \cdot 10^{-12}$ which expanded over short time periods were taken and compared to the ship movement. This analysis and the comparison with aerosol parameters allowed a clear characterization of pollution events. Especially on the last cloudy day the emission of H_2SO_4 by the ship became obvious since a "zig -zag" course along the coast, west of the research station at Mace Head, Ireland was chosen.

On three days the instrument mode of the second IT-CIMS (operated with a glow-discharge ion source at 60 hPa) was switched to the positive sampling mode for DMSO measurements. Detection of trace gases with a higher proton affinity than water can be achieved with the H_3O^+-ion as educt ion. A simplified proton exchange reaction is of the form:

$$H^+H_2O + X \rightleftharpoons H^+X + H_2O \tag{6.1}$$

If the water vapor concentration in the flow reactor is high, water molecules attache to the

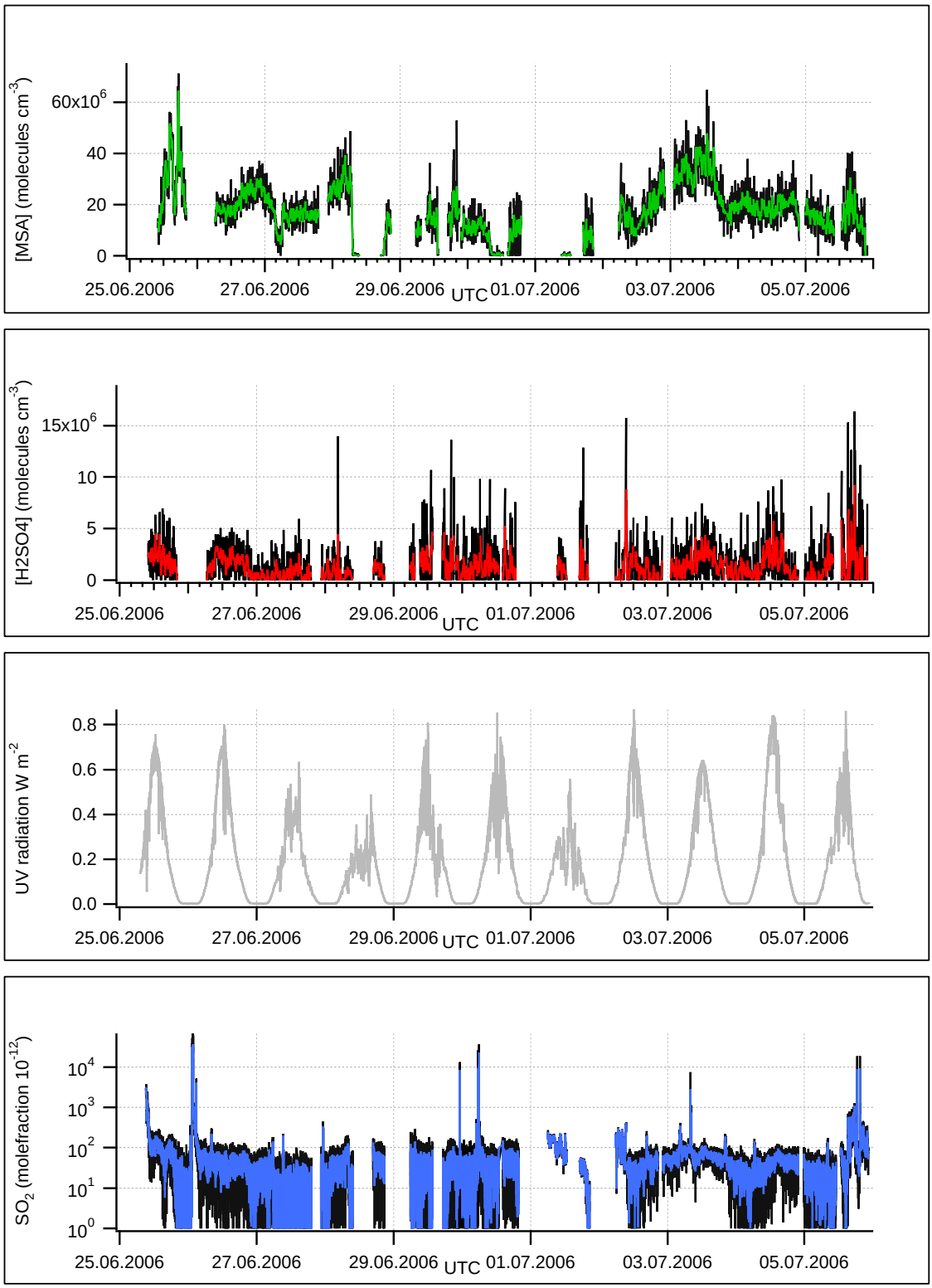

Figure 6.5: MSA, H_2SO_4, UV radiation and SO_2 (logarithmic scale) during the 2nd leg of the cruise. Colored timelines are averaged over five spectra.

hydronium-ions and form stable clusters. The rate coefficient for the back reaction in eq. 6.1 can be related to the forward reaction coefficient. It is temperature dependent and increases with increasing hydration. For a more detailed discussion with trace gases of similar proton affinity see [Aufmhoff, 2004]. The proton affinity of DMSO is with 221.4 kcal/mol higher than the proton affinity of DMS with 198.6 kcal/mol [Nowak et al., 2002]. Due to high relative humidities (mostly above 70%) only DMSO could be detected. An uncalibrated upper limit was derived to be at 10pptv.

F 6.5 shows the data acquired during the second leg of the cruise. The colored timelines are averaged over 5 mass spectra. A more detailed and complete overview of the daily measured concentrations will be given in the appendix. The data on the 13th of June have to be interpreted carefully because the tunefile used during that day was distinct from the other days. The voltage applied to the front electrode differed to the later settings by ~ 7 V, this however should have the same sampling effects on mass 125 and 160 and therefore the ratio of the two masses is not affected. A tune file used during the rest of the campaign was compiled on the 14th of June. Data analysis and evaluation of the SO_2, measured by the second CIMS-instrument was done by Anke Roiger (DLR) and Heinfried Aufmhoff (MPI-K) and have to be regarded as preliminary at this stage.

Comparison to additional data like aerosol parameters will give a more profound insight into origin and loss of the respective trace gases. Nucleation was only observed during the 13th of June.

Light Intensity

The light intensity was measured with an UV Sensor (Ultraviolet selective thin film sensor "TW30DY2", from sg lux GmbH) that was installed on the roof next to the inlet system. The wavelength of maximal spectral sensitivity S is at 300nm and ranges between 260 to 362 nm ($S=S_{max}\cdot 0.1$). Ozone photolysis at wavelengths ≤ 320 nm leads to the formation of $O(^1D)$ which can react with water molecules to form OH radicals. As explained in chapter 2, OH is the needed oxidant to form H_2SO_4 and MSA.

6.2.2 Additional Data: Aerosol parameters, Chlorophyll-a and Halocarbons

Differential Mobility Particle Sizer

Measurements of the particle number concentrations and size distributions were carried out by Mikael Ehn, University of Helsinki using a Differential Mobility Particle Sizer (DMPS).

The DMPS samples the number concentrations of particles between 3 and 800 nm in diameter, divided in 40 different size classes, with 10 minute time intervals. From these data the condensation sink was derived, which has already been explained in chapter 2. A more detailed description of a DMPS is given in [Laakso et al., 2004].

Aerosol Mass Spectrometer

Aerosol constituents such as mass concentrations of SO_4^{-2}, NH_4^+, NO_3^- and total organic compounds were measured by Paul Williams and Jonathan Crosier, University of Manchester, with an Aerodyne Time of Flight Aerosol Mass Spectrometer. An important feature of the AMS is the ability to equate the detected ion count rate of the mass spectrometer to a mass concentration of a given species in a sample. It uses thermal desorption at 500°C, electron impact ionization at 70 eV and a quadrupole mass spectrometer. The time resolution comprised 5 min and aerosols of sizes from 70 to 600 nm were sampled and sized aerodynamically. The AMS is not able to detect the composition of a single particle but of all particles successfully collected. Aerosol containing sea-salt or other low volatility solid particulate matter cannot be detected. A detailed description of the instrument is given in [Allan et al., 2003]. Both experiments (the DMPS and the AMS) were located on the front deck inside two sea-containers opposite to our container, with an inlet system mounted at about 10m above the ocean surface. At the time of the termination of this diploma thesis the data set has to be regarded as preliminary.

Chlorophyll

Chlorophyll is a photosynthetic pigment found in plants and algae. Chlorophyllfluorescence is a phenomenon of light absorption of chlorophyll at a specific wavelength, which is - if not being used for photosynthesis or lost due to heat dissipation - re-emitted at a longer wavelength. Chlorophyll-a measurements were used as an indicator for high biological activity in the ocean due to phytoplankton growth. Satellite observations as well as filter sample measurements were used to track the region of high plankton density. Chlorophyll-a concentration was measured by Janina Woeltjen, University of East Anglia (UEA), and the ships intern fluorometer (Turner Model 10 Fluorometer). The water for both measurements was taken from 2 m below the surface and flushed through the fluorometer where fluorescence by algae was continuously measured. The fluorometer was however affected during day light since no fluorescence was measured probably due to interference with other wavelength. The measurement technique by UEA is also based on detection of fluorescence emitted by algae:

Water samples were taken on a daily basis, filtered by 0.7 μm Whatman GF/F Glassfilter and shock frozen for later analysis in the laboratory. The fluorescence is stimulated at a wavelength of 436 nm and detected at 680 nm. The water for both measurements was taken from 2 m below the surface. The measurement techniques were compared to each other and showed an exponential dependency, meaning that the fluorescence measured by the ship was overestimated at high concentrations which was due to a lack of calibration. The data set is presented in the appendix.

Halocarbons

Surface water samples acquired by Janina Woeltjen, UEA, for measurements of halogenated hydrocarbons were degassed and enriched in a thermoabsorption tube and then analyzed by a Gas Chromatographic Mass Spectrometer (GC/MS) during the cruise. The measurements shall be presented and discussed with their respective relevance on MSA production. The following species could be detected: $CHBr_3$, CH_2ICl, CH_2Br_2, CH_2I_2; $CH_3CH_2CH_2I$, C_2H_5I, CH_3CHICH_3 and surfactants.

Chapter 7

Data Analysis and Discussion

The gaseous MSA and H_2SO_4 concentration values acquired during one day of the first leg and the last days of the second leg of the cruise will be analyzed and discussed in more detail in this section with a closer look at sources and sinks of the respective trace gases. This will be done by introducing certain phenomena observed during the cruise. A special focus will be on the last three sunny days in July, when H_2SO_4 showed diurnal trends and MSA concentrations and SO_2 mole fractions were among the highest observed during the cruise in clean air conditions.

7.1 Sulfuric Acid

Sulfuric acid concentrations during the MAP cruise were generally low compared to measurements in the planetary boundary layer in Finland and Germany [Fiedler, 2004] or coastal measurements at the northeastern coast of Crete [Bardouki et al., 2003], with an average between $1.69 \cdot 10^6 cm^{-3}$ and $2.56 \cdot 10^6 cm^{-3}$. Although comparable to average concentrations measured at the research station in Mace Head, at the west coast of Ireland by [Berresheim et al., 2002], midday concentrations rarely showed more than $1 \cdot 10^7 cm^{-3}$, which differs from the Mace Head measurements. All values are plotted vs the local time (-1h) in F 7.1. The timelines of MSA, H_2SO_4, SO_2 and the condensation sink are presented in the appendix.

Nucleation events

During the cruise of the Celtic Explorer lasting 21 days in total, only on one day nucleation was observed. On that day H_2SO_4 concentrations peaked up to $2 \cdot 10^7 cm^{-3}$ which were among the highest values observed. The 5th of July showed similar values, but the course was set along the coast and atmospheric measurements were influenced by the ship's exhaust and

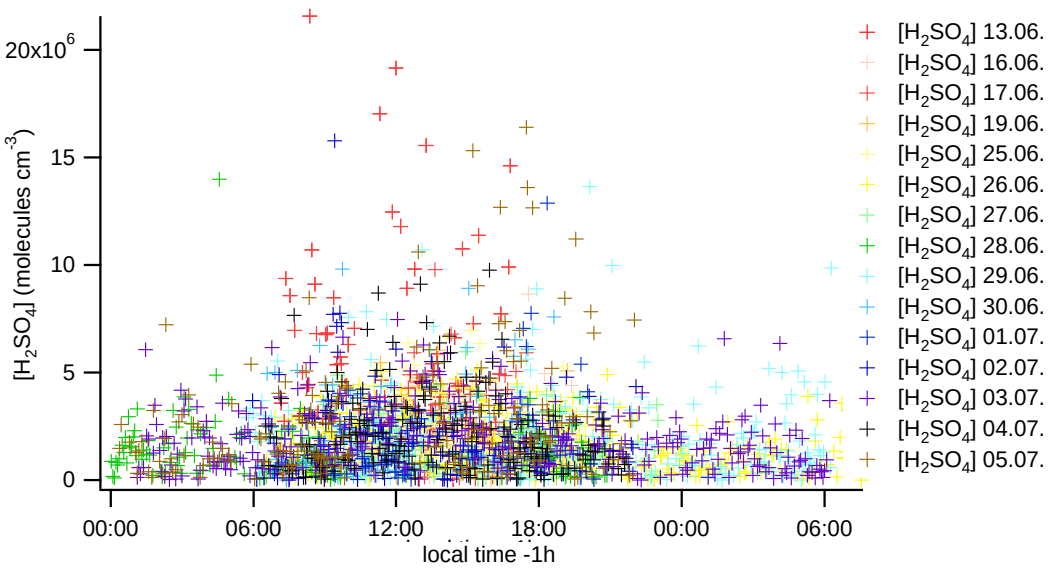

Figure 7.1: Sulfuric acid plotted vs local time (-1h). Different colored dots refer to different days. Except for the 13th of June and the 5th of July H_2SO_4 values stay mostly below $1{\cdot}10^7 cm^{-3}$

continental outflow. It was a sunny day with some cloud coverage. Wind speeds of 5 to 9 m/s were observed and the relative humidity was the lowest recorded throughout the whole cruise. It dropped till noon to values of RH = 60% and increased till midnight up to 85%. F 7.2 shows the data collected on the 13th of June. The first panel shows the time evolution of the condensation sink (CS), which decreased to values of $5{\cdot}10^{-4}s^{-1}$, corresponding to a very low particle concentration (shown in the last panel) of about 200 particles per cm^3. Similar observations were made before nucleation events occurred during continental measurements for example those described in [Fiedler et al., 2005]. Air mass trajectories (see appendix) show mostly clean air masses coming from north/northwest, with no significant contact to continental sites. Sulfuric acid concentrations were high throughout the whole day and did not covary with daylight, in fact high values between an 4 and 5 p.m. are visible. This particular peak was very likely due to burning of waste by the ship. Morning values can be explained by ship emissions, which were also evident in the enhancement of NO_x signatures in the spectra of the second CIMS-instrument. This method will be explained when discussing MSA formation. High night-time values of H_2SO_4 have been observed several times throughout the cruise and will be discussed later.

The DMPS plot(7.2) shows the time line of the particle diameter with the particle number

concentrations reflected in the color code. A clear "banana"- shape indicates the growth of the particles from diameters in the lower nm range up to 200 nm. On a first glance a time shift analysis explained in [Fiedler, 2004] between the increase of H_2SO_4 and the formation of nm-particles cannot be done, since no particles of 3 to 5 nm are present. The start of the nucleation event must have occurred earlier and the ship must have encountered the air masses with newly formed particles in a later evolution stage. If particle formation started before the observed enhancement of H_2SO_4, two interpretations are possible: Particle nucleation was hindered earlier during the day due to a high condensation sink, which dropped and reached a minimum around noon, or other gases were present that initiated the nucleation. Unfortunately at this stage of data availability no final conclusion is possible. Coastal nucleation events could not be explained by ternary nucleation through sulfurous gases, therefore a mechanism involving iodine containing vapors that originate from photolysis of biogenic iodocarbon, which are also emitted by marine algae, was proposed by [O'Dowd et al., 2002]. At the time of the termination of this thesis IO and OIO measurements were not evaluated therefore no statement of possible involvement of these gases can be made. However, since high values of H_2SO_4 were recorded on the 13th of June and this was the only day when nucleation occurred, one may arrive at the conclusion that there is a high probability that H_2SO_4 was the initiator of the nucleation event on this day, also recognizable through the indicated increase at the beginning of the formation of new particles. Furthermore very low concentrations of H_2SO_4 recorded during the following days of the cruise might explain why no other nucleation event was observed. This is consistent with the view that sulfuric acid is one of the most important substances leading to new particle formation in continental sites as well as over remote marine areas. The data set is however not sufficient to draw a final conclusion at this stage of the evaluation process.

Sulfuric acid during good weather conditions

A closer analysis of the evolution of H_2SO_4 concentrations during the last three sunny days in July (midday of 2nd of July till midnight of 4th of July) will be presented in the following section. These days were chosen for the following reason: Weather conditions were stable during these days with mostly uncovered sky accept for the 4th of July, when cirrus clouds were present. Additionally these days comprise values of measurements performed in areas of high plankton bloom (2nd and 3rd of July) and low plankton bloom (4th of July). Thus a comparison between the relative amounts of DMS oxidation products can be drawn.

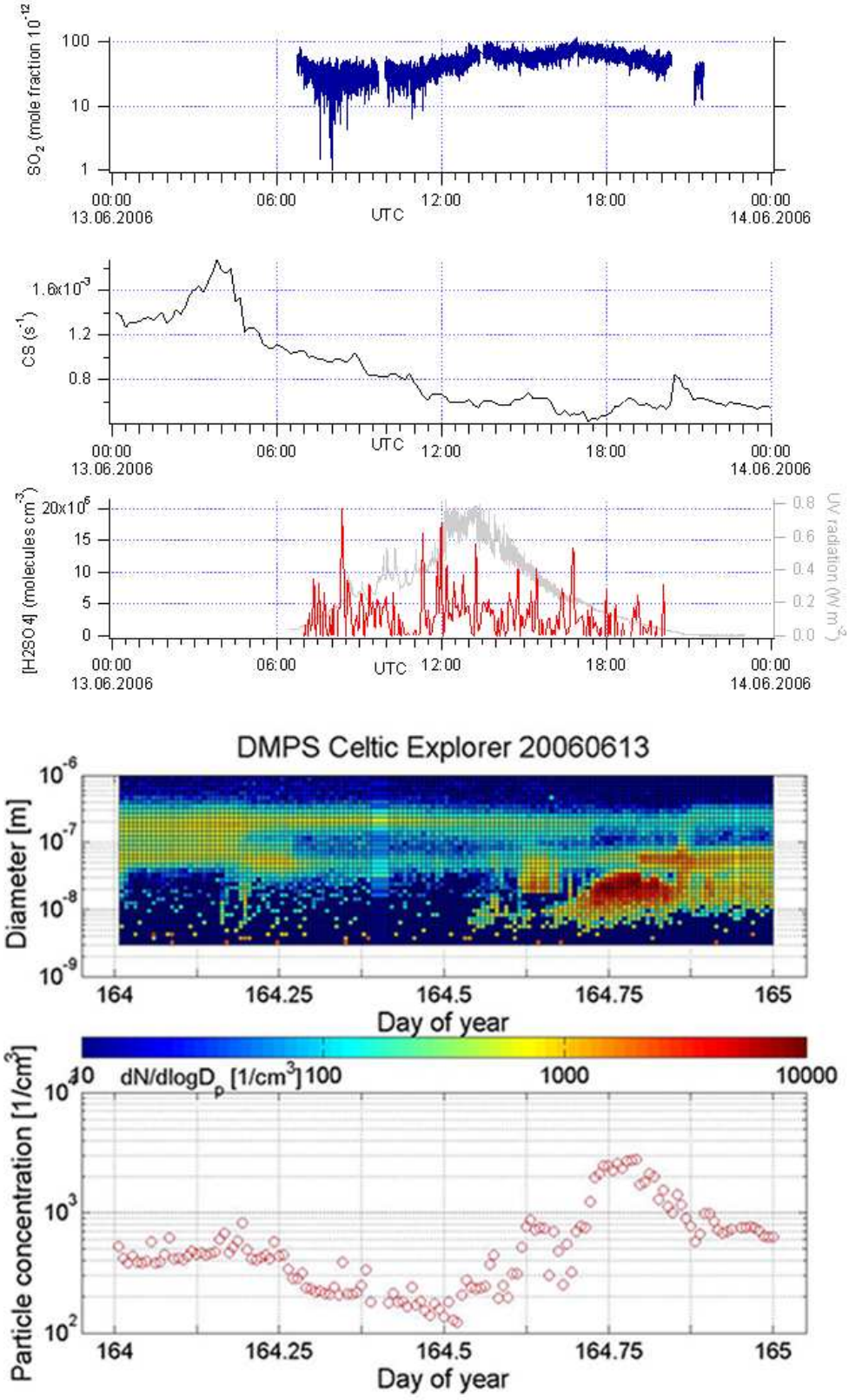

Figure 7.2: SO_2-mole fractions (first panel), gaseous H_2SO_4 concentrations, UV radiation (third panel, measured by MPI-K), CS, particle size distributions and particle number concentrations (measured by the University of Helsinki) during 13th of June. This day comprises the only data set when nucleation was observed.

To explain day- and nighttime values of H_2SO_4 as observed during this period one may consider the following aspects: The formation of secondary gaseous sulfuric acid depends crucially on the formation of OH-radicals (or other gaseous species with high oxidation power) and SO_2 concentrations. Apart from a strong correlation with the UV-radiation, a necessary element for the formation of OH-radicals (via O_3 photolysis), sinks and loss mechanisms have to be considered. In the presence of OH-radicals and clean air SO_2 is rapidly oxidized to H_2SO_4 via the Stockwell-Calvert-Mechanism presented in chapter 2.

F 7.3 shows the concentration of H_2SO_4 and the UV radiation during the three sunny days of July in mostly clean air masses stemming from west/northwesterly marine regions (see appendix for air mass trajectories). Pollution events caused by the ship, which are clearly marked in the time series of SO_2 and CS, for example on the 2nd of June at around 10 a.m. and on the 3rd of June at 8 a.m, are only partly reflected in the H_2SO_4 time series. This is probably due to fast removal of H_2SO_4 by condensation onto pre-existing aerosols or the fast change in air masses which goes with the movement of the ship. Diurnal patterns corresponding to the UV-radiation are visible but not pronounced. H_2SO_4 concentrations are generally low with values at midday around $4 \cdot 10^6 \mathrm{cm}^{-3}$. The signal is relatively "noisy", meaning the concentration differences can vary up to one magnitude from one spectra to the next and values are close to the detection limit which is plotted with a dashed horizontal line.

For an estimation of an average concentration of H_2SO_4 production the following steady-state calculation can be made: According to 2.8 the production rate of H_2SO_4 is determined via

$$k_{OH+SO_2}[SO_2][OH] = [H_2SO_4]\tau^{-1} \tag{7.1}$$

where k_{OH+SO_2} is the rate limiting reaction constant of the Stockwell-Calvert mechanism, τ the residence time of H_2SO_4 in the atmosphere that can be associated with the inverse CS. SO_2 mole fractions ranged between 20 and 80 pptv (in clean air) which corresponds to a concentration of 0.5 to $2.1 \cdot 10^9 \mathrm{cm}^{-3}$. Assuming an OH concentration of $1.0 \cdot 10^6 \mathrm{cm}^{-3}$ (taken from [Bey et al., 2001]) which corresponds to an average value in July in these latitudes and heights over the ocean, a SO_2 concentration of $2.1 \cdot 10^9 \mathrm{cm}^{-3}$ and a lifetime of H_2SO_4 of 700 s (1/CS) with respect to aerosol scavenging, we obtain a concentration of H_2SO_4 of $1.9 \cdot 10^6 \mathrm{cm}^{-3}$. Comparing this to our measured averaged values of $1.7 \cdot 10^6 \mathrm{cm}^{-3}$ it stands in good agreement but may not reflect diurnal trends and maximum values as measured at noon of the 3rd of July. As already mentioned a very noisy signal might explain the short term peaks

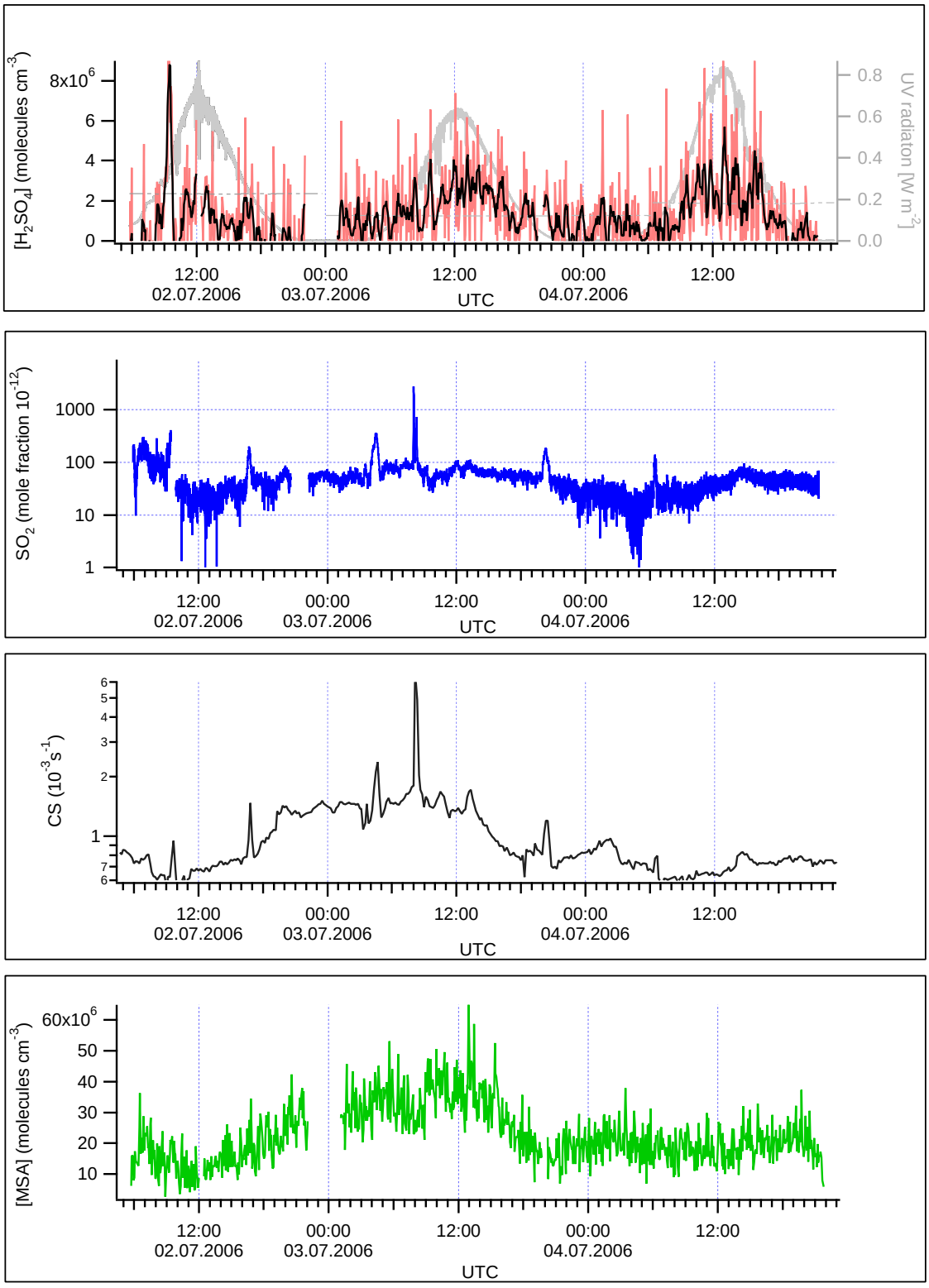

Figure 7.3: Sulfuric acid measurements (red), concentrations averaged over 5 spectra (black) during three days with high UV radiation (grey), CS (University of Helsinki) values range between $6{\cdot}10^{-4}$s^{-}1 and $6{\cdot}10^{-3}$s^{-}1 and SO_2 with 10 to 800 pptv (SO_2 values are averaged over 5 mass spectra).

which mostly last only one scan. All values are close to the detection limit therefore a smaller signal to noise ratio is expected. On the other hand is the steady state calculation a very limited description of the actual concentration and the variation of the OH-concentration is uncertain.
H_2SO_4 shows surprisingly high values with an average of $1.7{\cdot}10^6 cm^{-3}$ during the night which cannot be explained by photochemistry. Similar observations have been made during Antarctic H_2SO_4 measurements performed by Davis et al. (1998) and were attributed to a still not fully understood reaction pathway involving SO_3 which is directly formed from DMS through dissociation of CH_3SO_3, without involving SO_2 as an intermediate product [Lucas and Prinn, 2002]. It rapidly reacts (in the order of seconds) with water to H_2SO_4. [Lucas and Prinn, 2002] report a systematical underproduction of H_2SO_4 in their model study, if an enhanced production of SO_3, independent of the precursor SO_2 is not included. Evaporation processes of H_2SO_4 from aerosols at a relative humidity above 75%, which was the observed RH during these days, are expected to be small [Davis et al., 1999].

Vertical transport from atmospheric layers above the boundary layer, referred to as the buffer layer, have been reported during events of low relative humidity [Jefferson et al., 1998]. Dry air, enriched with DMS oxidation products such as DMSO, MSIA, SO_2 or other precursor gases of H_2SO_4 and MSA subside and mix with the Marine Boundary Layer air. Removal rates, due to high aerosol surface and number concentrations, of oxidized sulfur species in heights above 500 m are smaller and lead to a longer life time of these gases. Vertical entrainment and injection of H_2SO_4 from upper layers into the Marine Boundary Layer might be a possible explanation for high nighttime values. This assumption has partly been supported by the HYSPLIT calculation of air mass trajectories which show a subsidence of the respective air mass from altitudes of 1.5 km. The lifetime of H_2SO_4 in the boundary layer is of the order of 10 min therefore vertical transport can only partly account for the observed effect. The HYSPLIT calculation comprises only air mass trajectories with a time scale of 3 days, therefore may the observed effect only partly be explained by these backward trajectories.

Another explanation might be the process of degassing of primary H_2SO_4 from the ship and container surface as well as primary sulfuric acid emissions by the ships exhaust which causes a constant background value of H_2SO_4. Low wind speeds of 3 to 5 m/s might support this assumption. The effect of H_2SO_4 degassing from the surface of the sampling line can not be excluded either. A water-salt film covering the flow reactor surface might enhance the accumulation of H_2SO_4 inside this film during the day which then comes off at night. This

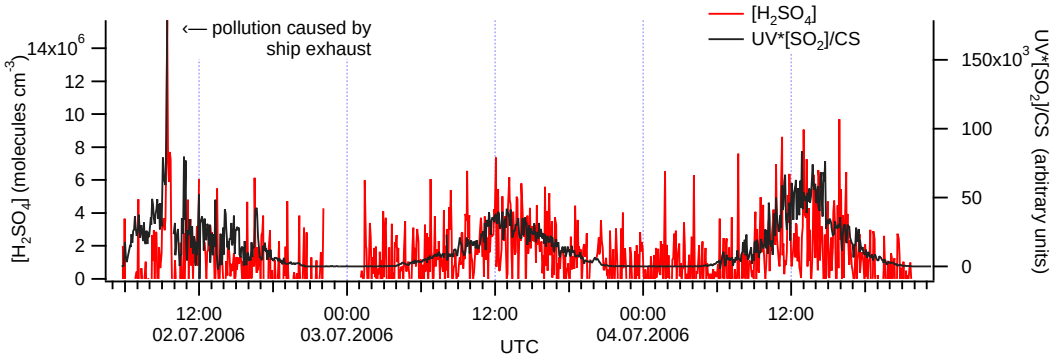

Figure 7.4: Measured H_2SO_4 compared to estimated photochemical production and loss onto aerosols

process however is very unlikely to have happened since the sampling line was heated (37°C) and condensation onto the walls was therefore inhibited.

For further analysis of the sinks and sources of H_2SO_4 by oxidation of SO_2 with OH-radicals and loss onto aerosols the following considerations can be made: Taking into account that the production rate of OH is proportional to the UV radiation and the CS reflects the inverse lifetime, one obtains

$$[H_2SO_4] \propto \frac{(\text{UV} - \text{radiation}) * [SO_2]}{\text{CS}} \tag{7.2}$$

which is just a trend. Loss rates of OH are not taken into account with this approach but it nevertheless reflects decently well the evolution of the measured H_2SO_4 concentration as can be seen in F 7.4. Except for night time values the calculated run of the curve describes the evolution of the measured values, suggesting that H_2SO_4 is mainly produced through OH oxidation of SO_2 and removed through aerosol scavenging. In this case the reason for the low H_2SO_4 values can be traced back to low SO_2 and OH concentration over the ocean. Due to reduced presence of ozon, less OH is present.

The influence of combustion processes of ship engines is clearly visible: The origin of the pollution peak at the 2nd of July can be associated with the fast oxidation of excessive SO_2 by OH radicals as well as emission of primary sulfuric acid. Comparing measured and calculated values, the yield of H_2SO_4 (relative values) derived from the above estimation might even accede the measured concentration, since the production rate of secondary H_2SO_4 is fast in the presence of abundant SO_2. Movement of the ship caused a fast change in air masses and with a low time resolution of 4 min, the measured values might not account for the

total H_2SO_4 produced by this pollution event. The measured values might underestimate the observed effect but still give an impression of the impact that ship emissions have onto H_2SO_4 injection into marine air.

Condensation Sink and Particle Composition

The effect of H_2SO_4 removal through aerosol scavenging can be demonstrated via the inverse relationship between gaseous H_2SO_4 concentrations and particle surface (F 7.5). At smaller values of CS more gaseous H_2SO_4 is present. The relation reflects condensation onto pre-existing aerosols as the most effective sink of H_2SO_4. The color code represents the relative humidity implicating an anti-correlation of gaseous H_2SO_4 concentrations with RH. This can partly be explained by re-evaporation of H_2SO_4 from aerosols, which however occurs only at a relative humidity <10%. Heating of the sampling tube might have contributed to the explained effect. The RH inside the sampling line comprises values of 17 to 20%. However the effect of water vapor content is twofold: High water vapor content in the MBL leads to a more effective production of OH radicals and to a more effective photochemical production of H_2SO_4 compared to higher layers where water vapor content is reduced [Mauldin III et al., 1999]. The variations of RH were low throughout the cruise therefore a sustainable statement of the effect of water vapor upon H_2SO_4 condensation can not be made.

The CS during the entire cruise ranged between $5{\cdot}10^{-4}s^{-1}$ up to $8{\cdot}10^{-3}s^{-1}$ resulting in a lifetime of H_2SO_4 of 125 to 2000 s with respect to aerosol scavenging with an average of 500 s.

At noon on the 2nd of July the CS starts to increase up to a plateau value of 0.001 s^{-1} decreasing almost 36 h later. Total aerosol number concentration increased during that time to levels of 1000 particles/cm^3 with a dominant mode between 60 to 80 nm in diameter (see appendix for DMPS plots).

Looking at the composition of these particles from the AMS measurements, performed by the University of Manchester, which delivers particle compositions from particles with diameter of 70 to 600 nm, an enhancement of non sea-salt sulphate ions emerges during this time. Other constituents like nitrate or ammonium show small changes only, compared to values with coastal influence. This was the case on the 1st of July when the course was set along the coast of Scotland (west of South Uist, Outer Hebredies).
Coe et.al. (2005) denoted values for the mass load of the organics between 0.5 μg m^{-3} and 1μg m^{-3} for marine conditions at similar measurements conducted at the research station

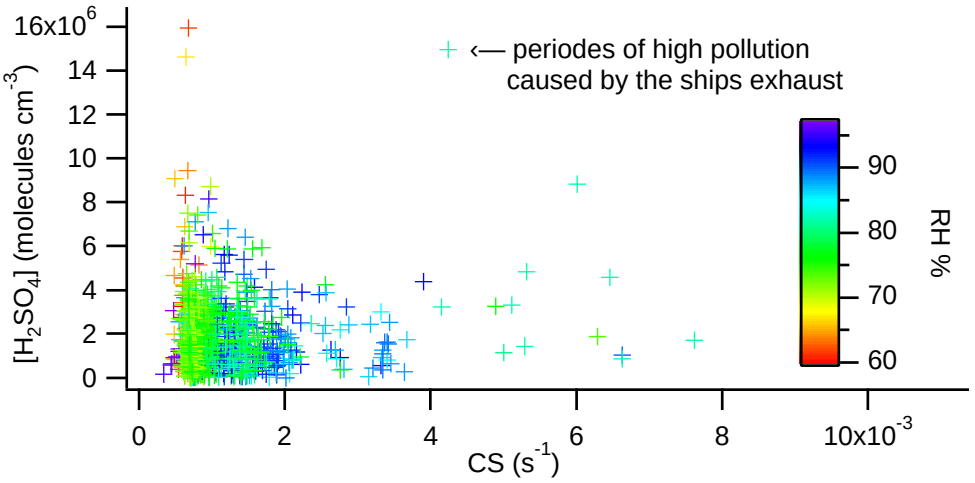

Figure 7.5: Scatterplot of H_2SO_4 (MPI-K) and CS (University of Helsinki) (data taken during the entire cruise); the color code represents the relative humidity

Mace Head in summer 2002. F 7.7 (upper two panels) shows an increase of the four aerosol constituents, SO_4^{2-}, NO_3^-, NH_4^+ and total organic compounds, within the aerosols, which is representative for continental outflow [Coe et al., 2005]. The 1st and the 5th of July were both days when the coast was in sight and mass loads comprised values around 2 μg m^{-3}. In comparison values of the 2nd, 3rd and 4th of July stayed mostly well below 0.5 μg m^{-3} except for the sulfate ions.

Ruling out the possibility that air masses during the selected days were in contact with continental boundary layer by comparing the aerosol composition during the coastal approach and the marine air, observations would represent a fingerprint of clean marine air at high plankton bloom, with typical compositions as for particle compositions as well as for gaseous species.

7.2 Sulfur Dioxide

Sulfur dioxide ranged around an average mole fraction of $\sim$ 100 pptv (including values of pollution events). The detection limit was at 30 pptv. Measurements showed great variability from values below the detection limit up to several ppbv, which were due to influences by the ship's exhaust or the coast. An upper limit of 200 pptv was set to distinguish between polluted and clean marine air. This value served as an initial guess to rule out the majority

of pollution events without extracting enhancement of SO_2 due to biogenic sources. A comparison with the CS helped to track down pollution events, since in most cases both showed significant increases on a short time scale as can be seen in the example of figure 7.3. However further comparison with measurements of black carbon might give a more sophisticated overview when pollution was dominant. Black carbon is mainly produced by combustion processes and may serve as an indicator for anthropogenic or continental influence.
The area of SO_2 production from DMS emission was not restricted to small spots and chlorophyll satellite data showed high values throughout the ship's route on a large area. Therefore one expects the biogenic enhancement of SO_2 to happen on a long term scale. However the possibility of extracting higher SO_2 values, which were not due to anthropogenic sources, can not be denied. Abrupt changing weather conditions might be a possible cause for short term enhancement. This however needs further analysis and comparison with meteorological data. Under the criteria given above values of clean marine air ranged around 30 to 40 pptv.

A unique phenomena occurred during the last three sunny days in July when SO_2 concentrations built up from 30 pptv to 80 pptv in a time scale of about 20 hours and stayed at that level (with small variations) till 6 p.m. on the 3rd of July, similar to the rise of CS. With a closer look on the chlorophyll satellite data, this was the time when the Celtic Explorer was in the highest plankton bloom until she left the region of high chlorophyll-a values in the evening of the 3rd of July. SO_2 values dropped down to values below the detection limit. SO_2 as one of the oxidation products of DMS showed a long term enhancement up to 80 pptv in areas of high plankton bloom and dropped down to values of 20 pptv, when the ship left these areas.

Chlorophyll

DMS representing a potential precursor of SO_2 was not measured during the cruise, so all assumptions of high DMS emissions have to be based on high chlorophyll-values. F 7.6 shows the satellite chlorophyll-a fluorescence data in the right panel OceanColor-Web by NASA [Draxler and Rolph, 2003] and in the left panel the course of the ship from midday of the 2nd of July 2006 till midnight of the 4th of July. Highest biological activity can therefore be attributed to the 2nd and 3rd of July, while the 4th of July was already in a less active area of plankton bloom. The two situations might therefore be taken for comparison of high plankton bloom and low plankton bloom. This however cannot be related to areas of high and low DMS emissions since up to now a correlation between the two factors has not been proved. One

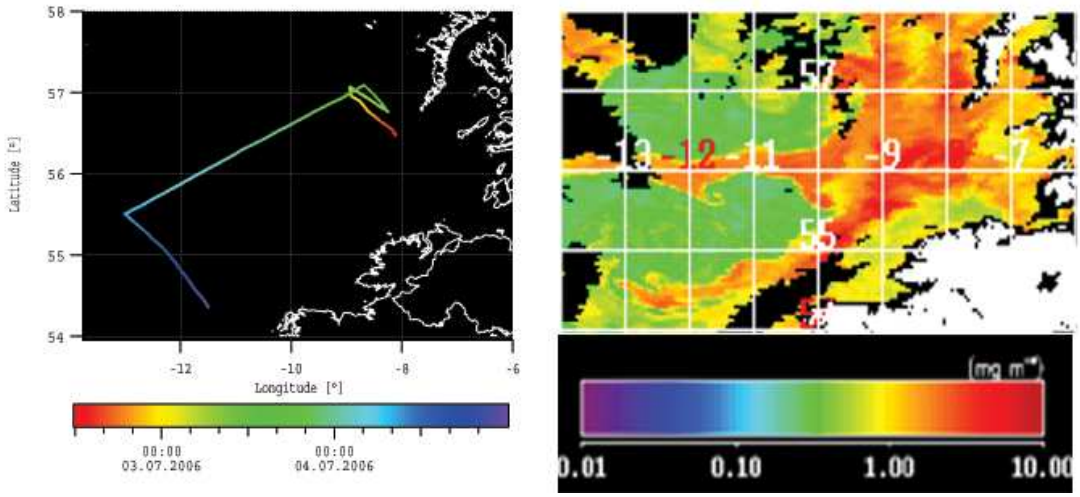

Figure 7.6: Chlorophyll satellite data taken from OceanColor-Web by NASA [Draxler and Rolph, 2003] and the course of the Celtic Explorer from midday of the 2nd of July in regions of high chlorophyll (10 mg m^{-3}) to midnight of the 4th of July with lower chlorophyll values (<1 mg m^{-3}).

problem that complicates the comparison of DMS emissions with chlorophyll-a observations is that chlorophyll fluorescence is caused by all algae while DMS emissions is restricted to certain algae species. Recent measurements of the ratio of chlorophyll-a and DMS emissions have shown a great variability due to different plankton species [Amouroux et al., 2002]. Furthermore fluorescence of plants was observed to increase not only in highly productive times of a plant's lifetime but also if the plant was under stress.

However, plankton samples were taken during the cruise and analyzed in the laboratory. The most abundant species found was a coccolithophore named Emiliania huxleyi (Ehux), which produces 100 times more DMS than related species such as diatoms [Matrai and Keller, 1993]. In conclusion one can say that in general chlorophyll fluorescence measured by satellite data or water samples may in general not be representative for DMS emission rates but for the present case chlorophyll can be taken as an indicator, since the respective species found is known to be a strong DMS emitter. Chlorophyll water samples showed in general high fluorescence with increased values only on the 1st of July during the coastal approach, thus reflecting higher plankton density near the coast. Atmospheric concentrations of H_2SO_4 and MSA were probably influenced by aerosol scavenging (high alkalinity of the aerosols decreases the vapor pressure of MSA and H_2SO_4 and will be discussed in the next section) and therefore showed no increase on this day.

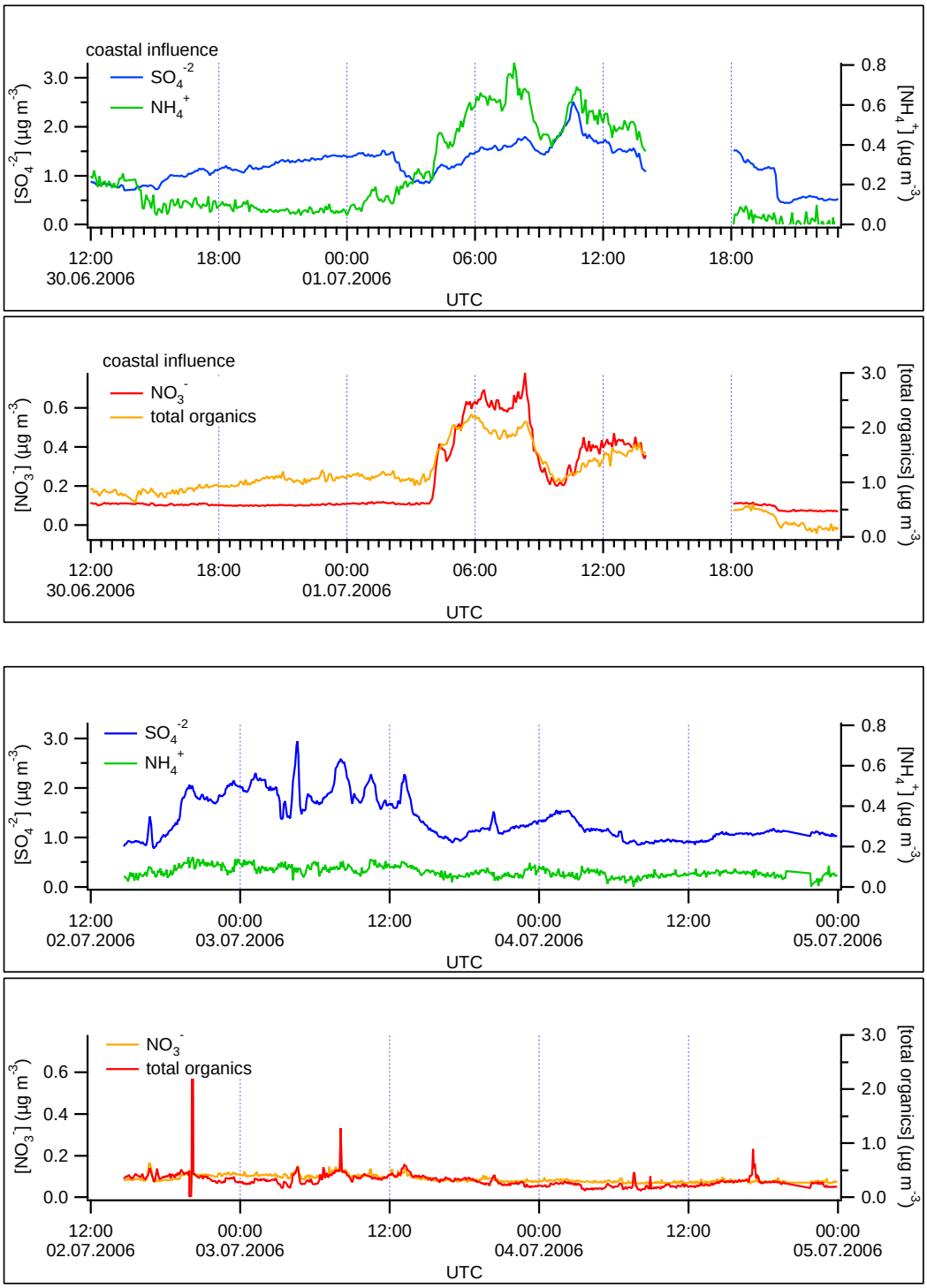

Figure 7.7: Sulphate, nitrate, ammonia and total organics measured by the AMS of the University of Manchester. During the coastal approach on the 1st of July all aerosol constituents are increased, while the 2nd and 3rd only show an enhancement of sulphate ions, correlating with an increased SO_2 concentration in the gas phase

7.3 Methanesulfonic Acid

MSA exceeded H_2SO_4 values most of the time by an order of magnitude with an average value of 2.0 $\cdot 10^7 cm^{-3}$ and stayed above the detection limit of 3.4 $\cdot 10^6 cm^{-3}$ on most days. This stands in big contrast to continental measurements performed in Finland by our group described in [Scholz, 2004] where concentrations only once reached values of $1 \cdot 10^6 cm^{-3}$ but stayed most of the time below 5.6 $\cdot 10^5 cm^{-3}$.

Diurnal patterns were rarely observed and did not correlate with UV radiation.
Panel 1 in F 7.8 shows the daily values of MSA plotted over the local time minus 1 hour. MSA concentrations were highest on the 13th of June with values above 1.0 $\cdot 10^8 cm^{-3}$. Although concentrations during the hours of sunlight were about 50% higher than during the night, they stayed constantly high at night with values above 1 $\cdot 10^7 cm^{-3}$.
This illustrates the different formation and loss mechanisms of H_2SO_4 and MSA and their different lifetimes in the MBL. MSA does not seem to be produced instantaneously by OH radicals, which are expected to be strongly correlated with the UV radiation. UV radiation had its maximum around 12 p.m., while the maximum concentrations of MSA often appeared to be shifted to afternoon and early evening times. Loss through aerosol scavenging seems to be less effective for MSA than it is for H_2SO_4 since values are high throughout the day and decrease only slowly at night. Similar observations have been made by [Jefferson et al., 1998], who estimated a 4 to 7 times longer lifetime of MSA compared to H_2SO_4 due to a smaller accommodation coefficient (α(MSA)= 0.12 [De Bruyn et al., 1994] and ($\alpha(H_2SO_4) \simeq$ 0.6 [Lucas and Prinn, 2002]) Thus the transition of gaseous MSA into the particulate phase is less effective than for H_2SO_4.

MSA data acquired in coastal areas [Davis et al., 1998],[Berresheim et al., 2002] were on average more than one order of magnitude lower but comparable to concentrations measured during the cruise at days when the coast was in sight. MSA concentrations during the 1st of July dropped down to values below the detection limit. Also a short term increase in CS, as observed on the 30th of June, results in a decline of MSA concentrations (see appendix). The concentration values on the 5th of July demonstrate that a mixture of continental and coastal air/polluted air can still be enriched in MSA. Possible production mechanisms involving NO_3 may have contributed to the enhanced values on this day. NO_3 has been named to be only of importance during night and in polluted air masses. NO_x signatures, detected at mass 62 (NO_3^-), were clearly marked in the spectra of the second ITMS (see appendix). Similar

explanations are valid in the case of the 13th of June when NO_3^- values were enhanced too. In clean marine air, these signatures were however one order of magnitude lower. Continental influence or combustion processes do not necessarily decrease concentrations, in fact they can even contribute to the formation of MSA, but they form a very large sink by providing additional surface for fast condensation.

Mostly clean air masses were encountered during the cruise, which may explain the high MSA values. In conclusion one can say that gaseous MSA is generally higher in remote marine areas than along the coast.

The third panel in F 7.8 exhibits an implication to an anti-correlation of MSA and relative humidity. This effect has been described by [Mauldin III et al., 1999] and reflects the increased volatility of MSA with decreasing RH. On most days this effect is very small, except for the 13th of June. The vapor pressure of MSA has been observed to only increase significantly at relative humidities below 70%. Observations comprise only values with RH above 60%. RH below 70 % has only been recorded on the 13th of June and in this case stand in good agreement with measurements performed by [Mauldin III et al., 1999]. The effect of particle neutralization upon MSA vapor pressure is reflected in panel 2 of figure 7.8. With decreasing particle neutralization, reflected in the mass load of NH_4^+ measured with the AMS, MSA increases, implicating that less MSA condenses on pre-existing particles with low alkalinity but instead stays in the gas phase.

An analysis of the data acquired during the selected days reveals a certain trend of MSA enhancement that can also be seen in the CS and SO_2 data (F 7.3). Concentrations start to increase at noon of the 2nd of July and decrease after 6 p.m. on the 3rd of July, when the Celtic Explorer left the area of high plankton bloom. MSA concentration did not drop during that night but remain almost constant at concentrations as high as 3.5 $\cdot 10^7 cm^{-3}$. Relative humidity dropped on the 2nd of July from RH =90% to 80% until the early afternoon of the 3nd and continued its decline down to 70% until midnight of the 4th of July.
Halocarbon measurements in the water show enhanced values of bromoform ($CHBr_3$)(see appendix). The photolytic destruction of bromoform leads (via multiple steps) to the formation of BrO which again takes part in the addition pathway of DMS oxidation
[von Glasow and Crutzen, 2004]. (see chapter 2). This might be a possible explanation for the enhancement of MSA during these days. Unfortunately BrO has not been measured, so this assumption is only based on measurements of its precursor and does not take into account possible loss mechanisms or other reaction pathways. Further possible explanations may comprise downwelling of dry, MSA enriched air from layers above the MBL as reported

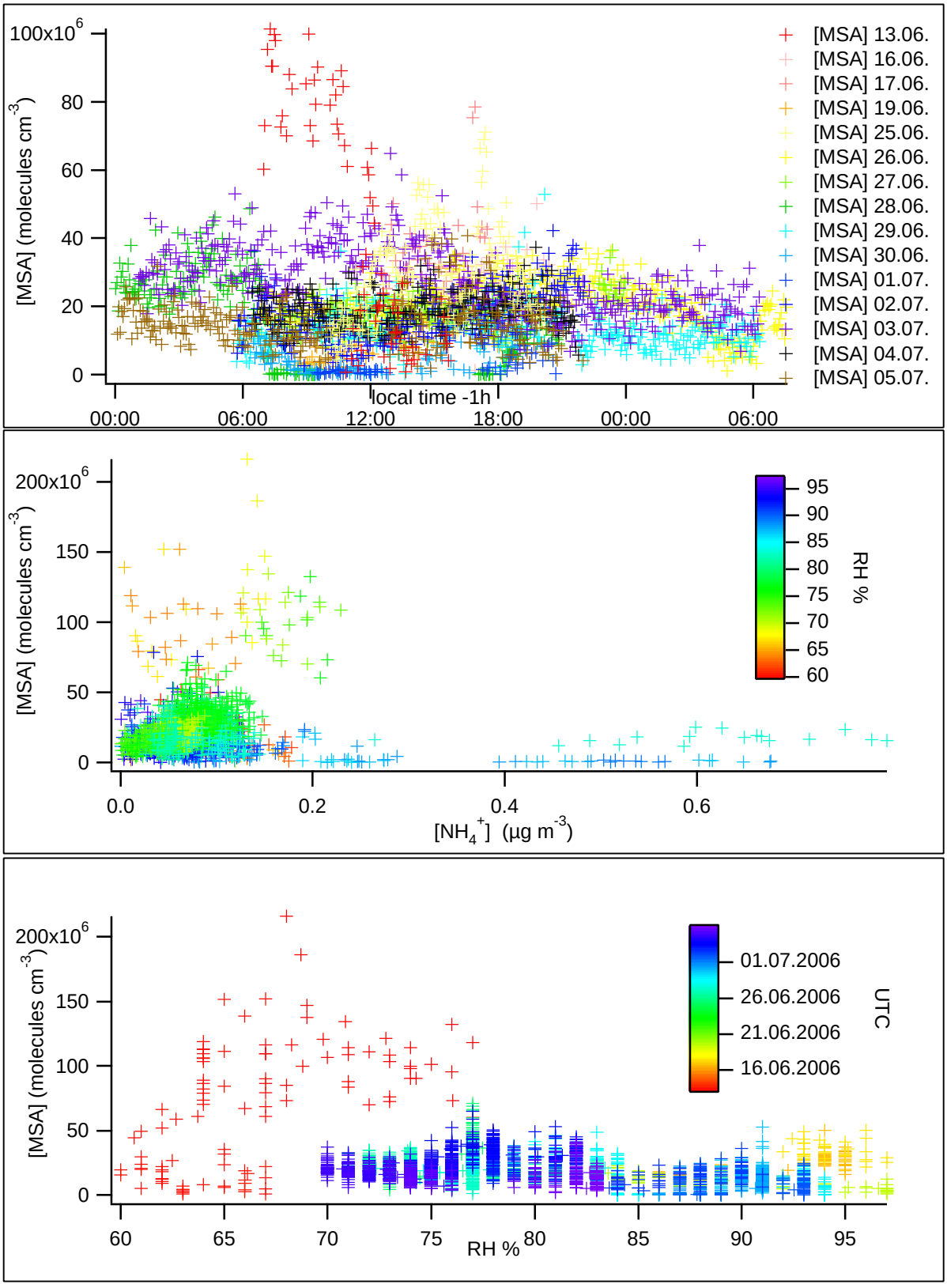

Figure 7.8: Panel 1 shows MSA concentrations plotted vs local time (-1h) for all days. Panel 2 shows the a scatterplot of MSA with NH_4^+ concentration (measured by the University of Manchester) in the aerosol (the color code represents the relative humidity). Panel 3 shows a scatter plot of MSA concentration with relative humidity

by [Davis et al., 1998] and [Jefferson et al., 1998]. Less aerosol surface in higher altitudes extends the lifetimes of MSA and its precursor. During airborne measurements of MSA and H_2SO_4 reported by [Lucas and Prinn, 2002] higher concentrations of MSA have been observed at altitudes of 3km.
On the 4th of July values of MSA dropped down to concentrations of $2 \cdot 10^7 cm^{-3}$ and stayed constant. Thus the values obtained during the 3rd of July are almost higher by a factor of two.

Scatter plots of all sulfur containing gases and particulate matter show a positive correlation in 3 of 4 cases shown in F 7.10. These plots do not contain values recorded during pollution events, assigned by the above discussed criteria and comprise only the selected days of July.
A weak linear correlation has been found between concentrations of MSA and SO_2 with a correlation of R=0.46 shown in F 7.10. The correlation coefficient was determined by means of linear regression. It measures the linearity between two variables X and Y. R^2 represents the quota of the variance of Y that is predicted by X. A better agreement shows the linear fit of MSA and sulphate, with R=0.65. Sulfuric acid shows no correlation trend with sulphate and SO_2 and sulfate have the weakest correlation coefficient of R=0.26.
The formation of non-sea-salt sulfate (NSS) in aerosols occurs through three known mechanisms, condensation of gaseous H_2SO_4, aqueous phase oxidation of SO_2 in cloud droplets and wet aerosols, and aqueous oxidation of MS^- to SO_4^-. Considering the low concentrations of H_2SO_4 in the gaseous phase, high sulfate concentrations reflect the efficient uptake by aerosols and can be regarded as the major sink. According to [Jefferson et al., 1998] most of the sulfate (of the precursor SO_2 and H_2SO_4) is expected to reside in particles with diameters smaller than 0.5 μm. The observed dominant mode was at 80nm, thus a factor of 4 smaller than needed.
According to [Huebert et al., 1993] MSA is being deposited on larger particles than the NSS with diameters of 1 to 1.5 μm, corresponding to diameters of sea salt particles. Low wind speeds of only 3 to 5 m/s lowered sea salt particle formation during these days therefore small loss rates due to aerosol scavenging may explain high MSA concentrations. Further comparison to particulate MSA will give more insight on the phase transition mechanism. Impactor samples were taken during the cruise but were not evaluated up to the day of the termination of this thesis.

In general one can observe that all sulfur components, whether gaseous or particulate

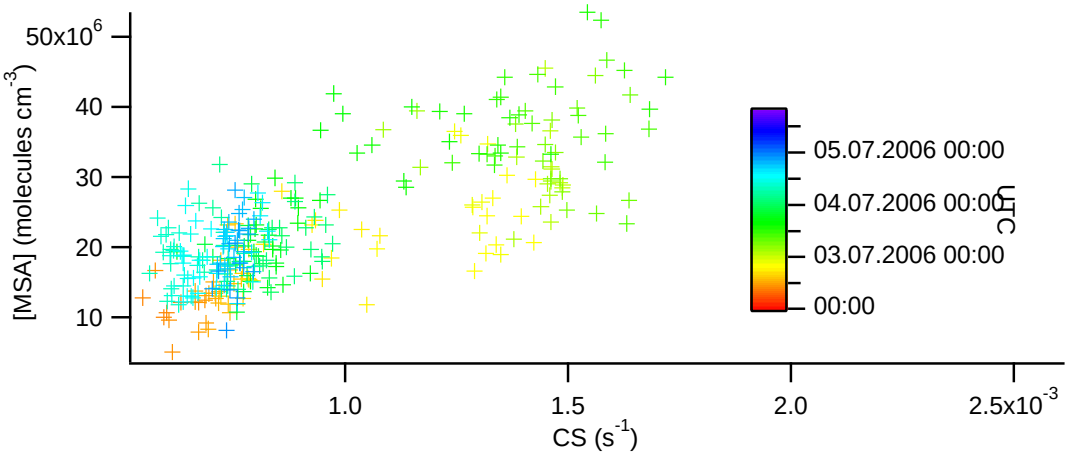

Figure 7.9: MSA (MPI-K) plotted vs the condensation sink (provided by the University of Manchester) for the selected days of July

show a simultaneous enhancement during the 2nd and 3rd of July, implicating that their common precursor is presumably DMS. High values were observed for all components in areas of high chlorophyll values and decreased (under similar weather conditions) to values of background concentrations.

A very counterintuitive observation has been made concerning the increase of MSA with a simultaneous increase in CS as shown in F 7.9.

The effect is counterintuitive since the increase of CS reflects an increase of aerosol surface by which gaseous MSA is removed through condensation. A possible explanation could be the evaporation of particulate MSA inside the sampling line. RH was reduced inside the sampling line due to a temperature gradient of about 20^oC with respect to ambient temperature. Heating belts kept the sampling flow at temperatures around 36^oC, which corresponds to a RH of 25%. A low concentration of ammonium ions which was observed on this day would support the idea, since the vapor pressure of MSA is decreased over a neutralized particle. Inhibited condensation onto pre-existing particles might also explain the high concentrations. The condensation sink showed a relative enhancement but with low absolute values.
Considering the large fraction of MSA production in the aqueous phase (see chapter 2) the high MSA values acquired during the cruise could be explained by phase transition from the particulate to the gaseous phase inside the flow reactor. A high volatility of MSA in the

atmosphere has been observed at RH around 20% [Mauldin III et al., 1999]. For a better understanding of these phase transitions further laboratory experiments have to be carried out.

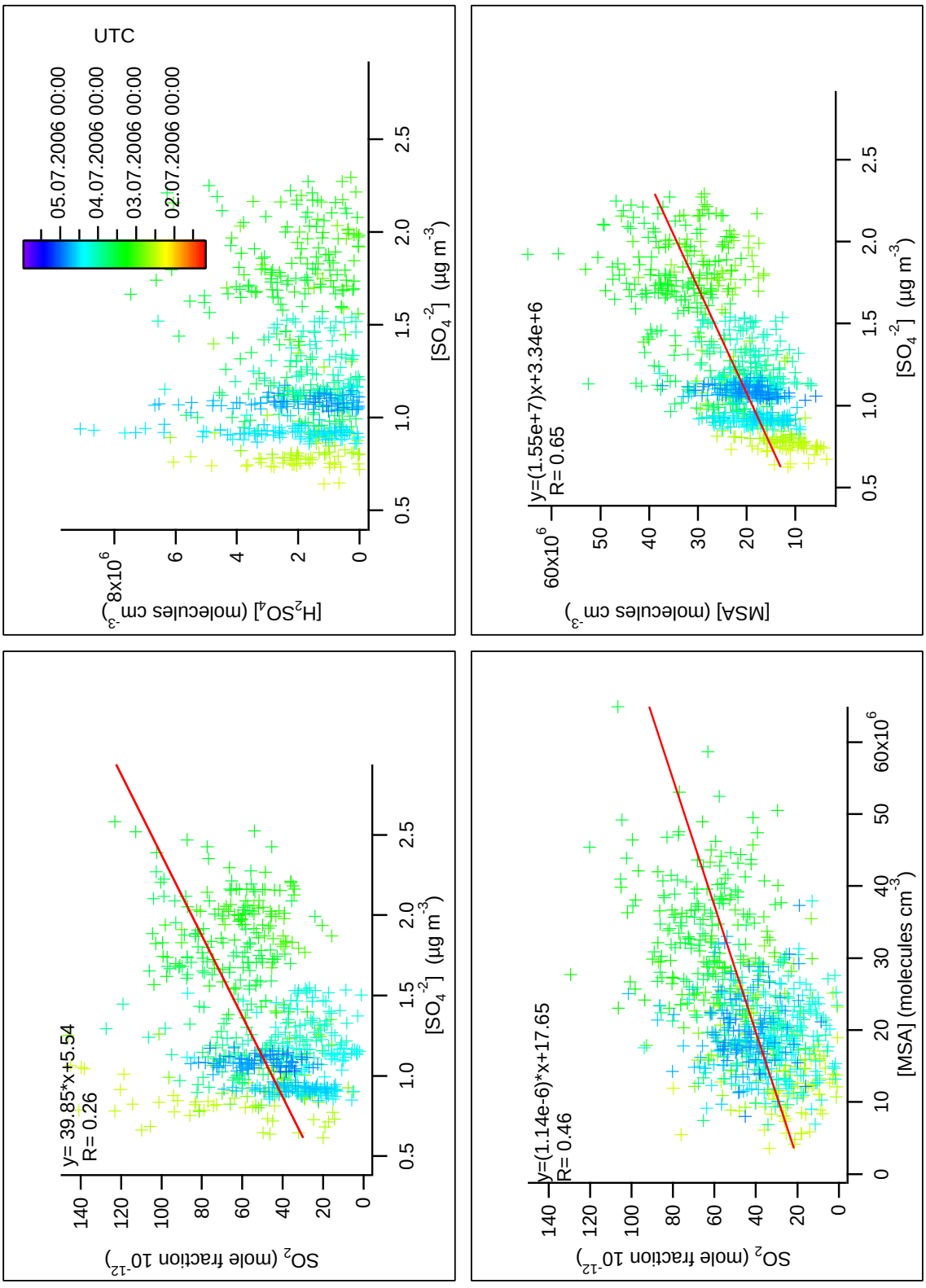

Figure 7.10: Scatterplots of the sulfur components in gaseous and particulate form. Except for H_2SO_4 all components show a strong correlation thus indicating that their precursor is of the same origin

Chapter 8

Conclusions and Perspectives

Measurements of sulfuric acid and methanesulfonic acid have been successfully carried out during a 21-day cruise on the Atlantic ocean in the season of high plankton bloom. The mounting of a sea-container and first application of the IT-CIMS-method by our group on a research vessel was described and discussed in detail. Problems that appeared during the operation of the instrument were discussed. Due to high relative humidity the sensitivity of the instrument was lowered. As a consequence detection limits comprised values of $\sim 1 \cdot 10^6 \mathrm{cm}^{-3}$. By heating the sampling line the efficiency of the the detection method was improved but might have provoked the evaporation of the particulate matter. Further laboratory work may help to understand the processes of evaporation and condensation onto sampling line walls at high relative humidities.

The actual objective of the campaign MAP was partly fulfilled, since only one nucleation event was observed, thus leaving many questions about the impact of DMS emissions or other aerosol precursors onto aerosol- and cloud formation over the ocean. Indications on the participation of sulfuric acid in the observed event are striking but cannot be specified at the present level of data evaluation. Iodine measurements have to be compared to H_2SO_4 measurements. Thus further investigation concerning the triggering elements of this event might lead to a better understanding of particle formation over the ocean. However the data set is in general insufficient for a broad analysis of nucleation over the ocean. Further field measurements raise the possibility to obtain a clear picture of appearance and evolution of nucleation.

Sources and sinks of sulfuric acid and methanesulfonic acid have been discussed and compared to similar measurements performed in the Marine Boundary Layer. H_2SO_4-concentrations were in general very low compared to continental sites which might be a possible explana-

tion that only one case of nucleation was observed. A steady state calculation indicates the reason for these low concentrations: low SO_2-concentrations. Especially enhanced night time values are difficult to explain. Since photochemistry is deactivated only vertical entrainment, degassing from the container surface or aerosol evaporation inside the flow reactor might account for an explanation. MSA on the other hand showed some of the highest values reported in literature. MSA exhibited a weak anti-correlation with RH and particle neutralization by NH_3.

Due to bad weather conditions during the first leg of the cruise, mainly data of the second leg were discussed with a focus on the last three sunny days in July. The course of the ship was maintained in areas of high plankton bloom during two of the three days, thus a good comparison of MSA production in the plankton bloom and outside the areas of high algae density was achieved. The enhancement of MSA was also reflected in the particle composition and all sulfur components, gaseous and particulate, except for H_2SO_4 showed a linear correlation. A coastal influence was discussed and leads to the assumption that combustion processes have a versatile influence on MSA production and loss: Both effects have been observed in the presence of polluted air.

These contradictory effects however might be of future research interest, clarifying the different loss and production mechanisms that lead to MSA production by DMS oxidation. Laboratory studies of the detection of DMS and intermediate products such as DMSO, as well as simultaneous measurements of additional oxidation candidates such as BrO and hydroxyl radicals might enlighten the different production pathways of MSA. Furthermore multi-phase reactions and transition of MSA from particulate to the gaseous phase are not fully understood yet. Simultaneous measurements of gaseous MSA and particulate MSA usind CIMS and an AMS could be of helpful to understand these processes.

The measurements give a small insight in the chemistry of remote marine air, contributing to the question of the validity of the CLAW hypothesis, proposed by Charlson, Lovelock, Andreae and Warren [Charlson et al., 1987], yet leaving the discussion on cloud formation over the ocean vital and filled with new questions.

Appendix A

Experimental Data

The following pages comprise the MSA(g) and H_2SO_4(g)-concentrations, the UV-radiation, and the SO_2 mole fraction measured by the MPI-K and the condensation sink calculated from aerosol size distribution measured by the University of Helsinki during the whole cruise. The data are presented in daily intervals, taking into account certain, varying measurement periods with the corresponding background corrections. SO_2 mole fractions are evaluated by Anke Roiger (DLR) and Heinfried Aufmhoff (MPI-K) and have been averaged over 5 spectra. The condensation sink and the UV-radiation are shown in Panel 3 of the daily figures and are colored in black and grey, respectively.

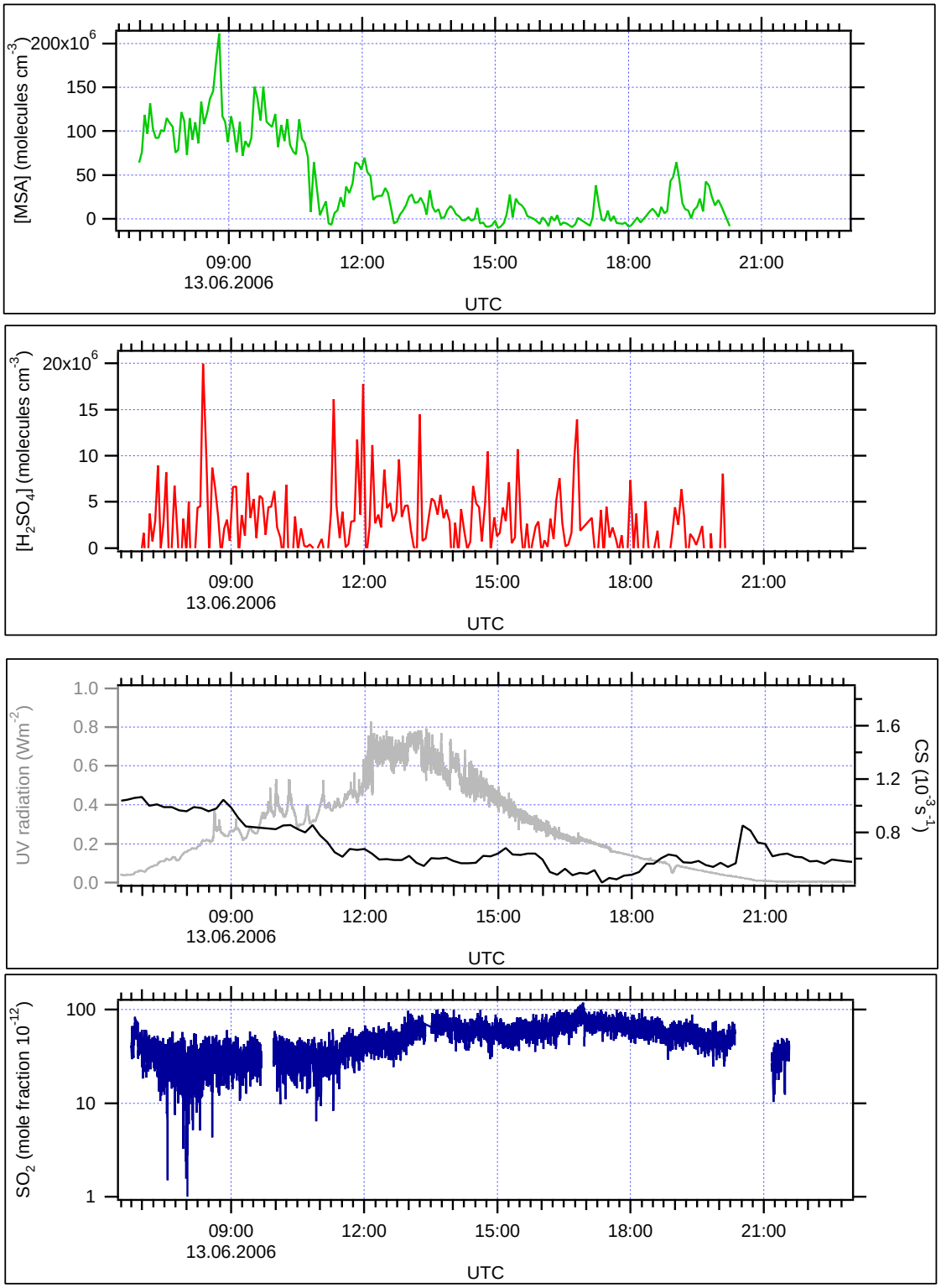

Figure A.1: MSA, H_2SO_4, UV radiation (grey) (MPI-K) and CS (black) (University of Helsinki), SO_2 (averaged over 5 mass spectra) (MPI-K) during 13.06.2006. The 13th of June was the only day when nucleation was observed

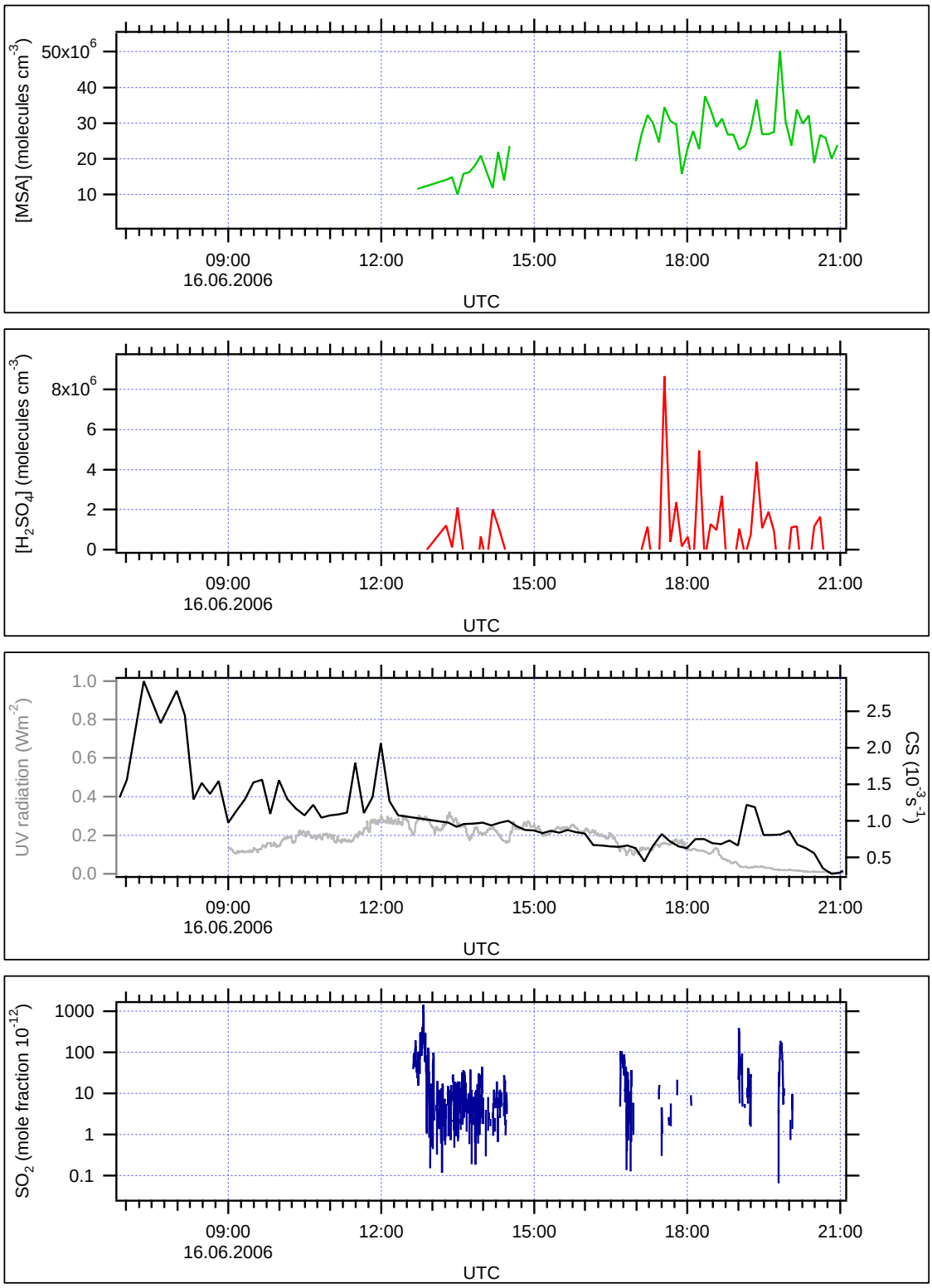

Figure A.2: MSA, H_2SO_4, UV radiation (grey) (MPI-K) and CS (black) (University of Helsinki), SO_2 (averaged over 5 mass spectra) (MPI-K) during 16.06.2006.

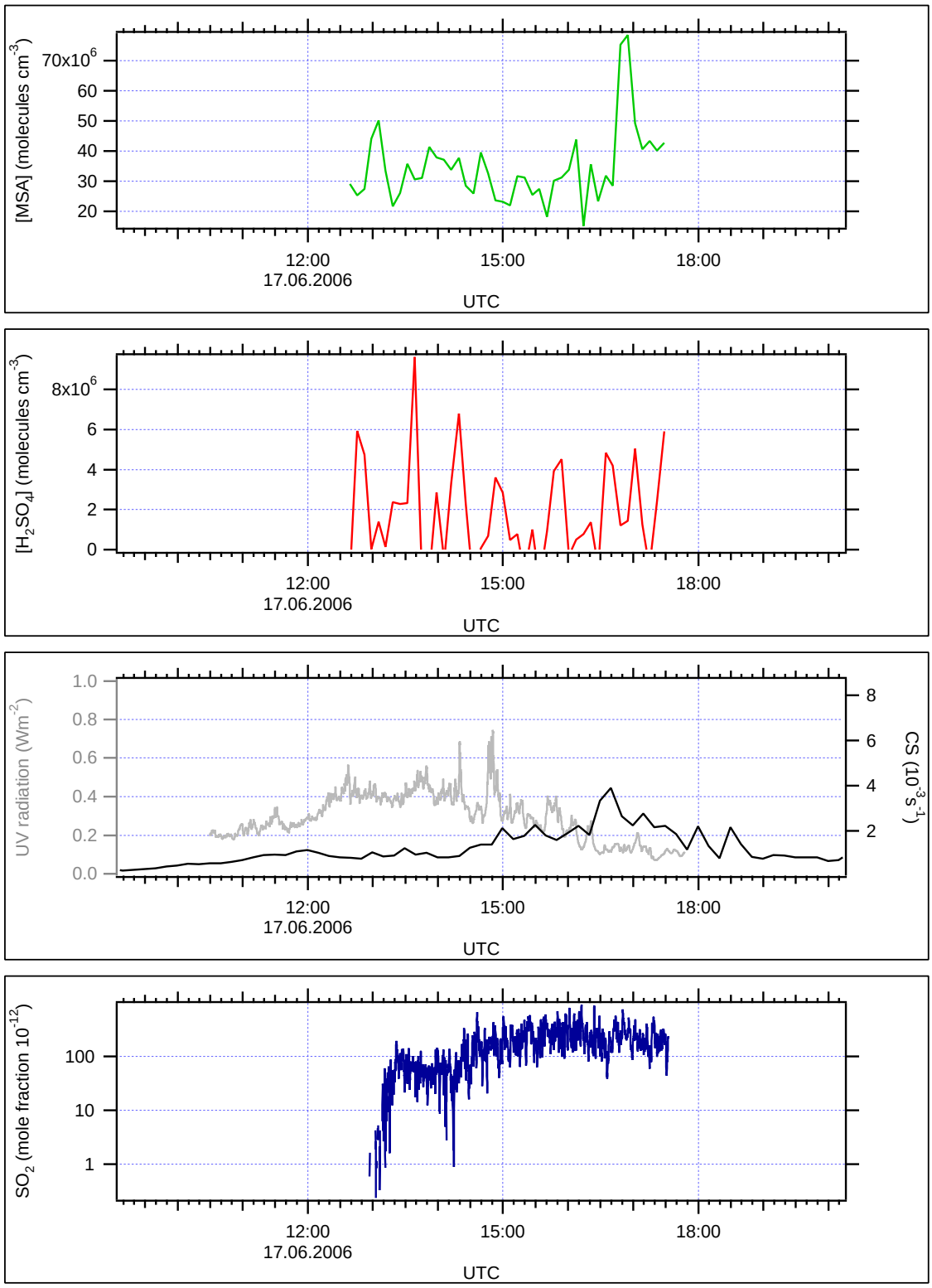

Figure A.3: MSA, H_2SO_4, UV radiation (grey) (MPI-K) and CS (black) (University of Helsinki), SO_2 (averaged over 5 mass spectra) (MPI-K) during 17.06.2006.

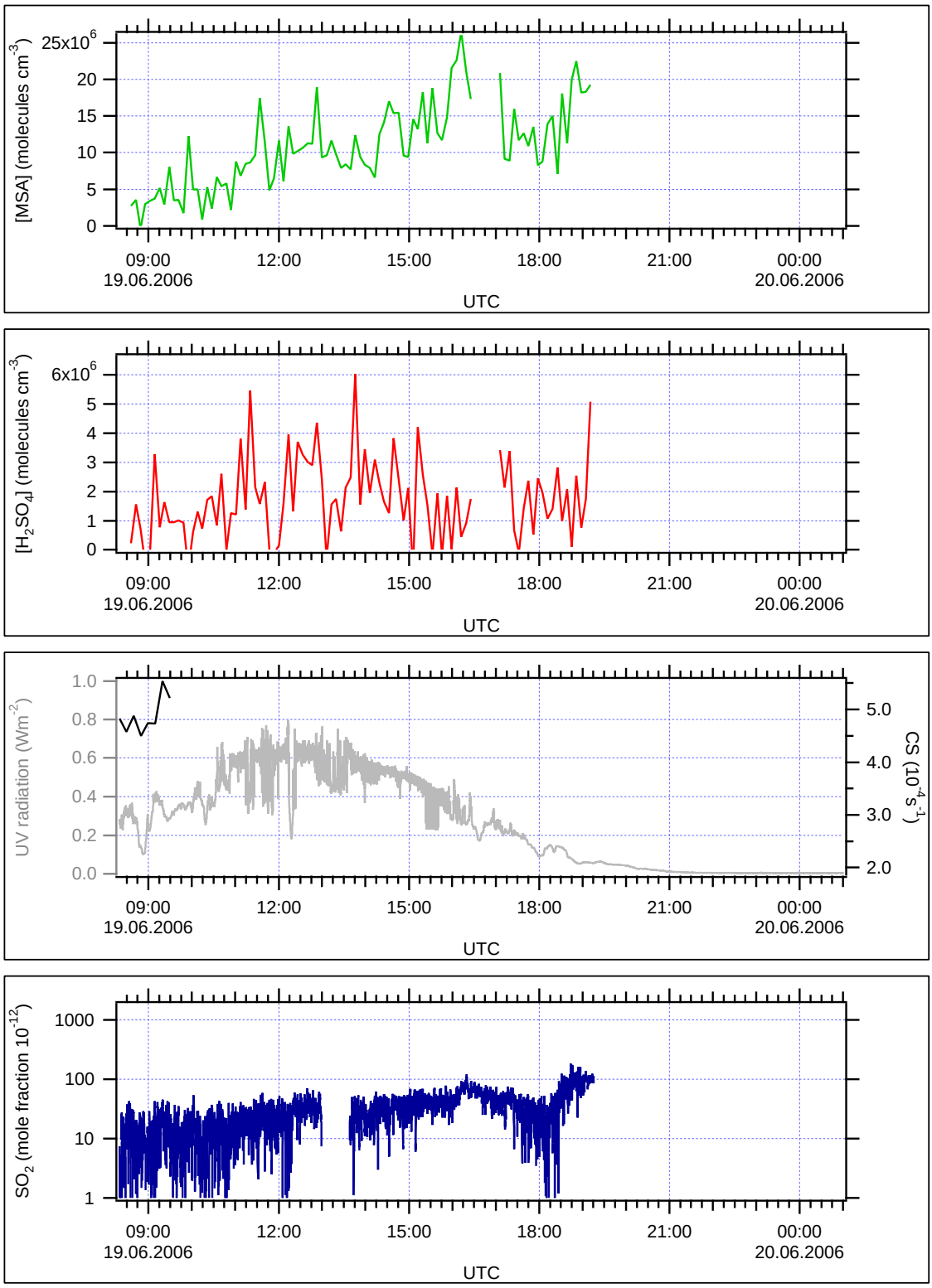

Figure A.4: MSA, H_2SO_4, UV radiation (grey) (MPI-K) and CS (black) (University of Helsinki), SO_2 (averaged over 5 mass spectra) (MPI-K) during 19.06.2006.

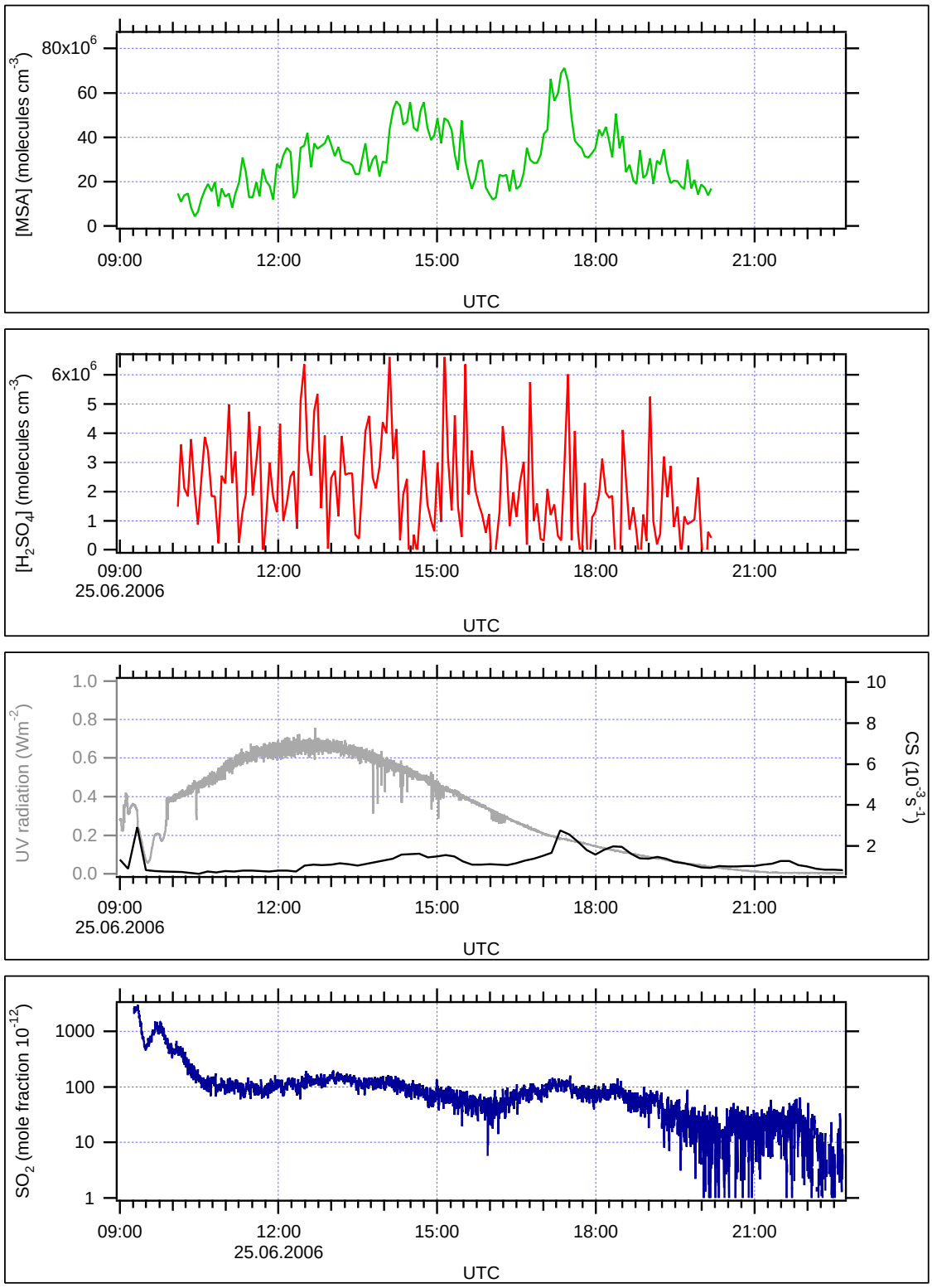

Figure A.5: MSA, H_2SO_4, UV radiation (grey) (MPI-K) and CS (black) (University of Helsinki), SO_2 (averaged over 5 mass spectra) (MPI-K) during 25.06.2006.

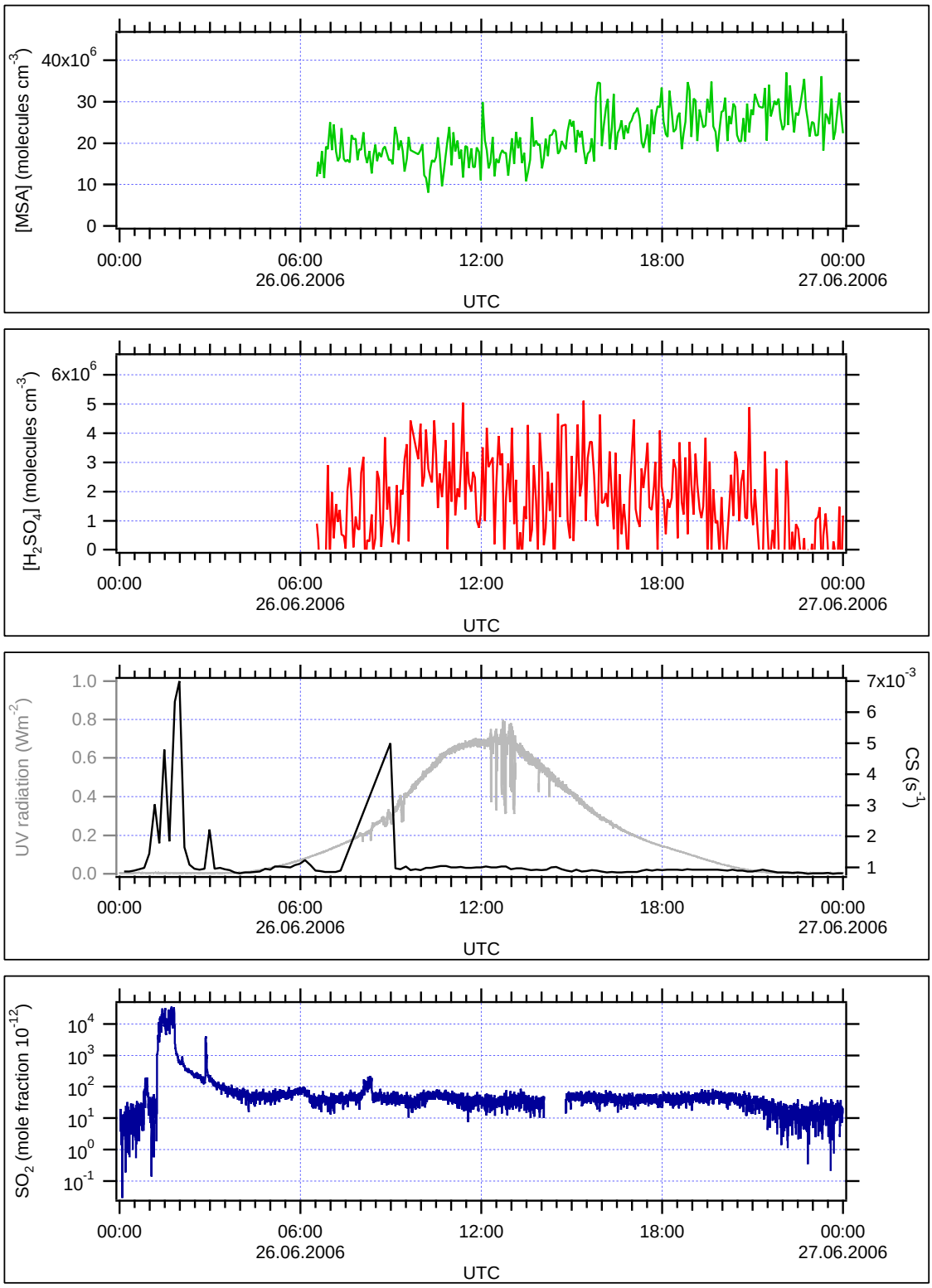

Figure A.6: MSA, H_2SO_4, UV radiation (grey) (MPI-K) and CS (black) (University of Helsinki), SO_2 (averaged over 5 mass spectra) (MPI-K) during 26.06.2006.

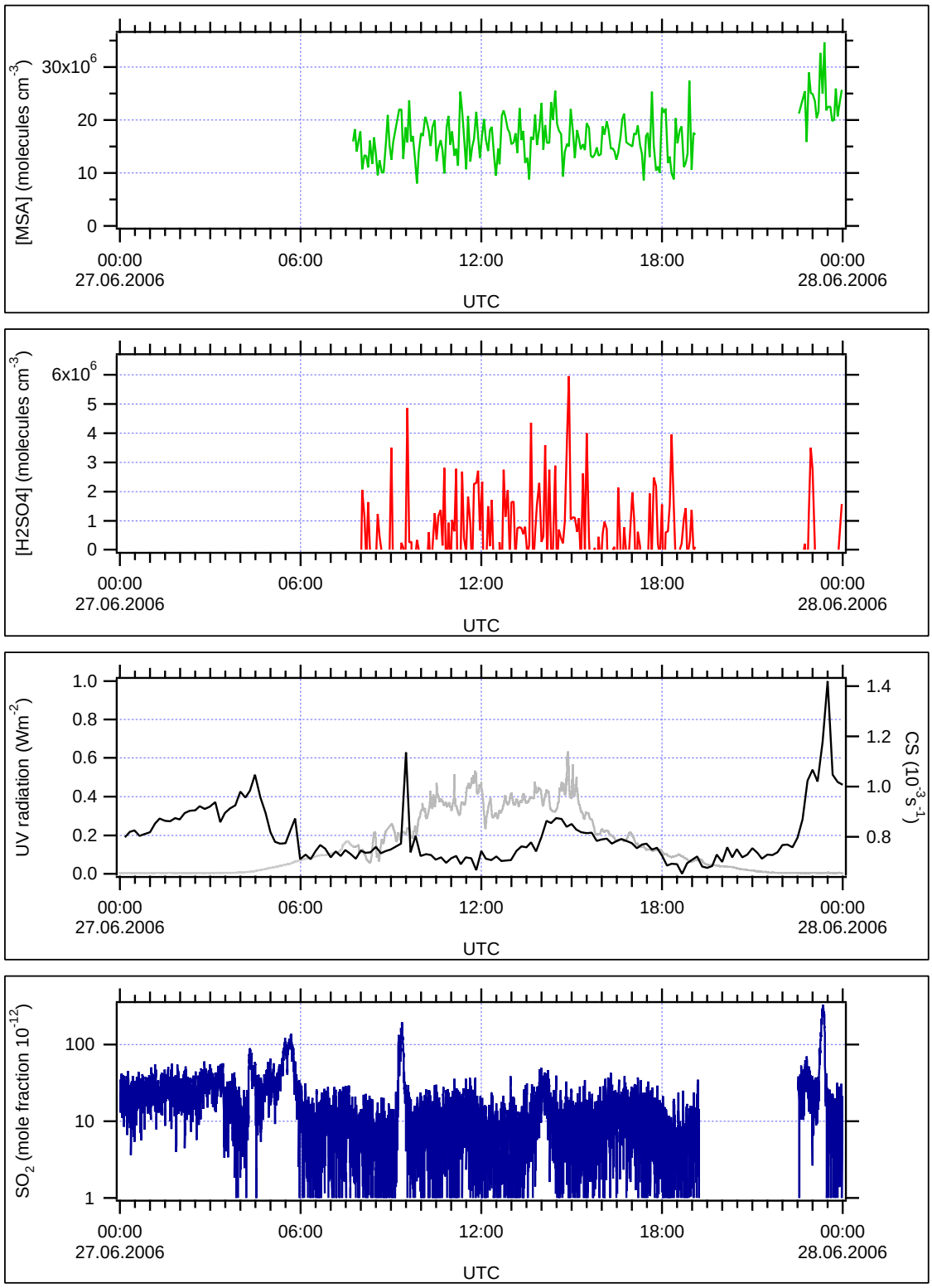

Figure A.7: MSA, H_2SO_4, UV radiation (grey) (MPI-K) and CS (black) (University of Helsinki), SO_2 (averaged over 5 mass spectra) (MPI-K) during 27.06.2006.

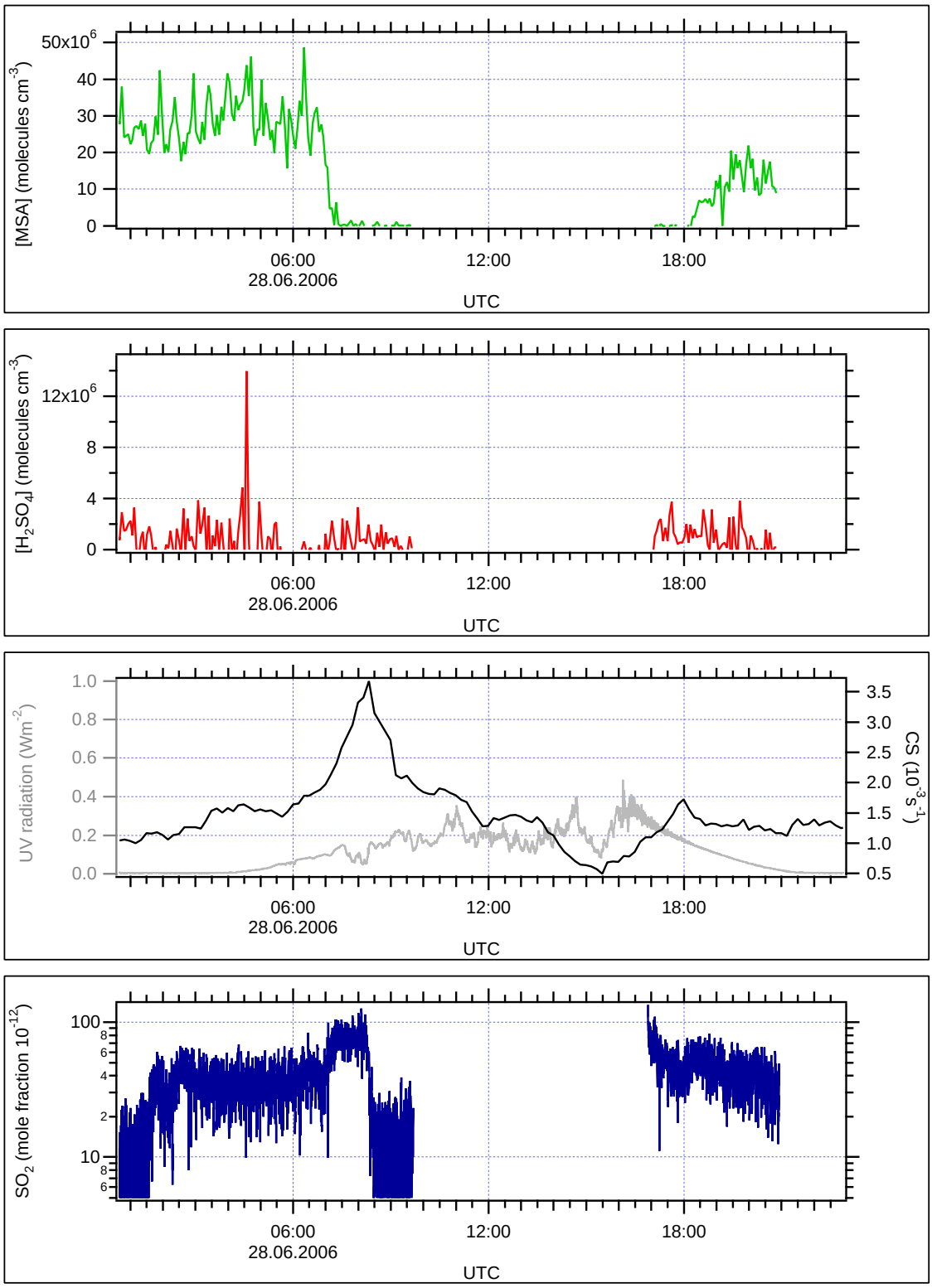

Figure A.8: MSA, H_2SO_4, UV radiation (grey) (MPI-K) and CS (black) (University of Helsinki), SO_2 (averaged over 5 mass spectra) (MPI-K) during 28.06.2006. The data show a clear tendency of MSA reduction with high values of CS.

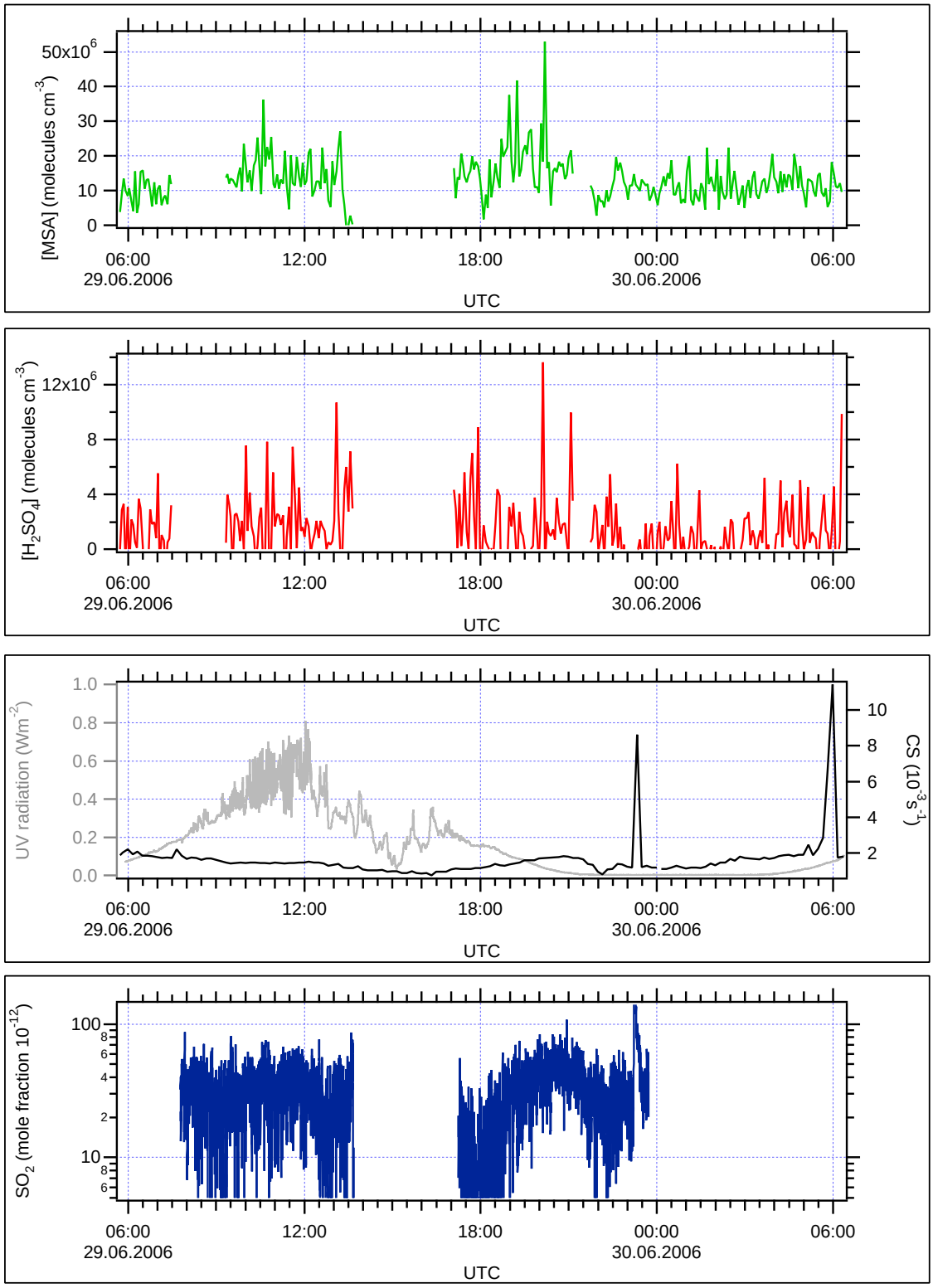

Figure A.9: MSA, H_2SO_4, UV radiation (grey) (MPI-K) and CS (black) (University of Helsinki), SO_2 (averaged over 5 mass spectra) (MPI-K) during 29.06.2006.

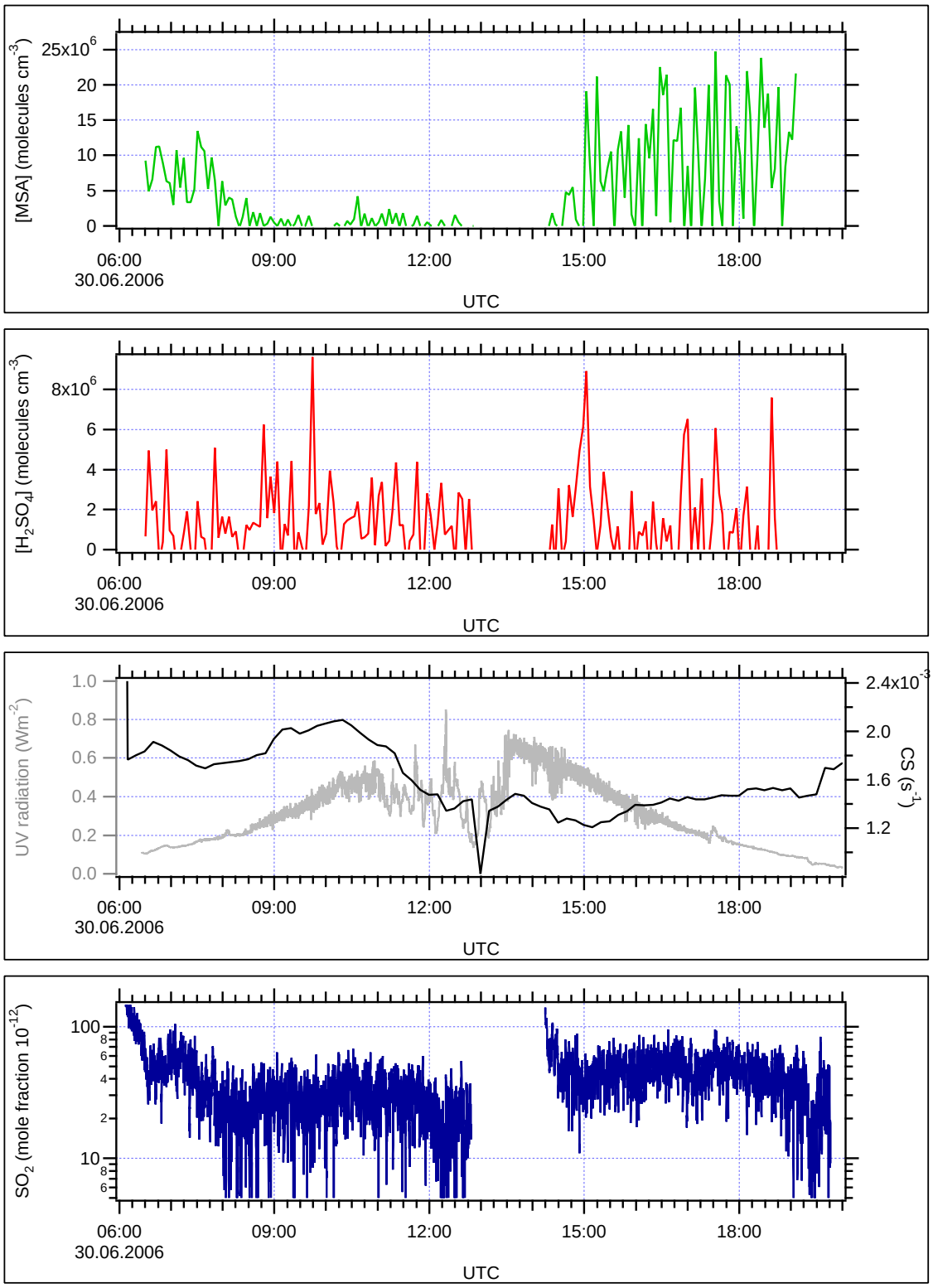

Figure A.10: MSA, H_2SO_4, UV radiation (grey) (MPI-K) and CS (black) (University of Helsinki), SO_2 (averaged over 5 mass spectra) (MPI-K) during 30.06.2006.

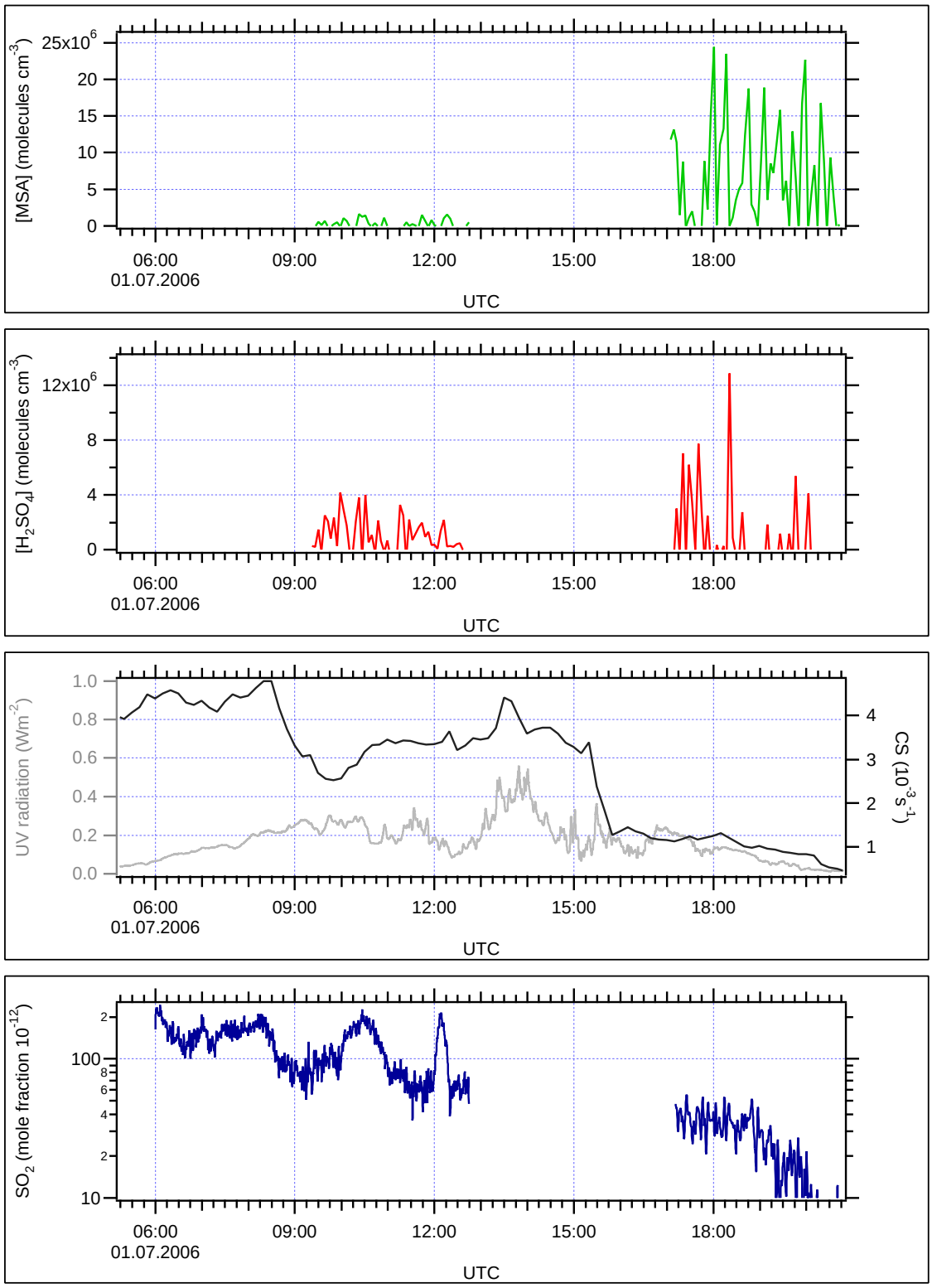

Figure A.11: MSA, H_2SO_4, UV radiation (grey) (MPI-K) and CS (black) (University of Helsinki), SO_2 (averaged over 5 mass spectra) (MPI-K) during 01.07.2006. The course was set along the coast of the Outer Hebridies, Scotland.

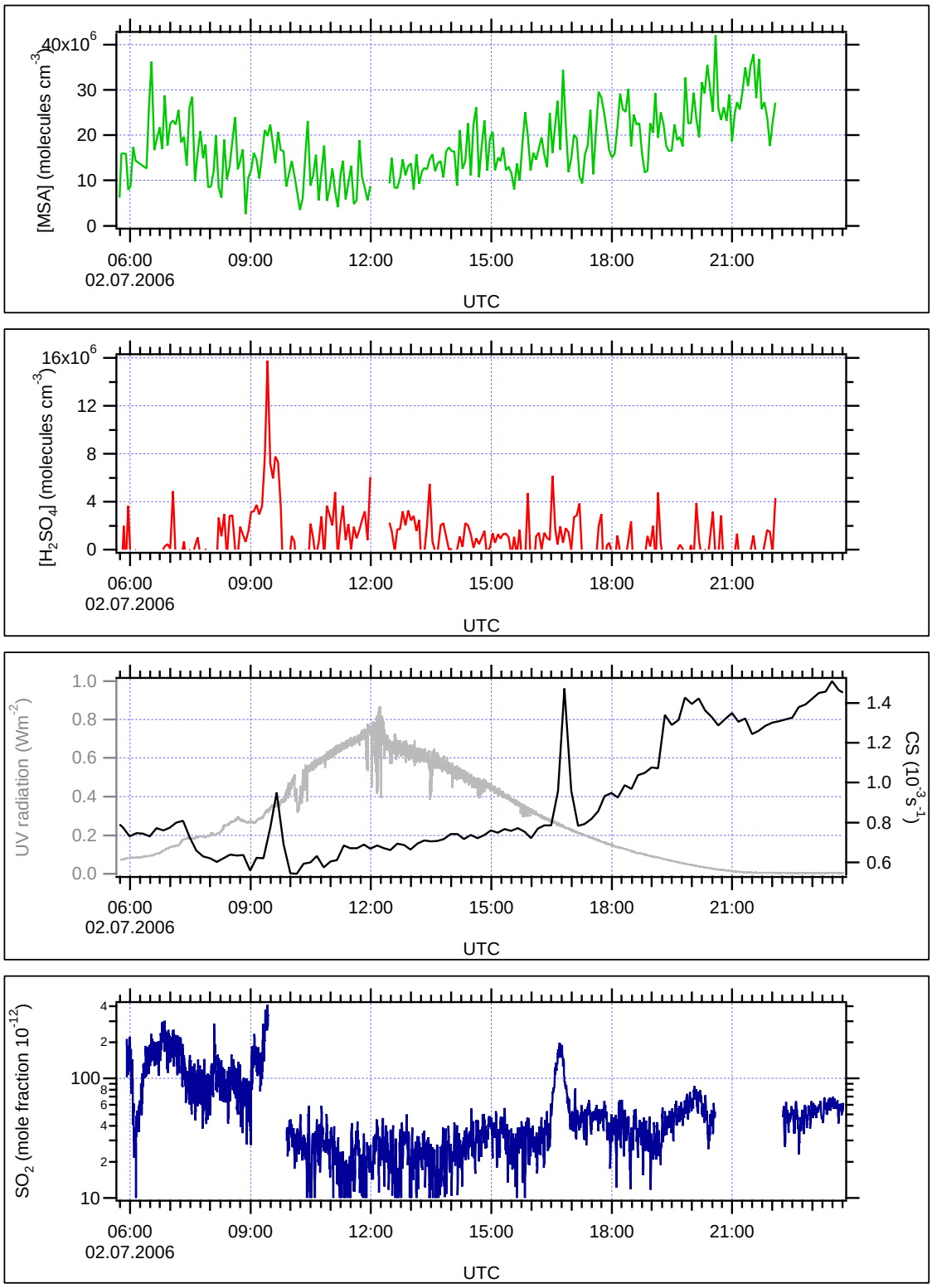

Figure A.12: MSA, H_2SO_4, UV radiation (grey) (MPI-K) and CS (black) (University of Helsinki), SO_2 (averaged over 5 mass spectra) (MPI-K) during 02.07.2006.

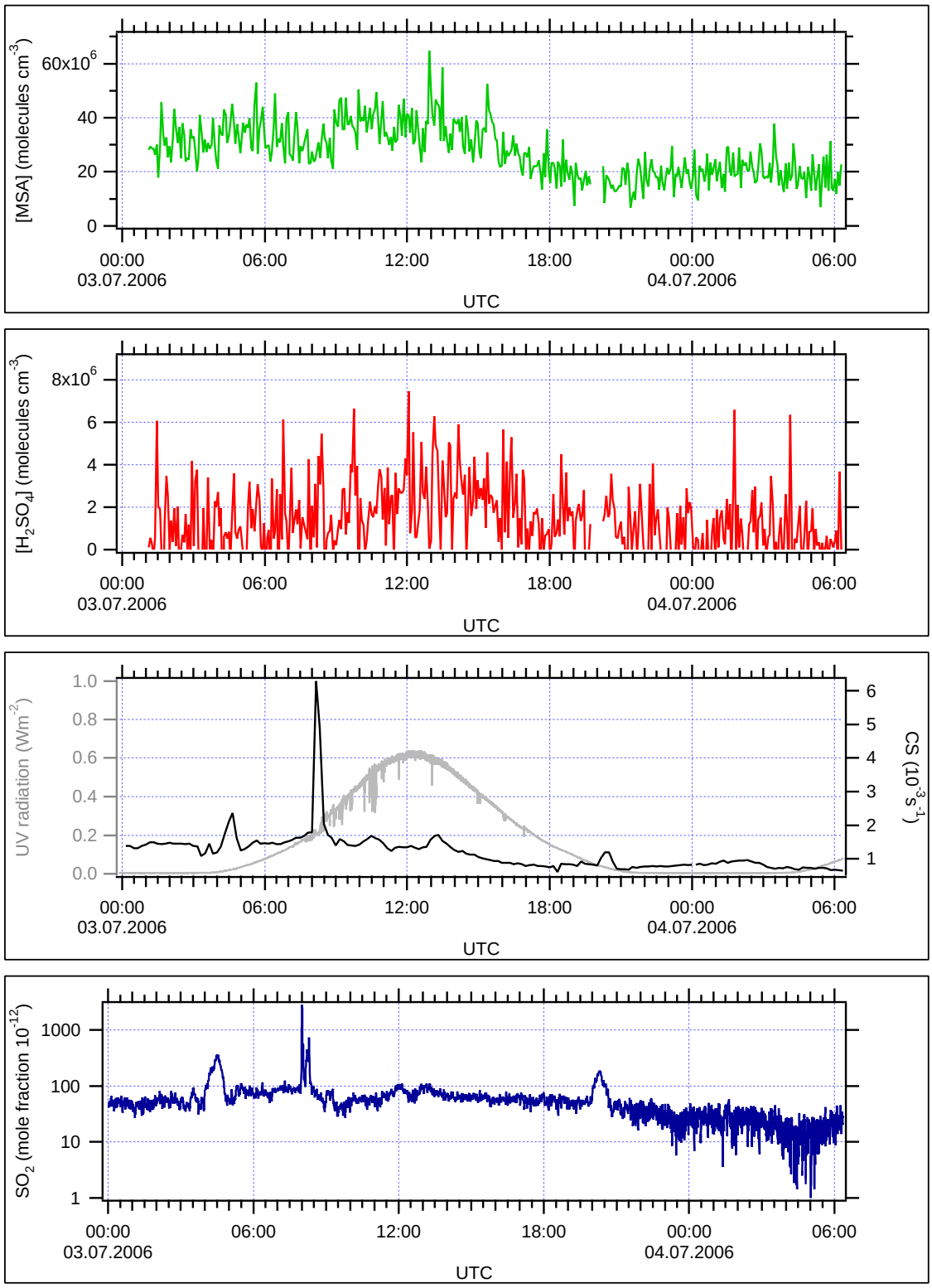

Figure A.13: MSA, H_2SO_4, UV radiation (grey) (MPI-K) and CS (black) (University of Helsinki), SO_2 (averaged over 5 mass spectra) (MPI-K) during 03.07.2006.

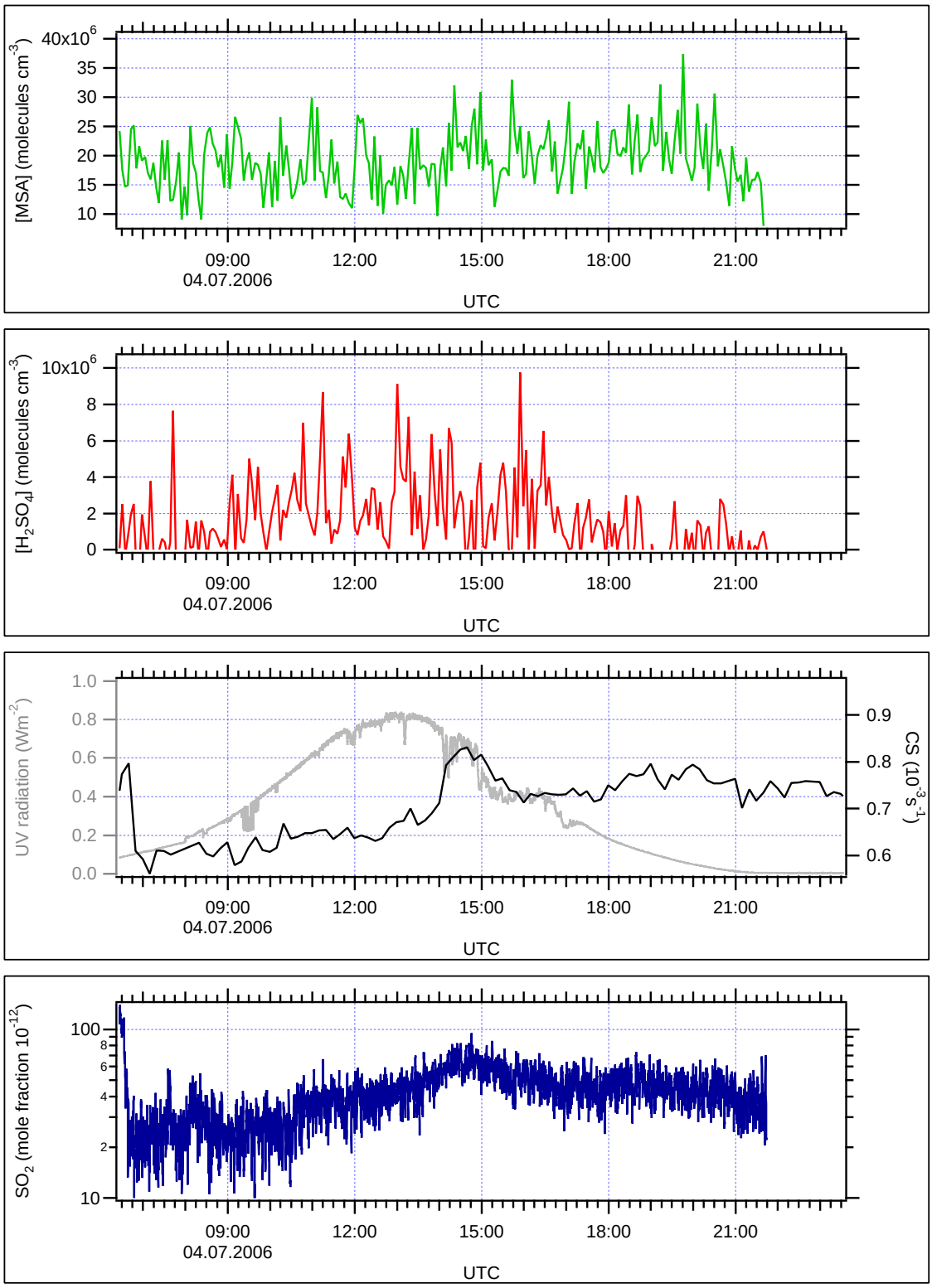

Figure A.14: MSA, H_2SO_4, UV radiation (grey) (MPI-K) and CS (black) (University of Helsinki), SO_2 (averaged over 5 mass spectra) (MPI-K) during 04.07.2006.

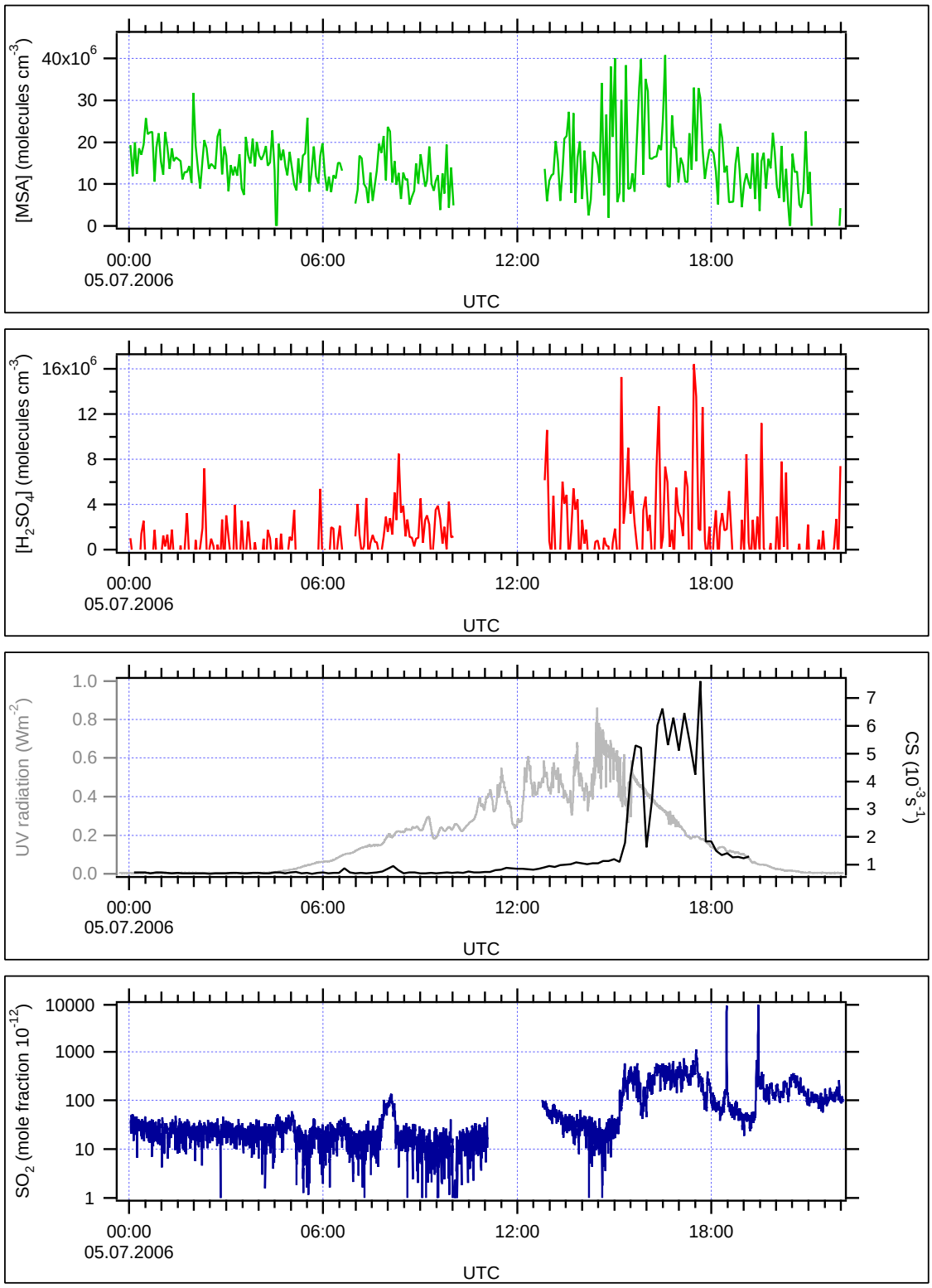

Figure A.15: MSA, H_2SO_4, UV radiation (grey) (MPI-K) and CS (black) (University of Helsinki), SO_2 (averaged over 5 mass spectra) (MPI-K) during 05.07.2006. In the afternoon, the coast of West Ireland near the research station Mace Head was in sight.

A.1 Influence of NO_x

The influence of contamination caused by the ship or air masses coming from the continent is also reflected in the mass m/z = 62 (NO_3^-), measured by the second IT-CIMS instrument. The NO_3^- ions are formed through electron association similar to the production of the educt ions CO_3^- as explained in chapter 6. They can also be produced through the reaction with CO_3^- ions. It is just a qualitative representation of the NO_x-concentration since the instrument is not calibrated and mass m/z 62 cannot be set in relation to an educt mass, since its generation is comparable to the educt mass itself. Therefore it shall be regarded as an indicator if high amounts of NO_x are present. At low concentrations the method may be very inaccurate since background corrections and changes in the instrumental settings were not considered. A comparison of data of different days is therefore associated with a great error.

F A.17 and F A.16 show MSA and H_2SO_4-concentrations and SO_2 mole fractions during the 13th of June and the 5th of July 2006. The 13th of June shows the highest MSA values throughout the cruise and might be associated with DMS oxidation with the help of NO_x, on this day possibly emitted by the ship's exhaust.

The correlation of mass 62 with MSA is not very clear on both days, in fact the highest MSA concentration on the 13th of June appears to be shifted to one hour after the highest NO_x-concentrations were seen. Taking into account that the ship is moving and air masses are changing, the reaction of DMS with NO_x is slow, no direct correlation is expected. A direct influence of NO_x on the MSA concentration is not visible on the 5th of July either but since MSA, NO_x and SO_2 show high values in the afternoon, the air masses could represent a mixture of coastal polluted air and MSA enriched air from the ocean. Again MSA might be high due to oxidation of DMS by NO_3. For comparison the two days 02.07. and 03.07. are included (F A.18 and F A.19). High SO_2 mole fractions are most of the time associated with high count rates of mass 62 if the measurements are influenced by the ship's exhaust. This is shown in the scatterplot of SO_2 and mass 62 in F A.20. However the increase of SO_2 on the 2nd of July as described in chapter 7 is not as pronounced in the timeline of mass 62. This may indicate that high concentrations of SO_2 during the 2nd and 3rd of July are not due to contamination from the ship but of natural origin.

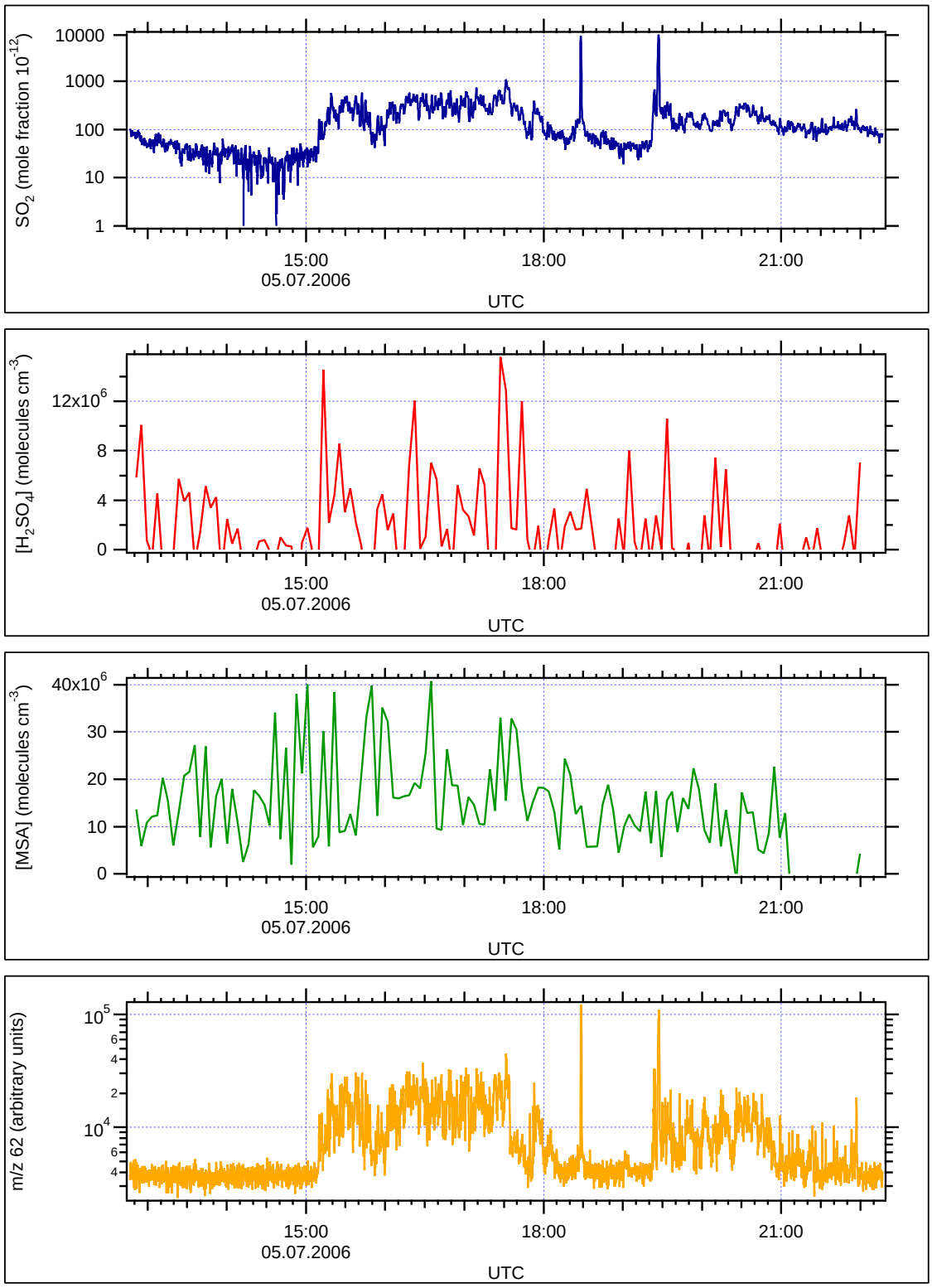

Figure A.16: The concentrations of MSA and H_2SO_4, SO_2 mole fraction during the 5th of July when the measurements were influenced by local pollution (presumably the coast or the ship's exhaust) and the NO_3^- signature at m/z = 62. High NO_x values might explain high MSA concentrations at the coast through oxidation of DMS

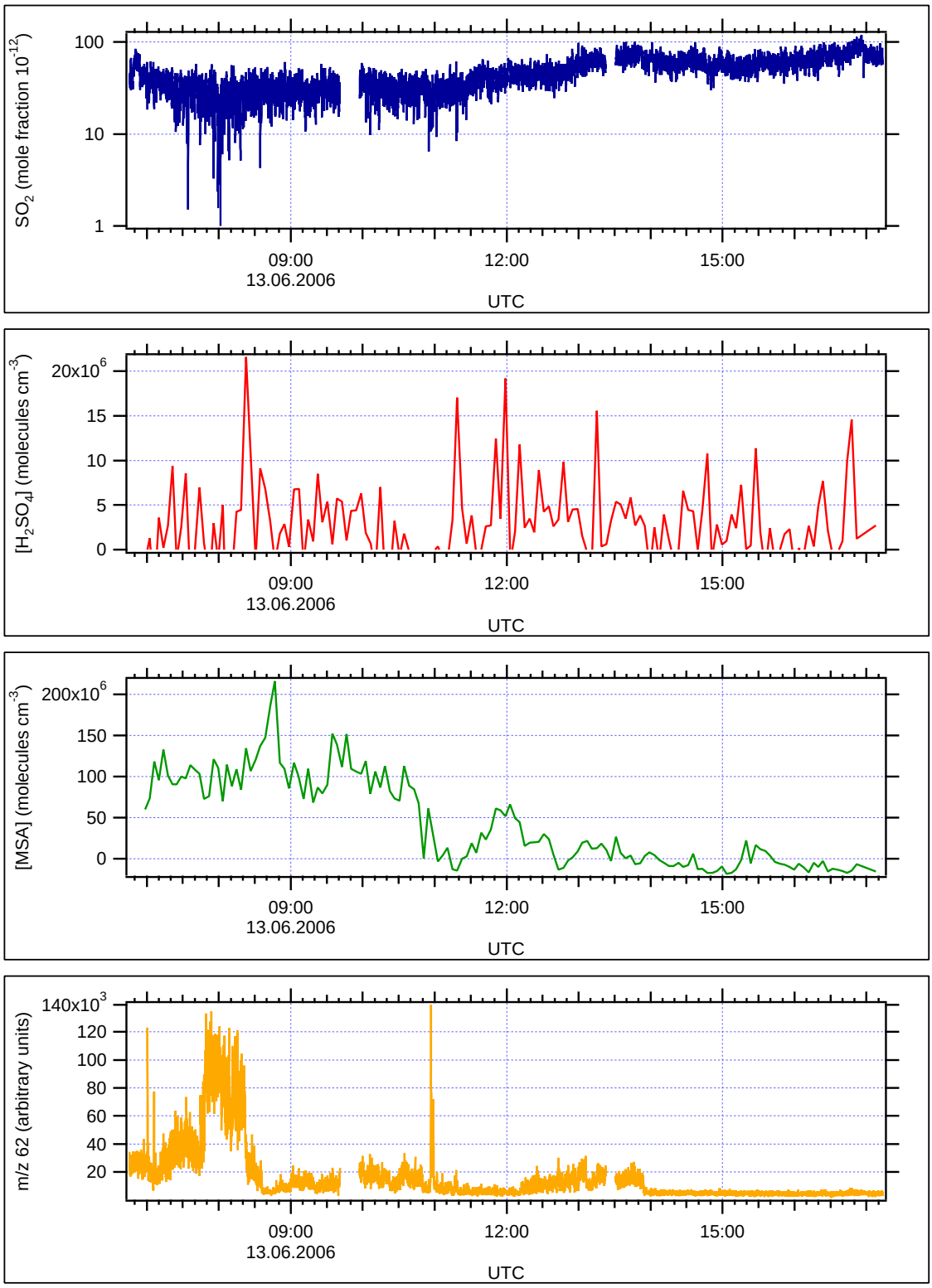

Figure A.17: The concentration of MSA and H_2SO_4, SO_2 mole fraction during the 13th of June and the NO_3^- signature at m/z = 62. Measurements might have been influenced by the ship's exhaust or other sources since only the NO_3^- signature is high. SO_2 does not show the same variations in the morning. MSA concentrations showed the highest values on the 13th of June presumably due to DMS oxidation through NO_3

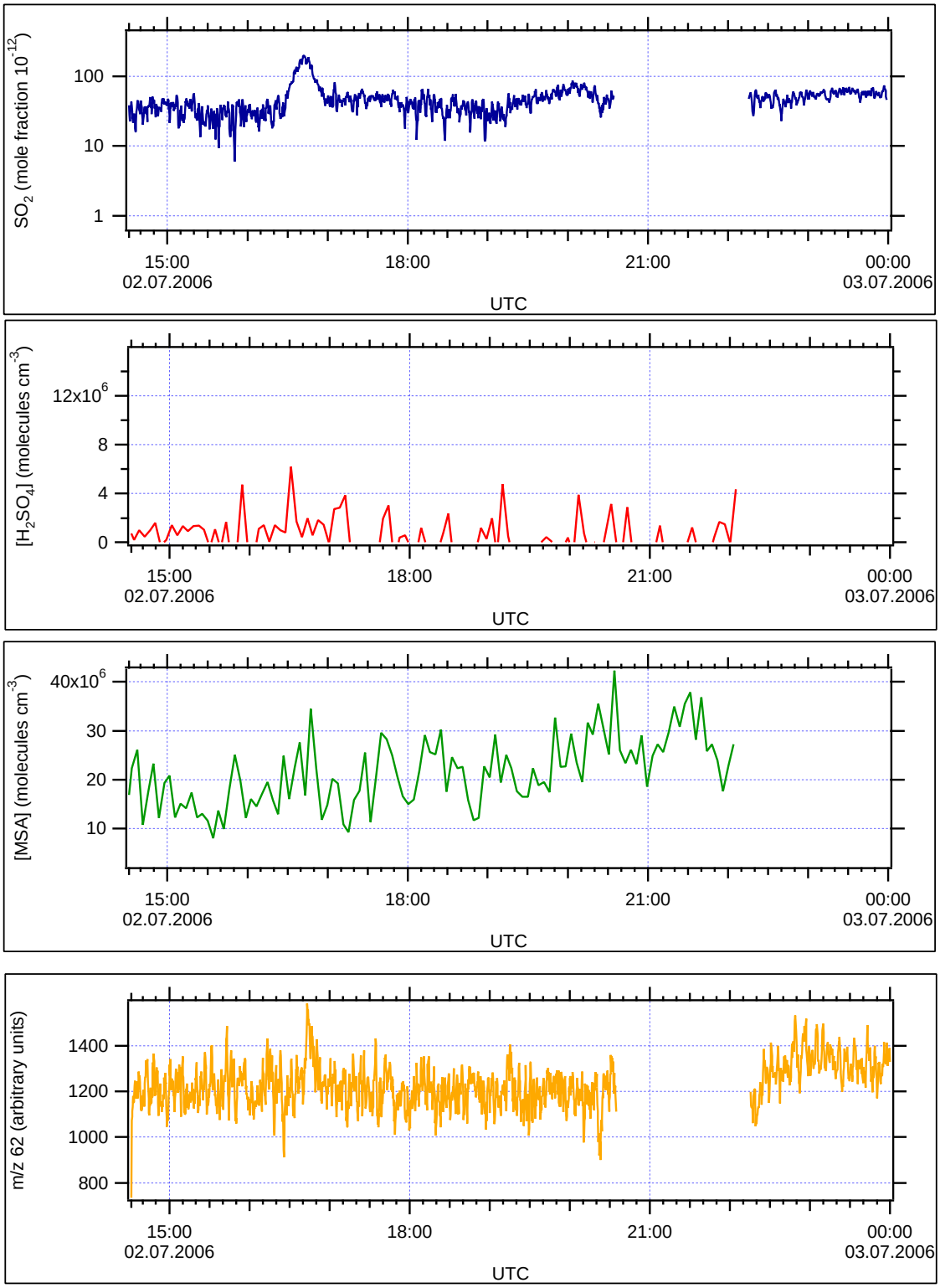

Figure A.18: The concentration of MSA and H_2SO_4, SO_2 mole fraction during the 2nd of July and the NO_3^- signature at m/z = 62.

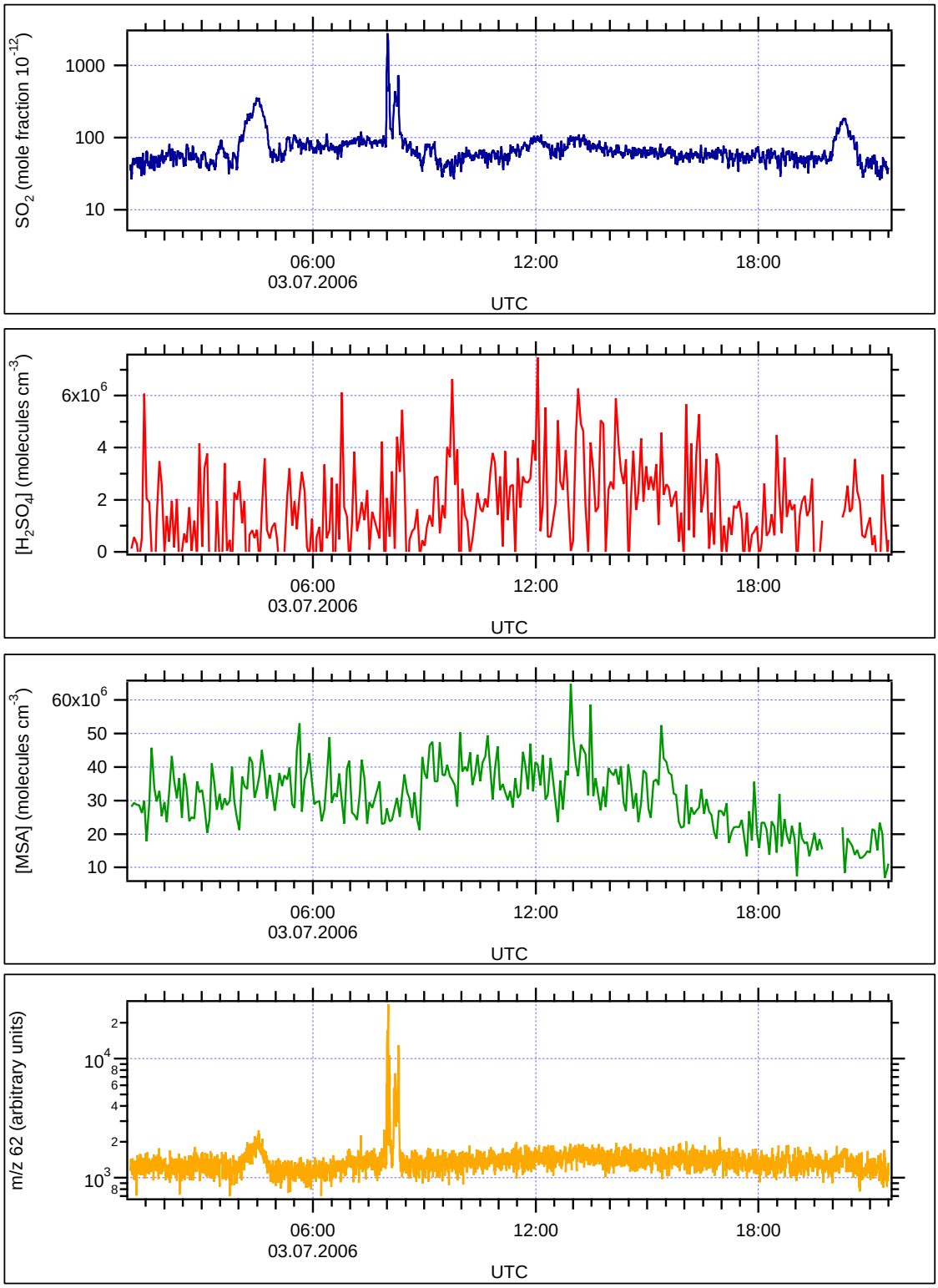

Figure A.19: The concentration of MSA and H_2SO_4, SO_2 mole fraction during the 3nd of July and the NO_3^- signature at m/z = 62.

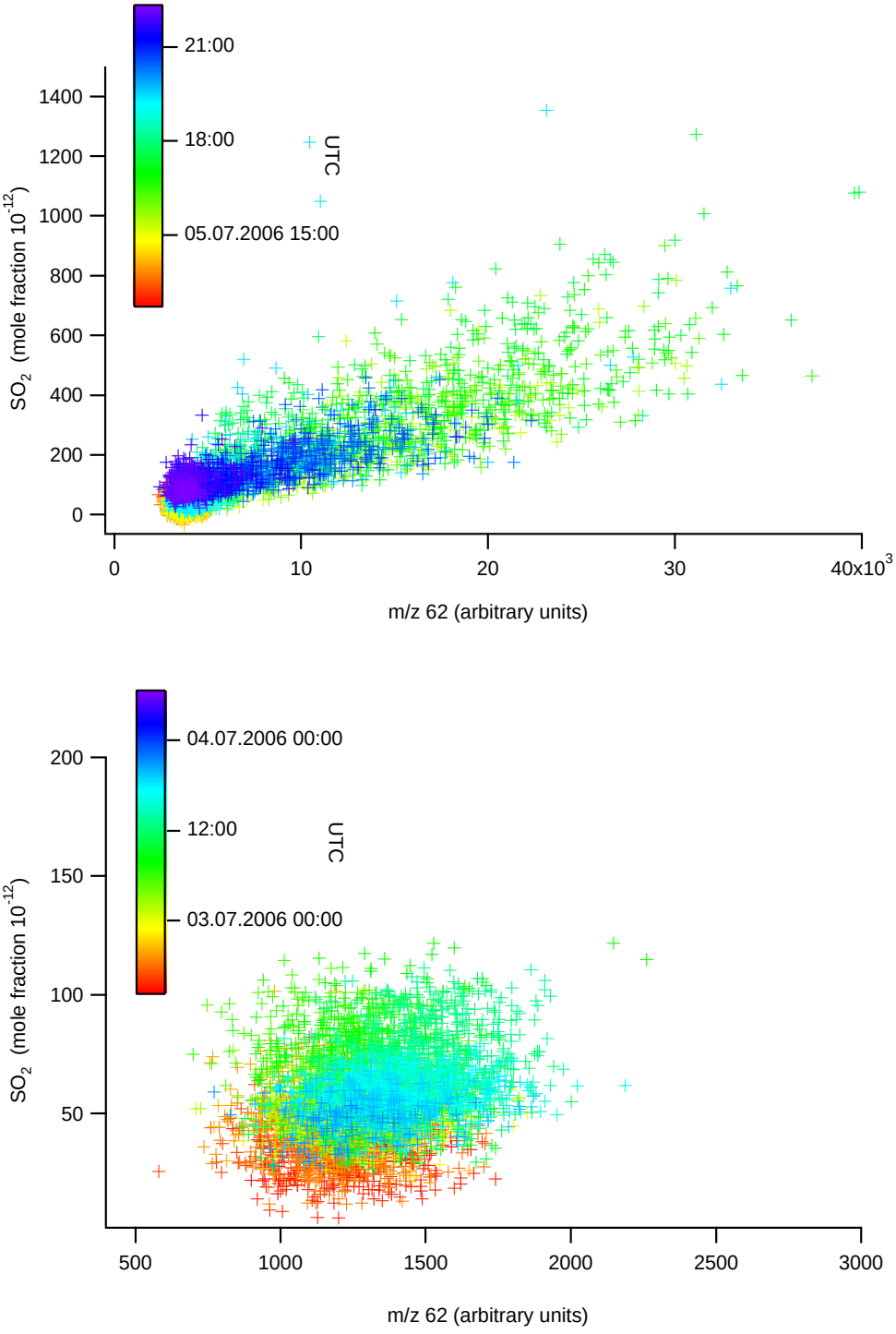

Figure A.20: A scatterplot of SO_2-mole fraction and mass 62 during the afternoon of the 5th of July and the 3rd of July. The positive correlation on the 5th indicates SO_2 and NO_x have the same origin, probably the ship's exhaust. On the 3rd no significant correlations are visible for small values of SO_2. In this scatterplot contamination events with SO_2 mole fractions above 200 ppt, which were only observed on a short time scale, are extracted. This might prove that SO_2 was of biogenic origin and not emitted by the ship's exhaust.

A.2 Experimental Setup

Figure A.21: Above: The Celtic Explorer in the harbor of Killybegs, North of Ireland. The MPI-K container is placed on the front deck while the exhaust is on the after deck. Below: Photograph of the IT-CIMS application inside the 20 feet sea-container; the right photograph shows the rack with supporting components, the left photograph shows the front of the spectrometer and the exhaust tube.

Appendix B

Additional Data

Particle size and number distributions during the 2nd, 3rd and 4th of July measured by the University of Helsinki and chlorophyll-fluorescence and halocarbon measurements performed by the University of East Anglia, as well as chlorophyll-fluorescence measured by the ship's fluorometer during the whole cruise are presented on the following pages. These are additional data that were discussed in chapter 7.

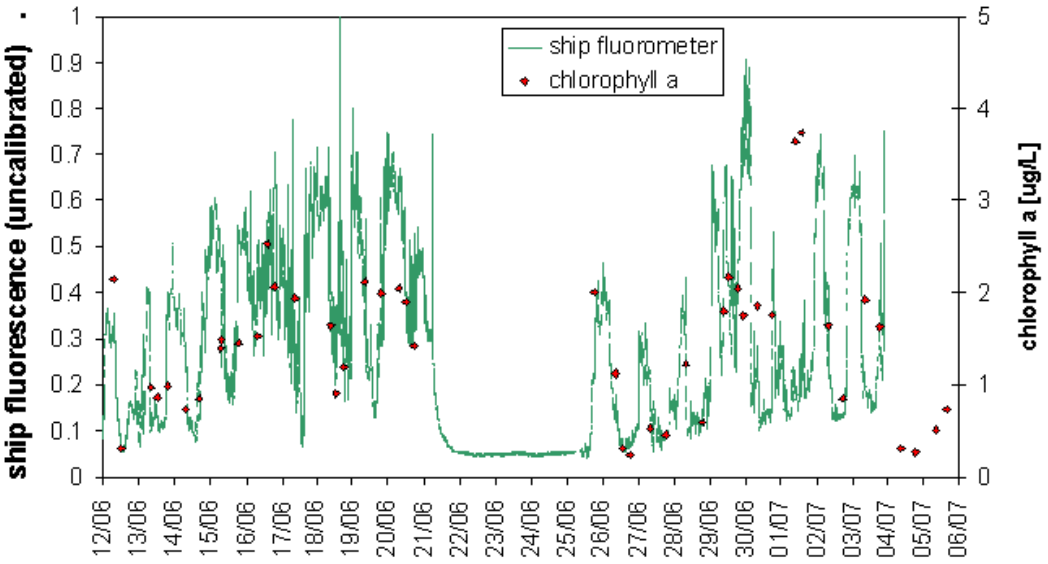

Figure B.1: Chlorophyll concentrations measured during the MAP-cruise by the University of East Anglia (red dots) and the ships fluorometer (green line). The ships fluorometer was not calibrated and only able to measure fluorescence during the night. Highest chlorophyll concentrations are found on the 1st of July (UEA measurements) when the CE was in coastal range.

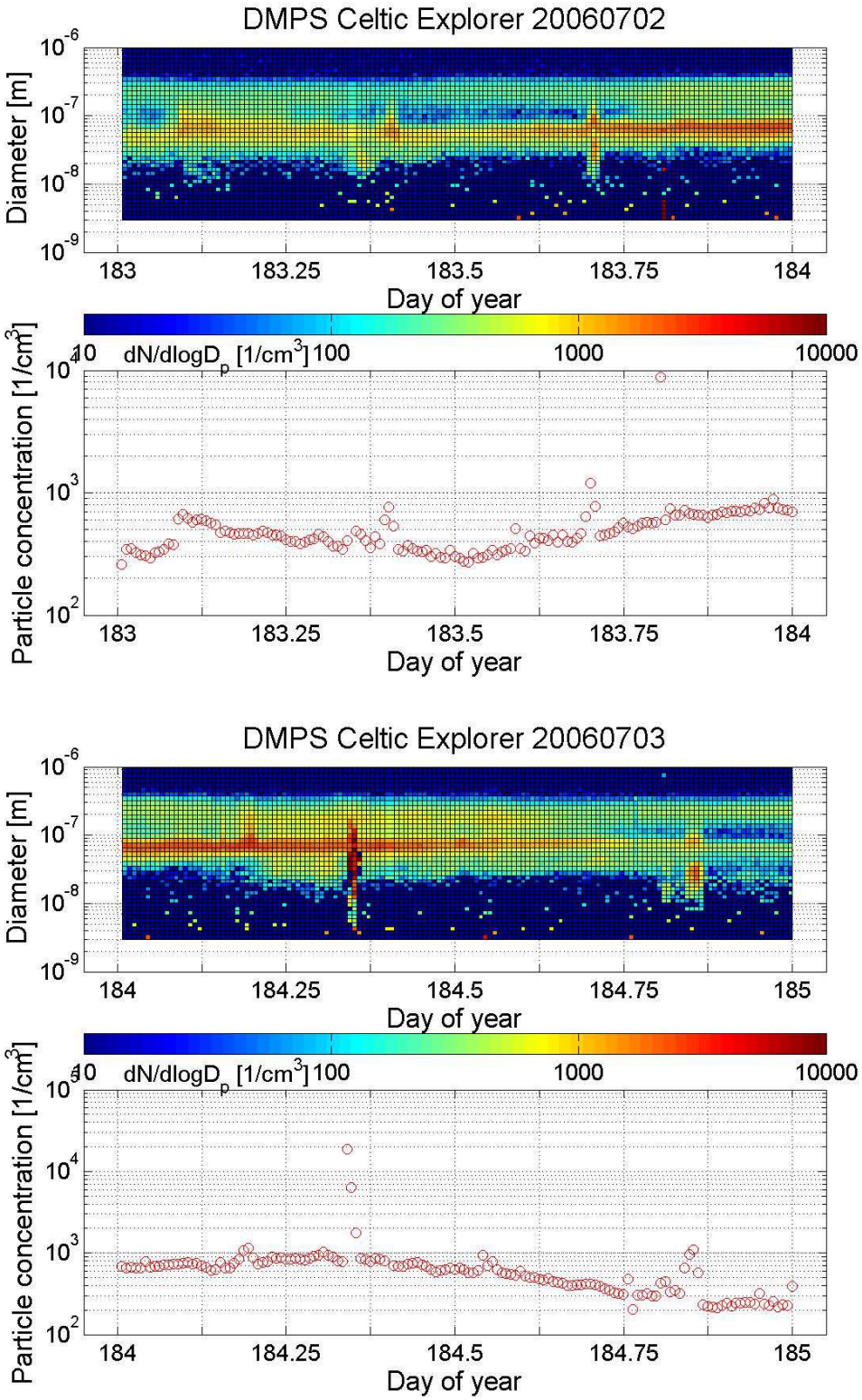

Figure B.2: Number and size distributions of particles between 3 and 800nm during the 2nd and 3rd of July. The color code represents the particle number concentration. A dominant mode is visible for particles of 60 to 80 nm in diameter. Measurements performed by the University of Helsinki

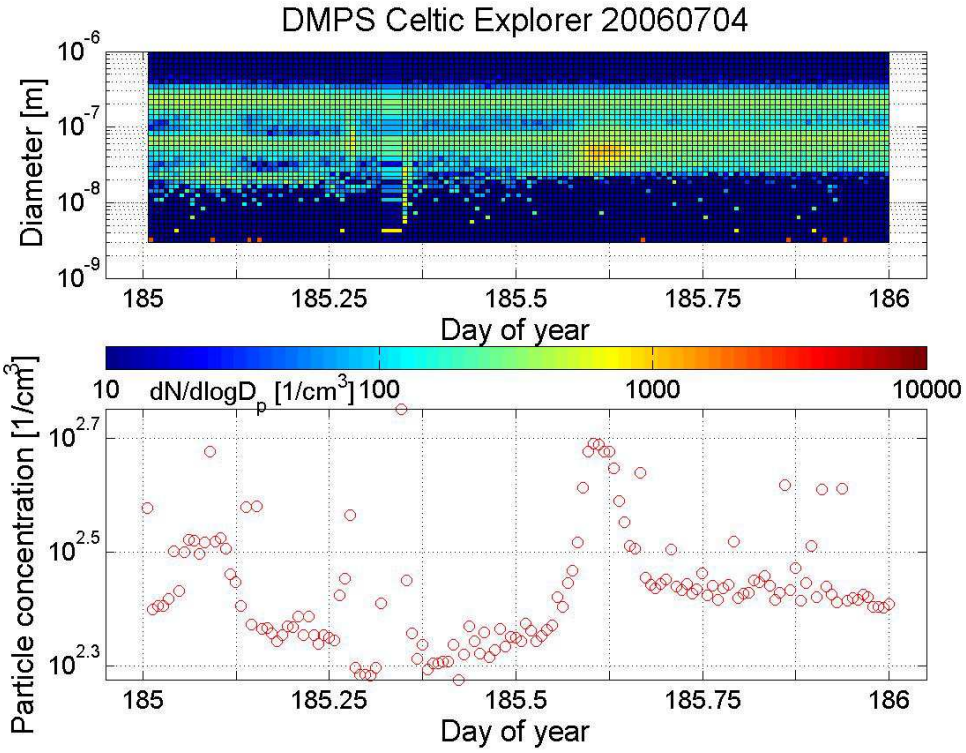

Figure B.3: Number and size distributions of particles with diameter between 3 and 800nm during the 4th of July. The color code represents the particle number concentration. Measurements performed by the University of Helsinki

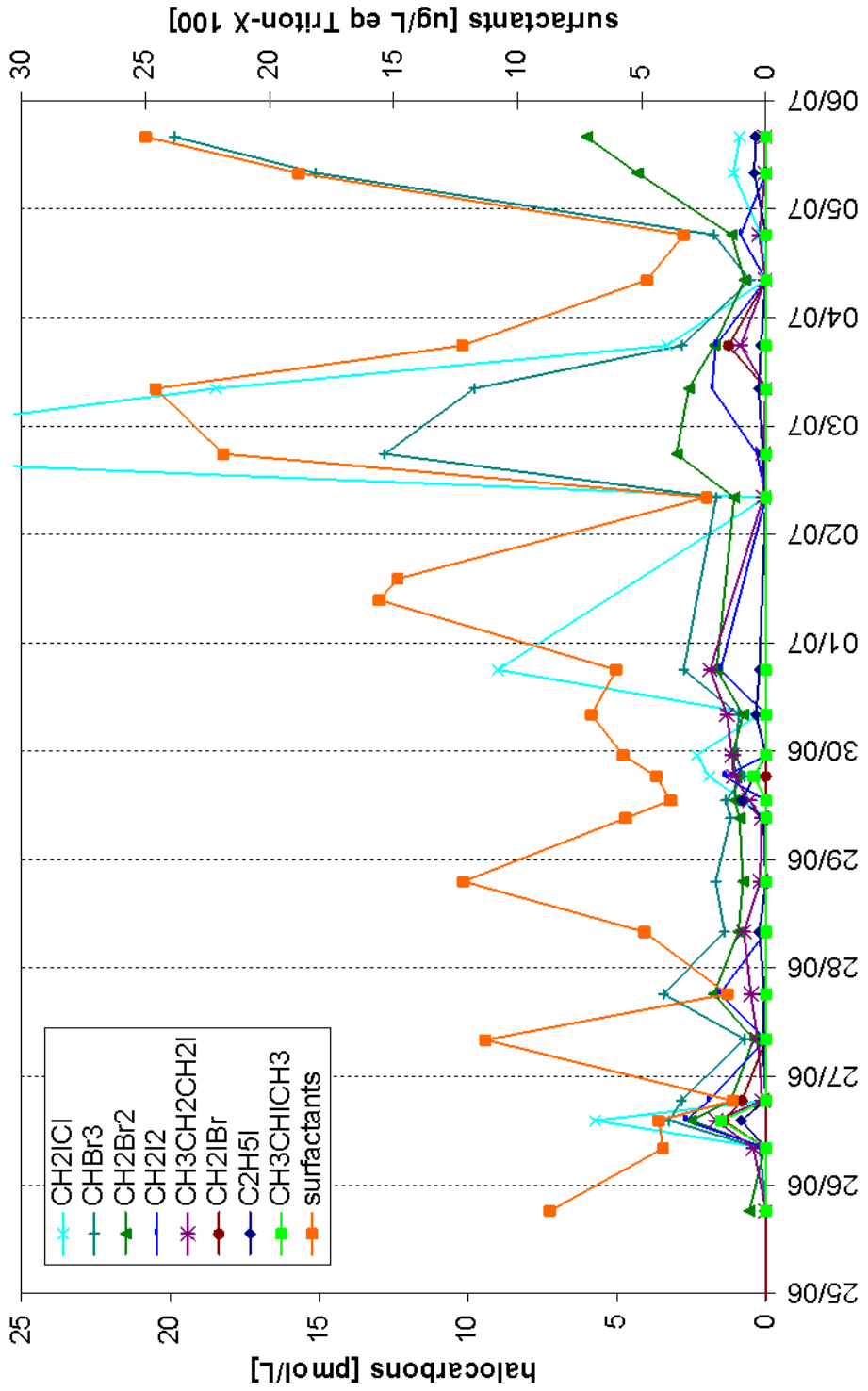

Figure B.4: Halocarbon-concentrations in the water measured during the MAP-cruise by the University of East Anglia. CH_2ICl, $CHBr_3$, surfactants and other halocarbons show the highest values on the 3rd of July when the CE was in the region of highest plankton bloom.

Appendix C

Air Mass Trajectories

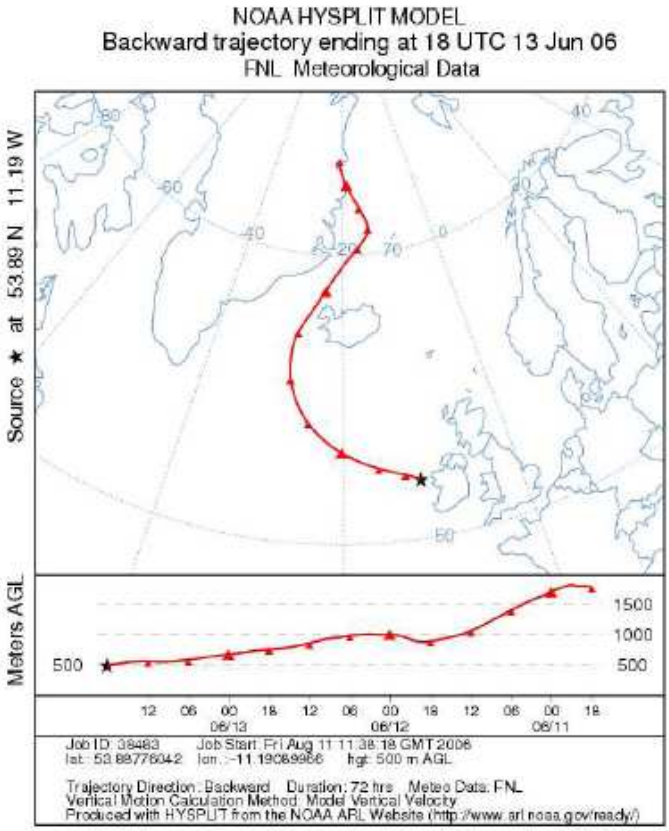

Figure C.1: HYSPLIT Backwards trajectories for the 13th of June when nucleation was observed. Indications of contact of the air masses with continental areas are visible.

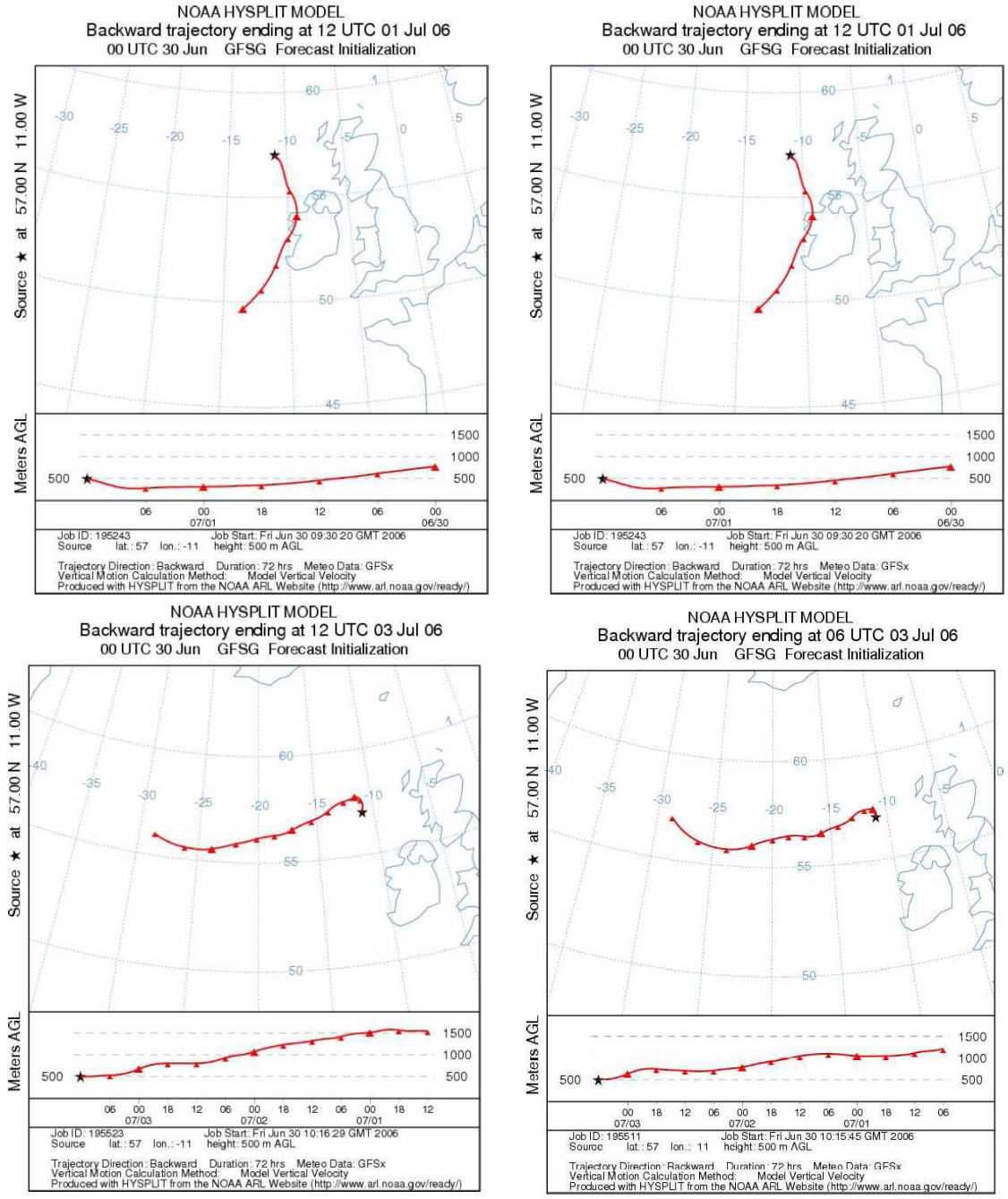

Figure C.2: HYSPLIT Backwards trajectories for the 1st, 2nd and 3rd of July at 12 p.m. and at the 3rd of July at 6 a.m. [Hardin and Kahn, 2005] The 1st of July was the day when the ship was close to the coast. The trajectory shows that the air masses have been in contact with continental air. On the 3rd of July air masses are coming mainly from western oceanic areas.

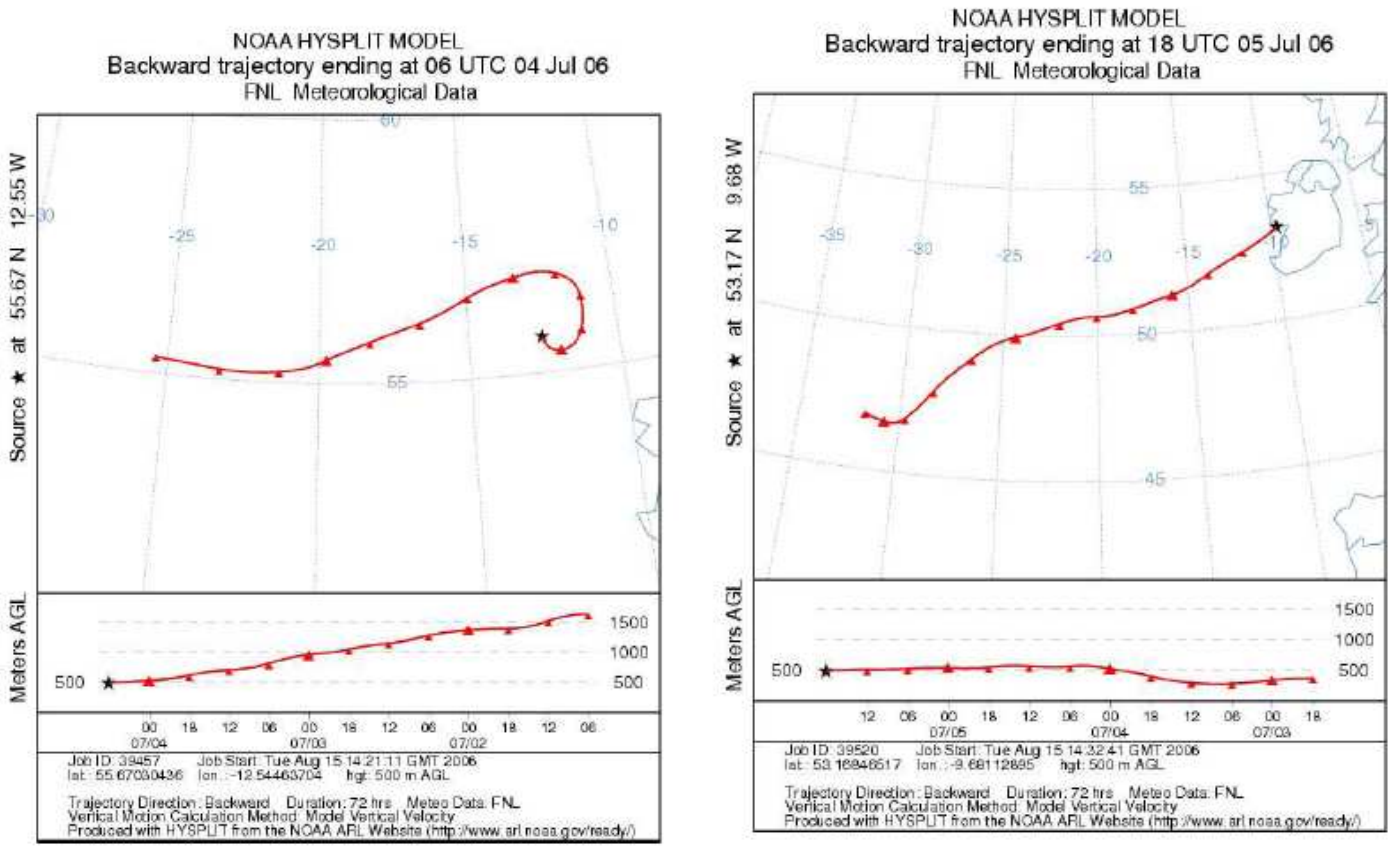

Figure C.3: HYSPLIT Backwards trajectories for the 4th of July at 6 a.m. when the CE was in areas of low plankton bloom and the 5th of July at 6 p.m. during the coastal approach. Both air mass trajectories indicate mostly clean marine air with no contact to continental areas.

List of Figures

2.1 Typical marine aerosol number distributions measured in North East Atlantic maritime air masses at the Outer Hebrides, taken from [O'Dowd et al., 1997] 7

2.2 The two reaction pathways leading to the formation of MSA and H_2SO_4 taken from [von Glasow and Crutzen, 2004]. 9

2.3 Δ G vs the particle radius, at T = 283 K and a supersaturation of S=p/p_0=1.01 . 17

2.4 Free enthalpy of cluster formation for binary nucleation. The saddle point is given through the minimum of Δ G with respect to both molecule numbers n_A and n_B. Graphic taken from [Seinfeld and Pandis, 1998]. 18

3.1 Scheme of the IT-CIMS apparatus (PITMAS) 26

3.2 Schematic of a Paul Ion Trap. 27

3.3 Stability diagram for the ITMS. Ions with a m/z ratio greater than the low-mass cut-off follow stable trajectories. Diagram taken from [March and Todd, 1995]. 29

4.1 Satellite photo taken on the 6th of June 2006. The milky-shaded belt along the coast indicates the area of high plankton density. 32

4.2 The course west of Ireland and Scotland going mainly from south to north with one port call on the 22nd of June at Killybegs, Ireland. The time is color-coded. 33

5.1 The inlet system on top of the sea-container. The smaller one in the back is the inlet for H_2SO_4 measurements while the bigger on in the front is the one for SO_2 measurements. On the top right side the setup for background measurement with the filter paper is shown. On the bottom right side the inlet icon cone in the center of the protection pipes is shown. 37

5.2 Experimental setup used during MAP for H_2SO_4 and MSA measurements. The air is drawn into a flow reactor and the H_2SO_4 and MSA molecules are ionized after approx. 91 cm by a radioactive ion source and then guided into the ITMS. 38

5.3 Schematic alignment of the instruments inside the container: to the left of the hatch (green square) is the IT-CIMS for SO_2 measurements, to the right the instrument to measure H_2SO_4. The green circles represent the openings for the two sampling lines. Two racks for supporting equipment are set next to the walls (black lined squares). The container has one window to the right and the exit to the left. The air conditioning system and the filter cartridges are placed in the front compartment. 38

5.4 The Polonium ion source. 40

5.5 Schematic of the experimental setup during calibration. 46

5.6 Mass spectra taken during calibration, the educt(m/z 125) and product(m/z 160) masses during background measurements (left) when the calibration source was turned off and calibration (right) with injection of SO_2 and turned on UV light source. 47

6.1 Background Measurements during MAP, mass 160 is plotted against the educt mass 125 with their respective 1σ standard deviation 54

6.2 Standard Deviation of mass 160 is plotted against the educt mass 125, a trend of increased noise with higher educt rates is observed, explaining the high detection limit 55

6.3 The intensity of mass 125 is plotted vs the relative humidity. At a relative humidity of 22% the count rates have already decreased by a factor of 4, thus resulting in a reduced sensitivity. Figure taken from [Uecker, 2002]. 56

6.4 1. Panel: Mass 125 during background measurements with a Pure Air Generator; 2. Panel: Mass 125 during background measurements with a filter . . . 57

6.5 MSA, H_2SO_4, UV radiation and SO_2 (logarithmic scale) during the 2nd leg of the cruise. Colored timelines are averaged over five spectra. 59

7.1 Sulfuric acid plotted vs local time (-1h). Different colored dots refer to different days. Except for the 13th of June and the 5th of July H_2SO_4 values stay mostly below $1{\cdot}10^7 \mathrm{cm}^{-3}$ 64

7.2 SO_2-mole fractions (first panel), gaseous H_2SO_4 concentrations, UV radiation (third panel, measured by MPI-K), CS, particle size distributions and particle number concentrations (measured by the University of Helsinki) during 13th of June. This day comprises the only data set when nucleation was observed. 66

7.3 Sulfuric acid measurements (red), concentrations averaged over 5 spectra (black) during three days with high UV radiation (grey), CS (University of Helsinki) values range between $6{\cdot}10^{-4}s^{-}1$ and $6{\cdot}10^{-3}s^{-}1$ and SO_2 with 10 to 800 pptv (SO_2 values are averaged over 5 mass spectra). 68

7.4 Measured H_2SO_4 compared to estimated photochemical production and loss onto aerosols 70

7.5 Scatterplot of H_2SO_4 (MPI-K) and CS (University of Helsinki) (data taken during the entire cruise); the color code represents the relative humidity . . . 72

7.6 Chlorophyll satellite data taken from OceanColor-Web by NASA [Draxler and Rolph, 2003] and the course of the Celtic Explorer from midday of the 2nd of July in regions of high chlorophyll (10 mg m^{-3}) to midnight of the 4th of July with lower chlorophyll values (<1 mg m^{-3}). 74

7.7 Sulphate, nitrate, ammonia and total organics measured by the AMS of the University of Manchester. During the coastal approach on the 1st of July all aerosol constituents are increased, while the 2nd and 3rd only show an enhancement of sulphate ions, correlating with an increased SO_2 concentration in the gas phase 75

7.8 Panel 1 shows MSA concentrations plotted vs local time (-1h) for all days. Panel 2 shows the a scatterplot of MSA with NH_4^+ concentration (measured by the University of Manchester) in the aerosol (the color code represents the relative humidity). Panel 3 shows a scatter plot of MSA concentration with relative humidity 78

7.9 MSA (MPI-K) plotted vs the condensation sink (provided by the University of Manchester) for the selected days of July 80

7.10 Scatterplots of the sulfur components in gaseous and particulate form. Except for H_2SO_4 all components show a strong correlation thus indicating that their precursor is of the same origin 82

A.1 MSA, H_2SO_4, UV radiation (grey) (MPI-K) and CS (black) (University of Helsinki), SO_2 (averaged over 5 mass spectra) (MPI-K) during 13.06.2006. The 13th of June was the only day when nucleation was observed 86

A.2 MSA, H_2SO_4, UV radiation (grey) (MPI-K) and CS (black) (University of Helsinki), SO_2 (averaged over 5 mass spectra) (MPI-K) during 16.06.2006. . 87

A.3 MSA, H_2SO_4, UV radiation (grey) (MPI-K) and CS (black) (University of Helsinki), SO_2 (averaged over 5 mass spectra) (MPI-K) during 17.06.2006. . 88

A.4 MSA, H_2SO_4, UV radiation (grey) (MPI-K) and CS (black) (University of Helsinki), SO_2 (averaged over 5 mass spectra) (MPI-K) during 19.06.2006. . 89

A.5 MSA, H_2SO_4, UV radiation (grey) (MPI-K) and CS (black) (University of Helsinki), SO_2 (averaged over 5 mass spectra) (MPI-K) during 25.06.2006. . 90

A.6 MSA, H_2SO_4, UV radiation (grey) (MPI-K) and CS (black) (University of Helsinki), SO_2 (averaged over 5 mass spectra) (MPI-K) during 26.06.2006. . . 91

A.7 MSA, H_2SO_4, UV radiation (grey) (MPI-K) and CS (black) (University of Helsinki), SO_2 (averaged over 5 mass spectra) (MPI-K) during 27.06.2006. . . 92

A.8 MSA, H_2SO_4, UV radiation (grey) (MPI-K) and CS (black) (University of Helsinki), SO_2 (averaged over 5 mass spectra) (MPI-K) during 28.06.2006. The data show a clear tendency of MSA reduction with high values of CS. . . 93

A.9 MSA, H_2SO_4, UV radiation (grey) (MPI-K) and CS (black) (University of Helsinki), SO_2 (averaged over 5 mass spectra) (MPI-K) during 29.06.2006. . 94

A.10 MSA, H_2SO_4, UV radiation (grey) (MPI-K) and CS (black) (University of Helsinki), SO_2 (averaged over 5 mass spectra) (MPI-K) during 30.06.2006. . 95

A.11 MSA, H_2SO_4, UV radiation (grey) (MPI-K) and CS (black) (University of Helsinki), SO_2 (averaged over 5 mass spectra) (MPI-K) during 01.07.2006. The course was set along the coast of the Outer Hebridies, Scotland. 96

A.12 MSA, H_2SO_4, UV radiation (grey) (MPI-K) and CS (black) (University of Helsinki), SO_2 (averaged over 5 mass spectra) (MPI-K) during 02.07.2006. . 97

A.13 MSA, H_2SO_4, UV radiation (grey) (MPI-K) and CS (black) (University of Helsinki), SO_2 (averaged over 5 mass spectra) (MPI-K) during 03.07.2006. . . 98

A.14 MSA, H_2SO_4, UV radiation (grey) (MPI-K) and CS (black) (University of Helsinki), SO_2 (averaged over 5 mass spectra) (MPI-K) during 04.07.2006. . . 99

A.15 MSA, H_2SO_4, UV radiation (grey) (MPI-K) and CS (black) (University of Helsinki), SO_2 (averaged over 5 mass spectra) (MPI-K) during 05.07.2006. In the afternoon, the coast of West Ireland near the research station Mace Head was in sight. 100

A.16 The concentrations of MSA and H_2SO_4, SO_2 mole fraction during the 5th of July when the measurements were influenced by local pollution (presumably the coast or the ship's exhaust) and the NO_3^- signature at m/z = 62. High NO_x values might explain high MSA concentrations at the coast through oxidation of DMS 102

A.17 The concentration of MSA and H_2SO_4, SO_2 mole fraction during the 13th of June and the NO_3^- signature at m/z = 62. Measurements might have been influenced by the ship's exhaust or other sources since only the NO_3^- signature is high. SO_2 does not show the same variations in the morning. MSA concentrations showed the highest values on the 13th of June presumably due to DMS oxidation through NO_3 103

A.18 The concentration of MSA and H_2SO_4, SO_2 mole fraction during the 2nd of July and the NO_3^- signature at m/z = 62. 104

A.19 The concentration of MSA and H_2SO_4, SO_2 mole fraction during the 3nd of July and the NO_3^- signature at m/z = 62. 105

A.20 A scatterplot of SO_2-mole fraction and mass 62 during the afternoon of the 5th of July and the 3rd of July. The positive correlation on the 5th indicates SO_2 and NO_x have the same origin, probably the ship's exhaust. On the 3rd no significant correlations are visible for small values of SO_2. In this scatterplot contamination events with SO_2 mole fractions above 200 ppt, which were only observed on a short time scale, are extracted. This might prove that SO_2 was of biogenic origin and not emitted by the ship's exhaust. 106

A.21 Above: The Celtic Explorer in the harbor of Killybegs, North of Ireland. The MPI-K container is placed on the front deck while the exhaust is on the after deck. Below: Photograph of the IT-CIMS application inside the 20 feet sea-container; the right photograph shows the rack with supporting components, the left photograph shows the front of the spectrometer and the exhaust tube. 107

B.1 Chlorophyll concentrations measured during the MAP-cruise by the University of East Anglia (red dots) and the ships fluorometer (green line). The ships fluorometer was not calibrated and only able to measure fluorescence during the night. Highest chlorophyll concentrations are found on the 1st of July (UEA measurements) when the CE was in coastal range. 109
B.2 Number and size distributions of particles between 3 and 800nm during the 2nd and 3rd of July. The color code represents the particle number concentration. A dominant mode is visible for particles of 60 to 80 nm in diameter. Measurements performed by the University of Helsinki 110
B.3 Number and size distributions of particles with diameter between 3 and 800nm during the 4th of July. The color code represents the particle number concentration. Measurements performed by the University of Helsinki 111
B.4 Halocarbon-concentrations in the water measured during the MAP-cruise by the University of East Anglia. CH_2ICl, $CHBr_3$, surfactants and other halocarbons show the highest values on the 3rd of July when the CE was in the region of highest plankton bloom. 112

C.1 HYSPLIT Backwards trajectories for the 13th of June when nucleation was observed. Indications of contact of the air masses with continental areas are visible. 113
C.2 HYSPLIT Backwards trajectories for the 1st, 2nd and 3rd of July at 12 p.m. and at the 3rd of July at 6 a.m. [Hardin and Kahn, 2005] The 1st of July was the day when the ship was close to the coast. The trajectory shows that the air masses have been in contact with continental air. On the 3rd of July air masses are coming mainly from western oceanic areas. 114
C.3 HYSPLIT Backwards trajectories for the 4th of July at 6 a.m. when the CE was in areas of low plankton bloom and the 5th of July at 6 p.m. during the coastal approach. Both air mass trajectories indicate mostly clean marine air with no contact to continental areas. 115

Bibliography

[Allan et al., 2003] Allan, J. D., Jimenez, J. L., Williams, P. I., Alfarra, M. R., Bower, K. N., Coe, J. T. J. H., and Worsnop, D. R. (2003). Quantitative sampling using an Aerodyne aerosol mass spectrometer; 1.Techniques of data interpretation and error analysis. *Journal of Geophysical Research*, 108(D3):4090.

[Amouroux et al., 2002] Amouroux, D., G. R., Rapsomanikis, S., and Andreae, M. (2002). Biogenic Gas(CH4, N2O, DMS) Emission to the Atmosphere from Near-shore and Shelf Waters of the North-western Black Sea. *Estuarine, Coastal and Shelf Science*, 54:575–587.

[Arnold, 1982] Arnold, F. (1982). Ion nucleation - a potential source for stratospheric aerosols. *Nature*, 299:134–137.

[Arnold and Fabian, 1980] Arnold, F. and Fabian, R. (1980). First measurements of gas phase sulfuric acid in the stratosphere. *Nature*, 283:55–57.

[Arnold and Viggiano, 1980] Arnold, F. and Viggiano, A. A. (1980). *Pl. Space Sci.*, 30:1295.

[Arnold, 1978] Arnold, F. und Henschen, G. (1978). First mass analysis of stratospheric negative ions. *Nature*, 275:521–522.

[Atkinson et al., 1997] Atkinson, R., Baulch, D., Cox, R., Hampson, R., Jr.J.A.Kerr, Rossi, M., and J.Troe (1997). Evaluated kinetic and photochemical data for atmospheric chemistry, supplement v. *J. of Phys. Chem. Ref. Data*, 26:521–1011.

[Aufmhoff, 2004] Aufmhoff, H. (2004). *Atmosphärische gasförmige Vorläufer von Aerosol und Ozon: Messungen mit CIMS-Methoden auf einem Flugzeug und am Boden.* PhD thesis, Universität Heidelberg.

[Bandy et al., 1993] Bandy, A., Thornton, D., and Driedger, A. (1993). Airborne measurements of sulfure dioxide, dimethyl sulfide, carbon disulfide and carbonyl sulfide by isotope

dilution gas chromatography/mass spectrometry. *Geophysical Research Letters*, 98:423–433.

[Bardouki et al., 2003] Bardouki, H., Berresheim, H., Vrekoussis, M., Sciare, J., Kouvarakis, G., K. Oikonomou, J. S., and Mihalopoulos, N. (2003). Gaseous(DMS, MSA, SO_2,H_2SO_4 and DMSO) and particulate (sulfate and methansulfonate) sulfur species over the north-eastern coast of Crete. *Atmospheric Chemistry and Physics*, 3:1871–1886.

[Barnes et al., 2006] Barnes, I., Hjorth, J., and Mihalopoulos, N. (2006). Dimethyl sulfide and dimethyl sulfoxide and their oxidation in the atmosphere. *Chem. Rev.*, 106:940–975.

[Bates, 1992] Bates, T. (1992). Sulfur emissions to the atmosphere from natural sources. *Journal of Atmospheric Chemistry*, 14:315–337.

[Bates et al., 1987] Bates, T., Cline, J., Gammon, R., and Kelly-Hanson, S. (1987). Regional and seasonal variations in the flux of oceanic dimethylsulfide to to the atmosphere. *Journal of Geophysical Research*, 92:2930–2938.

[Berresheim et al., 2002] Berresheim, H., Eisele, T., Tremmel, H., Allen, A., Hansson, H.-C., Rosman, K., Maso, M. D., J.M.Mäkelä, Kulmala, M., and O'Dowd, C. (2002). Gas-aerosol relationship of H_2SO_4, MSA and OH: Observations in the coastal marine boundary layer at Mace Head, Ireland. *Journal of Geophysical Research*, 107(D19):8100.

[Bey et al., 2001] Bey, I., Jakob, D. J., Yantosca, R., Logan, J., Field, B. D., A.M.Fiore, Q.Li, J.Mickley, H. L., and M.G.Schultz (2001). Global modeling of tropospheric chemistry with assimilated meteorology: Model description and evaluation . *Journal of Geophysical Research*, 106(D19):23,073–23,096.

[Boy et al., 2004] Boy, M., Kulmala, M., Ruuskanen, T., Pihlatie, M., Reissell, A., Aalto, P., Keronen, P., Hellen, H., Hakola, H., Jansson, R., Hanke, M., and Arnold, F. (2004). Sulphuric acid closure and contribution to nucleation mode particle growth. Submitted. *J. of Atmospheric Chemistry and Physics.*

[Brasseur et al., 1999] Brasseur, G. P., Orlando, J. J., and Tyndall, G. S. (1999). *Atmospheric Chemistry and Global Change.* Oxford University Press, New York, 1 edition.

[Charlson et al., 1987] Charlson, R. J., Lovelock, J. E., Andreae, M. O., and Warren, S. G. (1987). Oceanic phytoplankton, atmospheric sulphur, cloud albedo and climate. *Nature*, 326(16):655–661.

[Coe et al., 2005] Coe, H., Allan, J., M.R.Alfarra, Bower, K., Flynn, M., McFiggans, G., Topping, D., Williams, P., O'Dowd, C., Dall'Osto, M., Beddows, D., and Harrison, R. (2005). Chemical and physical characteristics of aerosol particles at the remote coastal location, mace head, ireland, during namblex. *Atmospheric Chemistry and Physics*, 6:3289–3301.

[Davis et al., 1999] Davis, D., G.Chen, A.Bandy, D.Thronton, F.Eisele, L.Mauldin, D.Tanner, D.Lenschow, H.Fuelberg, B.Huebert, J.Heath, A.Clarke, , and D.Blake (1999). Dimethyl sulfide oxidation in the equatorial Pacific: Comparison of model simulations with field observartions for DMS, SO2, H_2SO_4(g), MSA(g), MS, and NSS. *Journal of Geophysical Research*, 104(D5):5765–5784.

[Davis et al., 1998] Davis, D., G.Chen, P.Kasibhatla, A.Jefferson, D.Tanner, Eisele, F., D.Lenschow, W.Neff, and Berresheim, H. (1998). DMS oxidation in the Antartic marine boundary layer: Comparison of model simulations and field observations of DMS, DMSO, H_2SO_4(g), MSA(g), and MSA(p). *Journal of Geophysical Research*, 103(D1):1657–1678.

[De Bruyn et al., 1994] De Bruyn, W., Shorter, J., and Davidovits, P. (1994). Uptake of gas phase sulfur species methanesulfonic acid, dimethylsulfoxide, and dimethyl sulfone by aqueous surfaces. *Journal of Geophysical Research*, 99(D8):927–932.

[DeMore, 1997] DeMore, W. (1997). Chemical kinetics and photochemical data for use in stratospheric modeling. evaluation no. 12. *Jet Propulsion Laboratory Publication*, No.12:97–4.

[Draxler and Rolph, 2003] Draxler, R. R. and Rolph, G. D. (2003). *HYSPLIT (HYbrid Single-Particle Lagrangian Integrated Trajectory) Model access via NOAA ARL READY Website (http://www.arl.noaa.gov/ready/hysplit4.html).*

[Eisele and Tanner, 1993] Eisele, F. and Tanner, D. (1993). Measurements of the gas phase concentrations of H_2SO_4 and methane sulfonic acid and estimates of H_2SO_4 production and loss in the atmosphere. *Journal of Geophysical Research*, 98:9001–9010.

[Endresen and Sørgård, 2003] Endresen, Ø. and Sørgård, E. (2003). Emission from international sea transportation and environmental impact. *Journal of Geophysical Research*, 08(D17):4560.

[Fiedler, 2004] Fiedler, V. (2004). The Atmospheric Aerosol Precursor Gas Sulphuric Acid: Mass Spectrometric Measurements in the Atmospheric Boundary Layer in Finnland and Germany. Diplomarbeit, Universität Heidelberg.

[Fiedler et al., 2005] Fiedler, V., Dal Maso, M., Boy, M., Aufmhoff, H., Hoffmann, J., Schuck, T., Birmili, W., Arnold, F., and Kulmala, M. (2005). The contribution of sulphuric acid to atmospheric particle formation and growth: a comparison between boundary layers in northern and central europe. *Atmos. Chem. Phys. Discuss.*, 5:1–33.

[Fuchs and Sutugin, 1971] Fuchs, N. and Sutugin, A. (1971). Highly dispersed aerosol. *Hidy, G.M. and Brock, J.R. (eds): Topics in current aerosol research, Pergamon, New York.*

[Gosh, 1995] Gosh, P. (1995). *Ion Traps.* Clarendon Press, Oxford.

[Hanke, 1999] Hanke, M. (1999). *Development of a Novel Method for Measuring Atmospheric Peroxy Radicals : Calibration, Aircraft-Borne Measurements and Speciated Measurements of HO_2 and RO_2.* PhD thesis, Universität Heidelberg.

[Hanke et al., 2002] Hanke, M., Arnold, F., , Umann, B., Uecker, J., and Bunz, H. (2002). Atmospheric measurements of gas-phase HNO_3 using chemical ionization mass spectrometry during the Minatroc field campaign 2000 on Monte Cimone. *Atmospheric Chemistry and Physics Discussions*, 2:2209–2258.

[Hardin and Kahn, 2005] Hardin, M. and Kahn, R. (2005). Aerosols and climate change. *http://geography.berkeley.edu:16080/ProgramCourses/CoursePagesFA2005/Geog142.*

[Huebert et al., 1993] Huebert, B., S.Howell, P.Laj, J.E.Johnson, T.S.Bates, P.K.Quinn, V.Yegorov, A.D.Clark, and J.N.Porter (1993). Observations of the atmospheric sulfur cycle on SAGA 3. *J. Geophysical Research*, (98):985–995.

[Huebert, 1999] Huebert, B. J. (1999). Sulphur emissions from ships. *Nature*, 400:713–714.

[Jefferson et al., 1998] Jefferson, A., Tanner, D., Eisele, F., and Berresheim, H. (1998). Sources and sinks of H_2SO_4 in the remote Antarctic marine boundary layer. *Journal of Geophysical Research*, 103(D1):1639–1645.

[Knop and Arnold, 1985] Knop, G. and Arnold, F. (1985). Nitric acid vapour measurements in the troposphere and lower stratosphere by chemical ionisation mass spectrometry. *Planetary Space Science*, 33/II:983–986.

[Kolb et al., 1994] Kolb, C., Jayne, J., Worsnop, D., Molina, M., Meads, R., and Viggiano, A. (1994). Gas phase reaction of sulphur trioxide with water vapor. *J. Am. Chem. Soc.*, 116:10314–10315.

[Korhonen et al., 1999] Korhonen, P., Kulmala, M., Laaksonen, A., Viisanen, Y., McGraw, R., and Seinfeld, J. (1999). Ternary nucleation of H_2SO_4, NH_3 and H_2O in the atmosphere. *J. Geophys. Res.*, 104:26349–26353.

[Kreidenweis and Seinfeld, 1988] Kreidenweis, S. and Seinfeld, J. (1988). Nucleation of sulfuric acid-water and methanesulfonic acid-water solution particle: Implications for the atmospheric chemistry of organosulfur sprecies. *Atmospheric Environment*, (22):283–296.

[Kulmala, 2003] Kulmala, M. (2003). How Particles Nucleate and Grow. *Science*, 302:1000–1001.

[Kulmala et al., 2005] Kulmala, M., Lehtinen, K. E. J., and Laaksonen, A. (2005). Why formation rate of 3nm particles depends linearly on sulphuric acid concentration? *Atmospheric Chemistry and Physics Discussions*, 5:11277–11293.

[Kulmala et al., 2004] Kulmala, M., Vehkamäki, H., Petäjä, T., Dal Maso, M., Lauri, A., Kerminen, V.-M., Birmili, W., and McMurry, P. (2004). Formation and growth rates of ultrafine atmospheric particles: A review of observations. *J. Aerosol Science*, 35-2:143–176.

[Laakso et al., 2004] Laakso, L., Anttila, T., Lehtinen, K. E. J., Aalto, P. P., Kulmala, M., Horrak, U., Paatero, J., Hanke, M., and Arnold, F. (2004). Kinetic nucleation and ions in boreal particle formation events. *Atmos. Chem. Phys. Discuss.*, 4:39113945.

[Lee et al., 2003] Lee, S.-H., Reeves, J., Wilson, J., Hunton, D., Viggiano, A., Miller, T., Ballenthin, J., and Lait, L. (2003). Particle formation by ion nucleation in the upper troposphere and lower stratosphere. *Science.*, 301:1886–1889.

[Lee and Zhu, 1994] Lee, Y. and Zhu, X. (1994). Aqueous reaction kinetics of ozone and dimethylsulfide and its atmospheric implications. *Journal of Geophysical Research*, 99:3597–3604.

[Lovejoy et al., 1996] Lovejoy, E., Hanson, D., and Huey, L. (1996). Kinetics and products of the gas phase reaction of SO_2 with water. *J. Phys. Chem.*, 100:19911–19916.

[Lucas and Prinn, 2002] Lucas, D. and Prinn, R. (2002). Mechanistic studies of dimethylsulfide oxidation products using an observationally constrained model. *Journal of Geophysical Research*, (D14).

[March and Todd, 1995] March, E. R. and Todd, J. F., editors (1995). *Practical Aspects of Ion Trap Mass Spectrometry*, volume III. CRC Press, New York.

[Matrai and Keller, 1993] Matrai, P. and Keller, M. (1993). Dimethylsulfphide in a large scale coccolithophore bloom in the Gulf of Maine. *Continental shelf research*, 13:831–841.

[Mauldin III et al., 1999] Mauldin III, R., Tanner, D., Heath, J., Huebert, B., and Eisele, F. (1999). Observation of H_2SO_4 and MSA during PEM-Tropics-A. *Journal of Geophysical Research*, 104(D5):5801–5816.

[Mitchell, 2001] Mitchell, G. M. (2001). *Determination of Vertical Fluxes of Sulfur Dioxide and Dimethyl Sulfide in the Remote Marine Atmosphere by Eddy Correlation and an Airborne Isotopic Dilution Atmospheric Pressure Ioniziation Mass Spektrometer*. PhD thesis, Drexel University.

[Möhler et al., 1992] Möhler, O., Reiner, T., and Arnold, F. (1992). The formation of so_5^- by gas phase ion-molecule reactions. *Journal of Chemical Physics*, 97:8233–8239.

[Nau, 2004] Nau, R. (2004). Das atmosphärische aerosol-vorläufergas so_2: Messungen mit einem flugzeuggetragenen massenspektrometer. Diplomarbeit, University of Heidelberg.

[Nowak et al., 2002] Nowak, J., Huey, L., Eisele, F., Tanner, D., Mauldin III, R., Cantrell, C., Kosciuch, E., and Davis, D. (2002). Chemical ionization mass spectrometry technique for detection of dimethylsulfoxide and ammonia. *Journal of Geoph. Research*, 107(D18):4363.

[O'Dowd et al., 2002] O'Dowd, C. D., Jimenez, J. L., Bahreini, R., Flagan, R. C., Seinfeld, J. H., Hämeri, K., Pirjola, L., Kulmala, M., Jennings, S. G., and Hoffmann, T. (2002). Marine aerosol formation from biogenic iodine emission. *Nature*, 417:632–635.

[O'Dowd et al., 1997] O'Dowd, C. D., Smith, M., Consterdine, I. E., and Lowe, J. (1997). Marine Aerosol, Sea-Salt, and The Marine Sulphur Cycle: A Short Review. *Atmospheric Environment*, 31:73–80.

[Reimann, 2000] Reimann, J. (2000). Entwicklung und Aufbau einer Kalibrationsquelle für OH-, HO_2- und RO_2-Radikale. Diplomarbeit, Universität Heidelberg.

[Reiner and Arnold, 1993] Reiner, T. and Arnold, F. (1993). Laboratory flow reactor measurements of the reaction $SO_3 + H_2O + M \rightarrow H_2SO_4 + M$: Implications for gaseous H_2SO_4 and aerosol formation in the plume of jet aircraft. *Geophysical Research Letters*, 20:2659–2662.

[Reiner and Arnold, 1994] Reiner, T. and Arnold, F. (1994). Laboratory investigations of gaseous sulfuric acid formation via $SO_3 + H_2O + M \rightarrow H_2SO_4 + M$: Measurements of the rate constant and products identification. *J. Chem. Phys.*, 101:7399–7407.

[Reiner et al., 1998] Reiner, T., Möhler, O., and Arnold, F. (1998). Improved atmospheric trace gas measurements with an aircraft-based tandem mass spectrometer: Ion identification by mass-selected fragmentation studies. *Journal of Geophysical Research*, 103:31309–31320.

[Roedel, 2000] Roedel, W. (2000). *Physik unserer Umwelt: Die Atmosphäre*. Springer Verlag.

[Scholz, 2004] Scholz, S. (2004). Messung der atmosphärischen Spurengase Schwefelsäure und Methansulfonsäure mittels Ionen-Molekül-Reaktions-Massenspektrometrie. Diplomarbeit, Universität Heidelberg.

[Seinfeld and Pandis, 1998] Seinfeld, J. and Pandis, S. N. (1998). *Atmospheric Chemistry and Physics*. John Wiley & Sons, Inc.

[Simó and Pedrós-Alló, 1999] Simó, R. and Pedrós-Alló, C. (1999). Role of vertical mixing in controlling the oceanic production of dimethyl sulfide. *Nature*, 402:396–399.

[Speidel, 2005] Speidel, M. (2005). *Atmospheric Aerosol Particle Formation: Aircraft-Based Mass Spectrometric Measurements of Gaseous and Ionic Aerosol Precursors.* PhD thesis, University of Heidelberg.

[Speidel et al., 2007] Speidel, M., Nau, R., Arnold, F., Schlager, H., and Stohl, A. (2007). Sulfur dioxide measurements in the lower, middle and upper troposphere: Deployment of an aircraft-based chemical ionization mass spectrometer with permanent in-flight calibration. *Atmospheric Environment*. (accepted).

[Stockwell and Calvert, 1983] Stockwell, W. and Calvert, J. (1983). The mechanism of the HO-SO_2 reaction. *Atmospheric Environment*, 17:2231.

[Uecker, 2002] Uecker, J. (2002). *Messung der atmosphärischen Radikale OH, HO_2, RO_2 sowie des Ultraspurengases H_2SO_4 - Weiterentwicklung, Kalibration und Einsatz einer hochempfindlichen massenspektrometrischen Analysemethode.* PhD thesis, Universität Heidelberg.

[Viggiano et al., 1997] Viggiano, A., Seeley, J., Mundis, P., Williamson, J., and Morrison, R. (1997). Rate constants for the reaction of $XHO_3^-(H_2O)f(X = C$, HC and N) and $NO_3^-(HNO_3)_n$ with H_2SO_4 : Implications for atmospheric detection of H_2SO_4. *Journal of Physical Chemistry A*, 101:8275–8278.

[Volmer, 1939] Volmer, M. (1939). Kinetik der Phasenbildung. *Verlag Von Theodor Steinkopff, Dresden und Leipzig.*

[von Glasow and Crutzen, 2004] von Glasow, R. and Crutzen, P. (2004). Model study of mulitphase DMS oxidation with a focus on halogens. *Atmospheric Chemistry and Physics*, 4:589–608.

[Wayne, 2000] Wayne, R. P. (2000). *Chemistry of Atmospheres.* Oxford University Press.

[Wollny, 1998] Wollny, A. (1998). Flugzeugmessungen atmosphärischer Spurengase mittels Ionen-Molekül-Reaktions-Massenspektrometrie: Methodische Untersuchungen zur Reaktionskinetik. Master's thesis, Universität Heidelberg.

[Yue and Chan, 1979] Yue, G. and Chan, L. (1979). Theory of formation of aerosols of volatile binary solutions through the ion-induced nucleation process. *J. Colloid Interface Sci.*, 68:501.

[Zylka-Menhorn, 2005] Zylka-Menhorn, V. (2005). Luftschadstoffe: Feinstäube - Winzlinge mit grosser Wirkung. *Deutsches Ärzteblatt 102*, 14:A–954,B–808,C–755.

Erklärung :

Ich versichere, dass ich diese Arbeit selbstständig verfasst und keine anderen als die angegebenen Quellen und Hilfsmittel benutzt habe.

Heidelberg, den 04.01.2007